Structural Analysis of Serine/Threonine Protein Kinase B and Multiple Peptide Resistant Factor of *Staphylococcus aureus*

Dissertation

der Mathematisch-Naturwissenschaftlichen Fakultät

der Eberhard Karls Universität Tübingen

zur Erlangung des Grades eines

Doktors der Naturwissenschaften

(Dr. rer. nat.)

vorgelegt von

Sonja Natalie Rakette

aus Ostfildern-Ruit

Tübingen

2012

Tag der mündlichen Qualifikation:	18.12.2012
Dekan:	Prof. Dr. Wolfgang Rosenstiel
1. Berichterstatter:	Prof. Dr. Thilo Stehle
2. Berichterstatter:	Prof. Dr. Andreas Peschel

1 TABLE OF CONTENTS

2 ABBREVIATIONS

6xHis-tag	sixfold polyhistidine tag
ADP	adenosine diphosphate
AMP	adenosine monophosphate
AMP-CPP	α,β-methyleneadenosine 5′-triphosphate
AMP-PCP	β,γ-methyleneadenosine 5′-triphosphate
AMP-PNP	β,γ-imidoadenosine 5′-triphosphate
ATF2	activating factor 2
ATP	adenosine triphosphate
ATP-γS	adenosine 5′(γ-thio)triphosphate
CAMP	cationic antimicrobial peptide
cAMP	cyclic adenosine monophosphate
CA-MRSA	community-associated methicillin-resistant *Staphylococcus aureus*
CD	circular dichroism
C-spine	catalytic spine
DNA	deoxyribonucleic acid
DTT	dithiothreitol
EDTA	ethylenediaminetetraacetic acid
GST	gluthatione S-tranferase
HA-MRSA	hospital-associated methicillin-resistant *Staphylococcus aureus*
HEPES	4-(2-hydroxyethyl)-1-piperazineethanesulfonic acid
IEX	ion exchange chromatography
IMAC	immobilized metal ion affinity chromatography
IPTG	isopropyl β-D-1-thiogalactopyranoside
Lys-PG	*lysyl*-phosphatidylglycerol
M. tuberculosis	*Mycobacterium tuberculosis*
MBP	myelin basic protein
MES	2-(*N*-morpholino)ethanesulfonic acid
MIC	minimum inhibitory concentration
MprF	multiple peptide resistant factor
MRSA	methicillin-resistant *Staphylococcus aureus*
NCS	non-crystallographic symmetry

OD	optical density
ORF	open reading frame
PASTA	penicillin-binding protein and serine/threonine kinase associated
PBP	penicillin-binding protein
PDB	Protein Data Bank
PG	phosphatidylglycerol
PKA	protein kinase A
PknB	protein kinase B
$PknB_{SA\text{-}KD}$	kinase domain of *Staphylococcus aureus* PknB
$PknB_{SA\text{-}KD\text{-}short}$	kinase domain of *Staphylococcus aureus* PknB residues 1-274
PMSF	phenylmethanesulfonyl fluoride
R-spine	regulatory spine
RT-PCR	real-time polymerase chain reaction
SAP	Shrimp alkaline phosphatase
S. aureus	*Staphylococcus aureus*
SD	Superdex
SDS-PAGE	sodium dodecyl sulfate polyacrylamide gel electrophoresis
STK	serine/threonine kinase
TMS	transmembrane segment
Tris	tris(hydroxymethyl)aminomethane
VRSA	vancomycin-resistant *Staphylococcus aureus*

Units specified by the international system of units (SI) and compounds named by the IUPAC nomenclature are not listed here.

3 SUMMARY

Staphylococcus aureus (*S. aureus*) infections are becoming increasingly problematic. The bacteria gain resistance to new antibiotics in relatively short time periods. Besides the hospital associated methicillin-resistant *S. aureus* (HA-MRSA), infections with community-associated MRSA (CA-MRSA) are increasing.

The only serine/threonine kinase PknB of *S. aureus* is composed of an intracellular kinase domain, a transmembrane helix and three extracellular penicillin-binding protein and serine/threonine kinase associated (PASTA) domains. PknB is able to perform phosphorylation and autophosphorylation *in vitro*. Transcriptome and functional analysis of *S. aureus* showed that PknB is involved in regulating purine/pyrimidine synthesis, cell wall metabolism and central metabolic functions. In peptide arrays using eukaryotic peptides and PknB, the kinase was identified to be a proline-directed kinase. The crystal structure of the *S. aureus* PknB kinase domain ($PknB_{SA\text{-}KD}$) was solved in complex with a non-hydrolyzable adenosine triphosphate (ATP) analog at 3.0 Å resolution. Different ATP analogs, divalent cations and crystallization techniques were tested to improve crystal quality. The $PknB_{SA\text{-}KD}$ structure was compared to different eukaryotic and prokaryotic serine/threonine protein kinases. Similar to the full-length protein, $PknB_{SA\text{-}KD}$ is able to perform phosphorylation and autophosphorylation *in vitro*. In contrast to the active state in solution, the kinase crystallized in an inactive conformation.

The multiple peptide resistant factor (MprF) is a virulence factor of *S. aureus*. MprF is predicted to be composed of a large hydrophobic region, containing 14 transmembrane segments (TMS) and a hydrophilic C-terminal region. The hydrophilic portion and the six C-terminal TMSs form a synthase domain; the eight N-terminal TMSs harbor a flippase function. The synthase adds lysine to phosphatidylglycerol (PG); the flippase inserts this positively charged *lysyl*-phosphatidylglycerol (Lys-PG) into the outer membrane leaflet of *S. aureus*. This leads to a change in the membrane charge, and host defensins are thus no longer able to bind to the bacterial membrane. In this work, the initial constructs of the synthase of MprF contained all the C-terminal soluble part with varying N-terminal ends. In addition to the variations in the N-terminal end of the soluble part, the number of TMSs was varied. All these constructs were successfully cloned and expressed. Protein analysis indicated aggregation of the proteins. The linker region between the last TMS and the soluble part was in the main focus. Variations of only few amino acids influenced the behavior of the protein

during purification. Inclusions of increasing numbers of N-terminal TMSs into the construct lead to a decrease in solubility.

4 ZUSAMMENFASSUNG

Infektionen mit *Staphylococcus aureus (S. aureus)* werden problematischer, da die Bakterien in immer kürzerer Zeit Resistenzen gegen neue Antibiotika entwickeln. Zusätzlich zur steigenden Anzahl von im Krankenhaus erworbenen Infektionen mit Methicillin resistenten *S. aureus* Stämmen (HA-MRSA) häuft sich die Anzahl der MRSA Fälle in der nicht hospitalisierten Bevölkerung (CA-MRSA).

S. aureus besitzt eine einzige Serin/Threonin Proteinkinase. Diese besteht aus einer intrazellulären Kinasedomäne, einer Transmembranhelix und drei extrazellulären penicillin-binding protein and serine/threonine kinase associated (PASTA) Domänen. PknB ist dazu in der Lage sowohl andere Proteine als auch sich selbst *in vitro* zu phosphorylieren. Transkriptom- und Funktionalitätsstudien zeigten, dass *S. aureus* PknB an Regulation der Purin-/Pyrimidin-Synthese, dem Zellwand Metabolismus und zentralen metabolischen Funktionen beteiligt ist. Spezifitätsbestimmungen mittels Micorarrays, bei denen PknB und eukaryotische Peptide verwenden wurden, konnten zeigen, dass es sich bei PknB um eine prolingelenkte Kinase handelt. Die Kristallstruktur der Kinasedomäne von *S. aureus* PknB ($PknB_{SA\text{-}KD}$) wurde im Komplex mit einem nichthydrolysierbaren ATP (Adenosintriphosphat) Analogon bei einer Auflösung von 3.0 Å gelöst. Um die Kristallqualität zu verbessern, wurde $PknB_{SA\text{-}KD}$ mit verschiedenen ATP-Analoga und unterschiedlichen Kristallisationstechniken kristallisiert. Die Struktur wurde mit anderen eukaryotischen und prokaryotischen Serin/Threonin Proteinkinasen verglichen. Ebenso wie das gesamte Protein ist $PknB_{SA\text{-}KD}$ dazu in der Lage sowohl andere Proteine als auch sich selbst zu phosphorylieren. Im Gegensatz zu der aktiven Form der Kinase in Lösung ist die Kinasedomäne in einer inaktiven Konformation kristallisiert.

Das Protein MPRF (multiple peptide resistant factor) ist ein Virulenzfaktor von *S. aureus*. Voraussichtlich besteht es aus einem langen hydrophoben Teil, der 14 Transmembransegmente (TMS) besitzt, und einem hydrophilen C-terminalen Teil. Dieser hydrophile Teil bildet zusammen mit den sechs C-terminalen TMS die Synthase von MprF. Die acht N-terminalen TMS bilden die Flippase. Die Synthase verknüpft Phosphatidylglycerol (PG) mit Lysin zu Lysyl-Phosphatidylglycerol (Lys-PG), das dann von der Flippase in die äußere Schicht der Staphylococcenmembran integriert wird. Dies führt zu einer Änderung der Membranladung und verhindert so die Anlagerung von Defensinen. Die ersten MprF Konstrukte dieser Arbeit bestehen alle aus dem C-terminalen, löslichen Anteil

von MprF, wobei das N-terminale Ende dieser Konstrukte variiert. Zusätzlich zu den verschiedenen N-terminalen Enden wurde auch die Anzahl der TMS variiert. Alle Konstrukte konnten kloniert und exprimiert werden. Die Analyse der Proteine ergab allerdings, dass sie aggregiert sind. Das Hauptaugenmerk lag auf dem Verbindungstück zwischen der letzten TMS und dem löslichen Anteil von MprF. Bereits kleine Veränderungen der Anzahl der Aminosäuren in dieser Region beeinflussten das Verhalten des Proteins merklich. Eine Verlängerung des Proteins durch zusätzliche TMS in N-terminale Richtung verringerte die Löslichkeit.

5 CONTRIBUTION TO PUBLICATIONS

5.1 First author paper

Structural analysis of *Staphylococcus aureus* serine/threonine kinase PknB.

Rakette S, Donat S, Ohlsen K, Stehle T;
PLoS One, 2012, **7**, e39136

Construct design, cloning, purification, crystallization, data collection, structure solving, structural analysis, structure interpretation, surface analysis, crosslinking, figures and text.

5.2 Contributing author papers

Staphylococcal PknB as the first prokaryotic representative of the proline-directed kinases.

Miller M, Donat S, Rakette S, Stehle T, Kouwen TR, Diks SH, Dreisbach A, Reilman E, Gronau K, Becher D, Peppelenbosch MP, van Dijl JM, Ohlsen K.;
PLoS One. 2010 Feb 4;5(2):e9057.

Construct design, cloning and purification of the kinase domain, used for kinome array analysis.

Transcriptome and functional analysis of the eukaryotic-type serine/threonine kinase PknB in *Staphylococcus aureus*.

Donat S, Streker K, Schirmeister T, Rakette S, Stehle T, Liebeke M, Lalk M, Ohlsen K.;
J Bacteriol. 2009 Jul; 191(13):4056-69. Epub 2009 Apr 17.

Construct design, cloning and purification of the kinase domain, used for initial tests.

6 THE SERINE/THREONINE PROTEIN KINASE PKNB

6.1 PknB - Introduction

6.1.1 *Staphylococcus aureus*

The human pathogen *Staphylococcus aureus* (*S. aureus*) was discovered in 1881 by Ogston (Ogston, 1882, 1884). These gram-positive bacteria form grape-like clusters of globular, golden pigmented cells. The typical size of the cocci lies between 0.5 and 1.5 µm (Madigan, 2012). *S. aureus* can produce virulence factors such as coagulase or toxins such as toxic shock syndrome toxin, protein–alpha toxin, enterotoxin A or Panton-Valentine leukocidin (Lowy, 1998; Madigan, 2012). The bacteria mainly colonize the respiratory tract or the skin as part of the natural skin flora. Colonization increases the risk of endogenous infections with *S. aureus* (Edwards et al., 2012). The severity of *S. aureus* infections symptoms can range between mild to life threatening symptoms such as bacteremia, pneumonia, meningitis, osteomyelitis, sepsis and toxic shock syndrome (Aguilar et al., 2010; Bohach et al., 1990; Deftereos et al., 2009; Lowy, 1998).

The mayor public health concern with *S. aureus* infections is their increasing resistance against antibiotics. In the 1940s, the first resistance against penicillin was discovered (reviewed in Otto, 2010). The antibiotic methicillin is a semisynthetic penicillin derivative, insensitive to β-lactamase. The first methicillin-resistant *S. aureus* (MRSA) was discovered shortly after the introduction of methicillin in the early 1960s. Originally, MRSA infections were restricted to hospital-associated infections (HA-MRSA), but the first infections of healthy, non-hospitalized people (community-associated MSRA; CA-MRSA) appeared in the 1990s. In addition to methicillin, several MRSA strains became resistant to additional antibiotics such as erythromycin, tetracycline and ciprofloxacin (Otto, 2010). In 2002, MRSA infections exhibiting a resistance against the glycopeptide antibiotic vancomycin (vancomycin-resistant *Staphylococcus aureus*; VRSA) have been reported (CDC, 2002).

The increasing antibiotic resistances of *S. aureus* represent a severe problem for the therapy of bacterial infections. More and more antibiotics become ineffective, and thus new antibacterial strategies must be developed. It is crucial to understand as much as possible about the processes in the bacterial life cycle to identify new bacterial targets for future antibiotics.

6.1.2 Protein kinases

Reversible phosphorylation is an important mechanism for organisms to regulate molecular processes in response to changes in the environment. The phosphorylation of specific amino acids can change the characteristics of target proteins and influence their activity (Pereira et al., 2011). The reversible process of phosphorylation is regulated by kinases and their antagonists the phosphatases. Protein kinases are transferases using the γ-phosphate of adenosine triphosphate (ATP) to phosphorylate protein residues such as serine, threonine, tyrosine, histidine and aspartic acid.

Among the homologous group of proteins, the eukaryotic protein kinases make up the largest superfamily (Hunter, 1995). They can be divided into the subgroups of serine/threonine kinases and tyrosine kinases. Before the early 1990s, prokaryotic protein phosphorylation was thought to take place only at histidine and aspartic acid residues in signal transduction by two component systems (Bakal and Davies, 2000).

6.1.3 Prokaryotic serine/threonine protein kinases

Phosphorylation of serine, threonine and tyrosine by prokaryotic kinases was first observed in the 1990s (Bakal and Davies, 2000). As these prokaryotic kinases share high homology with eukaryotic serine/threonine kinases in their kinase domain, they have been classified as eukaryotic serine/threonine kinases (STKs) (Pereira et al., 2011). (A detailed description of the conserved structure elements and motifs of eukaryotic serine/threonine kinases is given in chapter 9.1 “Structural features determining the activation of eukaryotic serine/threonine protein kinase.”). The number of STKs in bacteria species differs. While there are 11 STKs known in *Mycobacterium tuberculosis* (*M. tuberculosis*), only one is known in *S. aureus*, the protein kinase B (PknB).

STKs in gram-positive bacteria consists of an intracellular the kinase domain, a transmembrane region and a variable amount of extracellular penicillin-binding protein and serine/threonine kinase associated domains (PASTA) (Fig. 1). The domain structure of *S. aureus* PknB follows this template. The protein contains an intracellular kinase domain, a transmembrane helix and an extracellular part of the protein consisting of three PASTA domains (Fig. 1).

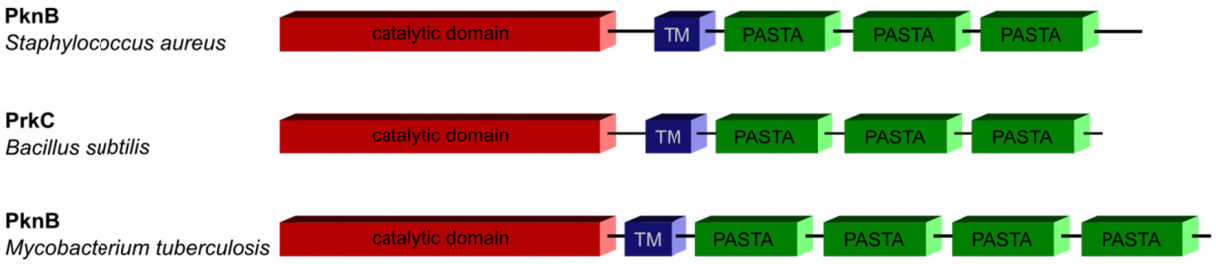

Fig. 1: Schematic representation of the domain structure of bacterial serine/threonine protein kinases. The catalytic kinase domain is shown in red, the transmembrane helix (TM) in blue and the extracellular PASTA domains in green. The figure is adapted from Ohlsen and Donat, 2010 and Yeats et al., 2002.

The physiological roles of STKs are very diverse. STKs were reported to be involved in many bacterial processes such as development, secondary metabolism, cell division, cell wall synthesis, virulence and the central metabolism (Pereira et al., 2011).

6.1.4 The PASTA domain

PASTA domains occur as parts of STKs and of penicillin–binding proteins (PBPs), such as PBP2x of *Streptococcus pneumoniae* (Gordon et al., 2000; Yeats et al., 2002). PBPs are predicted to bind peptidoglycan and to be the contact area of β-lactam antibiotics (Barthe et al., 2010; Yeats et al., 2002).

The number of PASTA subunits differs among STKs between two and five. Schematic views of three kinases important for this work are shown in Fig. 1. In *S. aureus* PknB, the extracellular part is composed of three PASTA domains. Each domain consists of three β-strands and one α-helix. The structure of the PknB PASTA domains was determined by competing groups during this thesis. The structure exhibit a linear extended conformation in contrast to the compact conformation of PBP2x (Paracuellos et al., 2010; Ruggiero et al., 2011). For *S. aureus* PknB, three binding sites for peptidoglycan could be predicted in docking experiments. They are located between subunits A and B, between subunits B and C and at subunit C (Paracuellos et al., 2010).

6.2 PknB - Aims

The aim of this work was the structure analysis of the serine/threonine protein kinase PknB using X-ray crystallography. This kinase shares 37% sequence identity with the well-studied PknB of *M. tuberculosis*. The crystal structure of *M. tuberculosis* PknB is known (Ortiz-Lombardia et al., 2003; Young et al., 2003). For *S. aureus* PknB, no such structure was available. It will provide insights into the differences and similarities of bacterial STKs in different species in comparison to eukaryotic kinases. As *S. aureus* PknB is the only STK in *S. aureus*, it is also a potential drug target. This work is focused on the structure of the kinase domain $PknB_{SA\text{-}KD}$. Besides obtaining the crystal structure, the aim was further to characterize PknB function, possible binding to phosphorylation targets and its activation or inactivation mechanism of this kinase.

6.3 PknB - Results

As the full-length PknB contains multiple domains, presumably flexible linkers and a transmembrane domain, the crystallization of the full-length protein is highly challenging. Therefore it is a more promising strategy to crystallize the domains individually. The PknB domains were predicted by domain searches using the TIGR- and SMART-databases (http://tigr.org and http://smart.embl-heidelberg.de) (Donat et al., 2009). The identified serine/threonine kinase at locus SA1063 showed 37% sequence identity with *M. tuberculosis* PknB, and the name PknB was adapted from this protein. The *S. aureus* PknB kinase domain was predicted to comprise residues 10 to 268 (Donat et al., 2009). The crystal structure of the kinase domain of *M. tuberculosis* PknB has been solved to resolutions of 2.2 and 3.0 Å (Ortiz-Lombardia et al., 2003; Young et al., 2003, respectively). In these structures, the C-terminal end of the kinase domain is visible up to residues 278 (Ortiz-Lombardia et al., 2003) and 286 (Young et al., 2003), respectively. These correspond to residues 272 and 282 in *S. aureus.*

6.3.1 $PknB_{SA\text{-}KD\text{-}short}$

6.3.1.1 Cloning of $PknB_{SA\text{-}KD\text{-}short}$

The first designed construct included *S. aureus* PknB kinase domain residues 1-274 ($PknB_{SA\text{-}KD\text{-}short}$) in pET-28b according to the higher resolution structure of *M. tuberculosis* PknB (Ortiz-Lombardia et al., 2003). The vector contained a kanamycin resistance, a sixfold polyhistidine tag (6xHis-tag), thrombin cleavage site and a second, C-terminal 6xHis-tag. The second 6xHis-tag was not used by including a stop codon directly after the $PknB_{SA\text{-}KD\text{-}short}$ sequence. The primers used were PknBfw and PknB274rev listed in Table 1.

Table 1: Primers for PknB constructs

PknBfw	5'-GGAGCTCCATATGATAGGTAAAATAATAAATGAACG-3'
PknB274rev	5'-CCGCTCGAGCTAATTTTCATGTAAAACACTACTCAAATC-3'
PknB291rev	5'-CCGCTCGAGCTATACCGCTATCGTTTTCATTTTATCG-3'

6.3.1.2 Expression and purification of $PknB_{SA\text{-}KD\text{-}short}$

Expression and purification of the protein was performed according to chapter 9.2 ("Structural analysis of *Staphylococcus aureus* serine/threonine kinase PknB"(Rakette et al., 2012)). The final expression time was determined by expression trials with varying the expression time

and running a sodium dodecyl sulfate polyacrylamide gel electrophoresis (SDS-PAGE) of the soluble supernatant after lysis. An expression time of 24 hours resulted in a visible overexpression on SDS-PAGE. After thrombin digest, the protease usually can be removed by the use of benzamidine columns. In case of PknB this was not possible. PknB binds strongly to the benzamidine column and could only be removed by elution with high concentrations of urea. As no nonspecific cleavage or other problems caused by remaining thrombin occurred and the thrombin represents only a very small percentage of the purified protein, no further purification efforts to remove the thrombin were performed. Selected steps of the purification are shown in Fig. 2. The purification yield was 10 mg of pure protein from a 1 L culture.

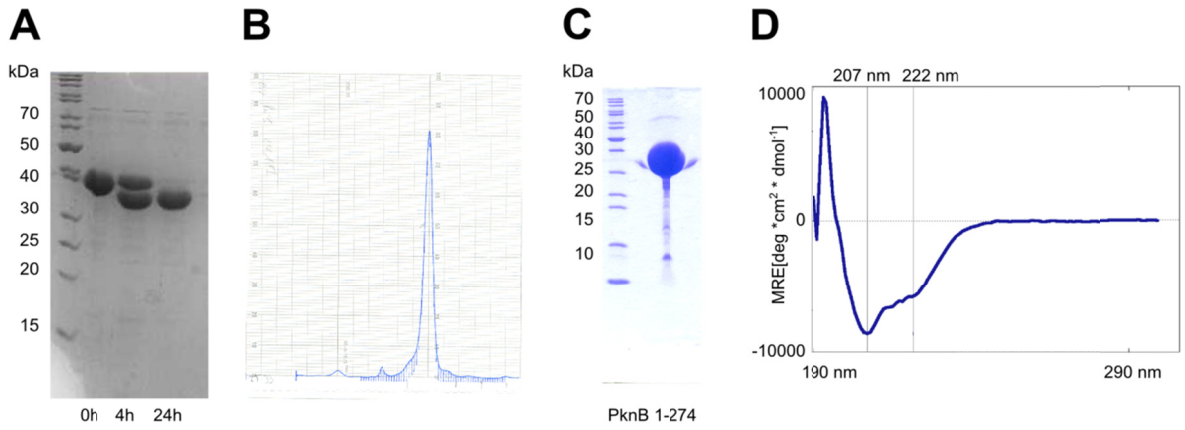

Fig. 2: Purification and characterization steps of $PknB_{SA\text{-}KD\text{-}short}$. **A:** SDS-PAGE of thrombin digests at different time points were loaded. The digest is complete after 24 h. **B:** Superdex75 (SD75) size exclusion run. **C:** SDS-PAGE of the pure, highly concentrated protein. **D:** CD spectrum of the sample.

6.3.1.3 Protein characterization of $PknB_{SA\text{-}KD\text{-}short}$

Bradford assay (Bradford, 1976) was used for concentration measurements of all PknB constructs because the PknB sequence does not contain tryptophan and the UV-absorbance of the other residues is weak. SDS-PAGE was used to analyze the purity and size in all purification steps.

Typically circular dichroism (CD) spectra of α-helices are positive at around 192 nm and negative at 208 and 222 nm. For β-sheets they are negative at 218 nm and positive at 196 nm. CD-spectra of random coil are positive at 212 nm and negative at 198 nm (Ranjbar and Gill, 2009). The spectra were compared to the spectra of known proteins. CD experiments revealed that $PknB_{SA\text{-}KD\text{-}short}$ is folded and suggests the presence of both, α-helices and β-sheets (Fig. 2D).

The purified protein was usually stored at -30 °C. To verify that the protein is not damaged by freezing or thawing procedures, multiple steps of freezing and thawing were performed with one sample. CD-spectra and SDS-PAGEs were used to compare the $PknB_{SA\text{-}KD\text{-}short}$ before, during and after this test. No change in the protein fold and purity was observed also no degradation or unfolding occurred.

6.3.1.4 Crystallization of $PknB_{SA\text{-}KD\text{-}short}$

As the protein was pure, folded and monomeric in gel filtration, crystallization experiments were performed. The protein concentration used was 8 mg/mL. Hanging and sitting drop experiments were performed with commercial screens such as Crystal Screen 1&2 (Hampton Research), JBScreen Wizard 1&2 (Jena Bioscience), PEG/Ion Screen 1&2 (Hampton Research) and Crystal Screen Lite (Hampton Research) both at 4 °C and 20 °C.

Kinases are known to be composed of two flexibly linked lobes, so a useful strategy is to bring the two lobes together and stabilize the protein in a more rigid conformation for crystallization. This can be done, for example, by cocrystallization together with non-hydrolyzable ATP analogs and divalent cations such as magnesium or manganese.

In addition to the protein in the size exclusion chromatography buffer, the ATP analog β,γ-methyleneadenosine 5′-triphosphate (AMP-PCP) and magnesium chloride ($MgCl_2$) were used as additives in the protein solution. Varied concentrations of all compounds, including dithiothreitol (DTT), were tested. Needles, spherulites, precipitation, phase separation and salt crystals could be observed but no threedimensional crystals could be grown (Fig. 3).

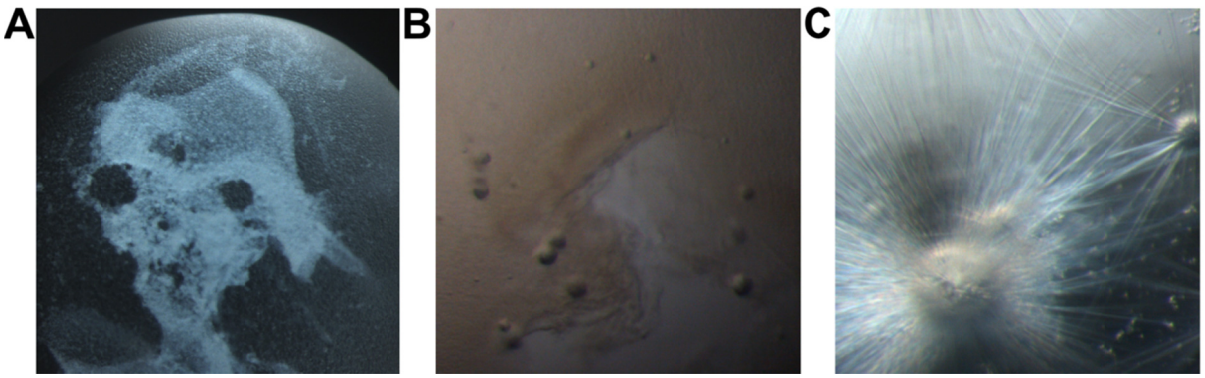

Fig. 3: Crystallization experiments of $PknB_{SA\text{-}KD\text{-}short}$. **A:** Example of precipitated protein. **B:** Spherulites in zinc acetate-containing conditions. **C:** Reproducible needle clusters growing in high citrate conditions after several months.

The needles and spherulites appeared only in conditions containing AMP-PCP and $MgCl_2$. The spherulites appeared in a condition containing zinc acetate, the needles and needle

clusters grew in citrate concentrations of 1.0-1.8 M citrate. The spherulites never diffracted, and the needles were too thin to be measured. Fine screens, additive screens, and seeding techniques did not improve their size.

6.3.2 $PknB_{SA\text{-}KD}$

6.3.2.1 Cloning, expression and purification of $PknB_{SA\text{-}KD}$

The C-terminal end of $PknB_{SA\text{-}KD\text{-}short}$ was first chosen according to the higher resolution structure of *M. tuberculosis* PknB (Ortiz-Lombardia et al., 2003) and the domain prediction of *S. aureus* PknB (Donat et al., 2009). A second construct was designed next, including more C-terminal residues similar to the lower resolution structure of *M. tuberculosis* PknB (Young et al., 2003). *S. aureus* PknB residues 1-291 ($PknB_{SA\text{-}KD}$) were cloned in pET-28b introducing a stop codon after the last residue. Cloning, expression, purification and protein characterization are described in to chapter 9.2 ("Structural analysis of *Staphylococcus aureus* serine/threonine kinase PknB"(Rakette et al., 2012)) (Fig. 4). The primers used were PknBfw and PknB291rev listed in Table 1. In contrast to the $PknB_{SA\text{-}KD\text{-}short}$ construct, the yield of the longer construct in purification was over 100 mg/L LB. The purity of the protein was confirmed by SDS-PAGE, and its identity was verified by mass spectrometry (Andreas Maurer, Kalbacher Laboratory; IFIB, University of Tübingen).

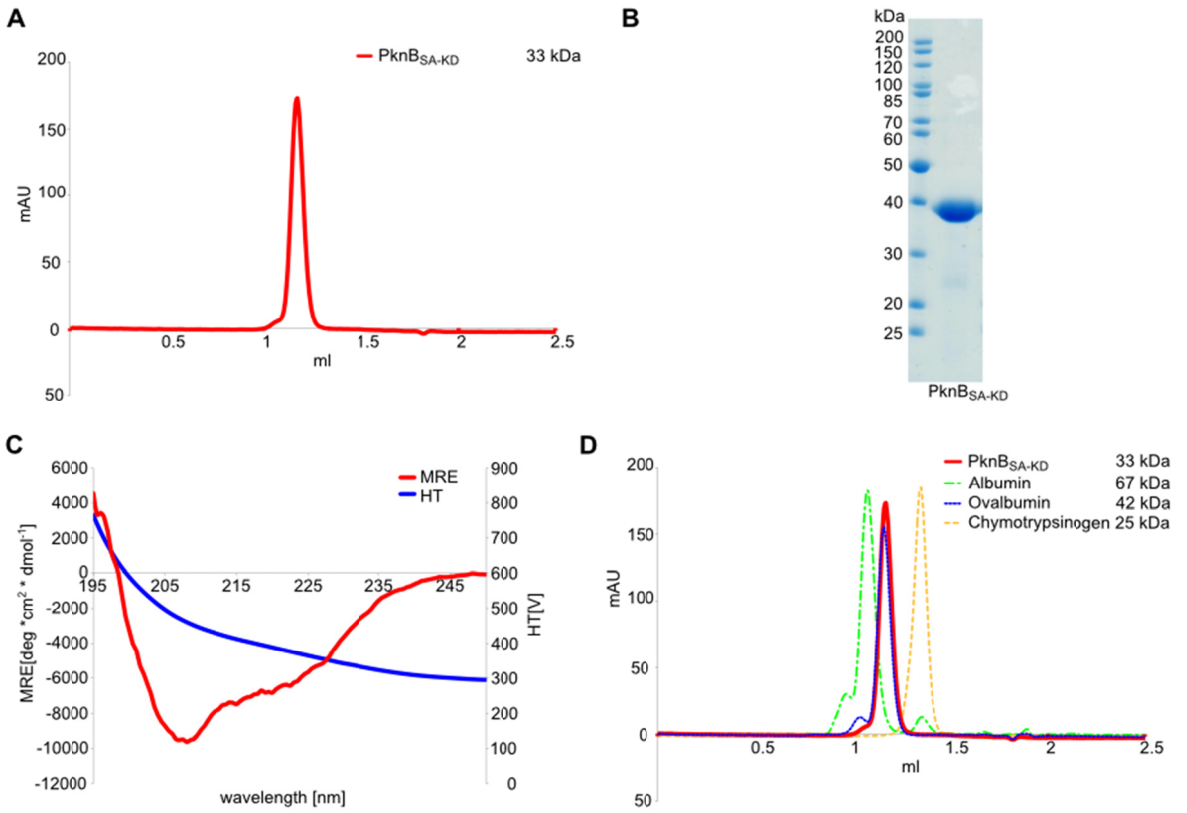

Fig. 4: Purification and analysis of PknB$_{SA-KD}$. **A:** Size exclusion chromatography run of the pure protein. **B:** SDS-PAGE of pure PknB$_{SA-KD}$. **C:** CD spectrum of PknB$_{SA-KD}$. **D:** Size exclusion runs of PknB$_{SA-KD}$ and commercially available proteins for column calibration. This picture is adapted from supplementary Figure 1 in chapter 9.2 ("Structural analysis of *Staphylococcus aureus* serine/threonine kinase PknB"(Rakette et al., 2012))

6.3.3 Crystallization of PknB$_{SA-KD}$

The purified PknB$_{SA-KD}$ eluted from size exclusion was concentrated up to 12 mg/mL. The kinase alone did not crystalize at different temperatures in all commercial screens available in the lab and at different protein concentrations. Cocrystallization with different ATP analogs (Fig. 5) and $MgCl_2$ was therefore carried out next.

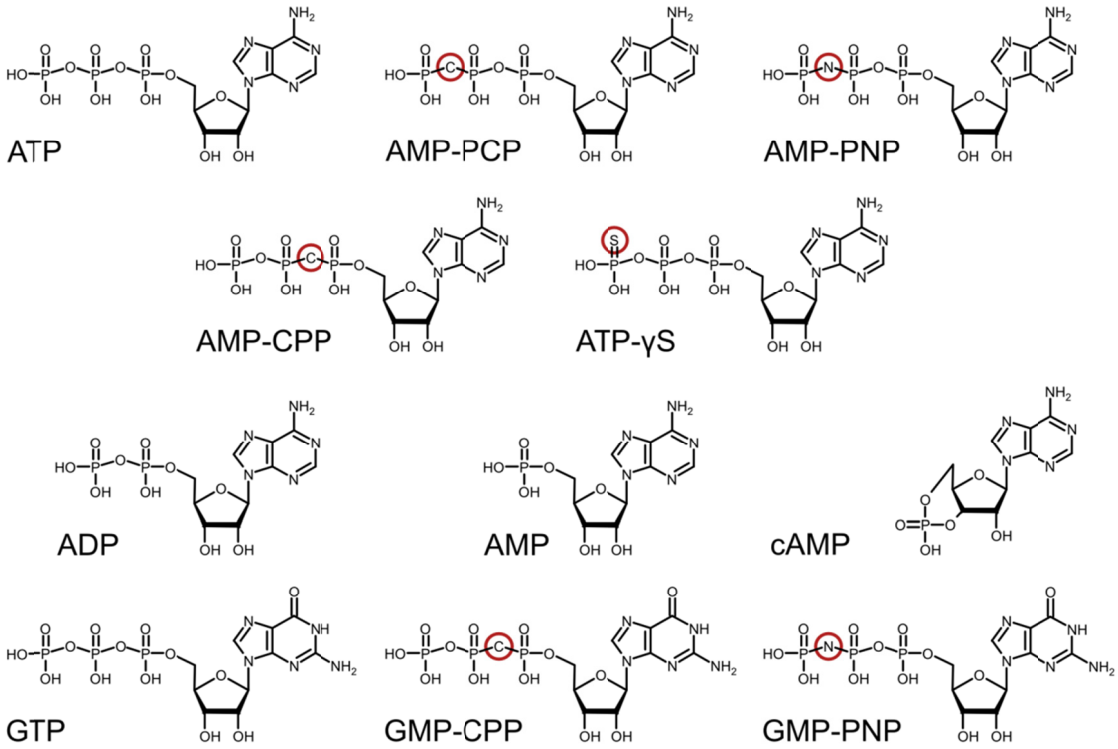

Fig. 5: Nucleotides. The substituted atoms to generate non-hydrolyzable compounds are marked with a red circles

The first ATP analog tested was AMP-PCP, followed by adenosine 5′-(γ-thio)triphosphate (ATP-γS) and finally β,γ-imidoadenosine 5′-triphosphate (AMP-PNP). Similar to $PknB_{SA\text{-}KD\text{-}short}$, reproducible needle-like crystals of $PknB_{SA\text{-}KD}$ grew in the presence of 5 mM AMP-PCP and 5mM $MgCl_2$ at 20 °C in both hanging and sitting drops in 100 mM 4-(2-hydroxyethyl)-1-piperazineethanesulfonic acid (HEPES) pH 7.5 and 1.4 M citrate after several weeks (Fig. 6A). As these needles were too thin to be measured, the Additive Screen (Hampton Research) was used to refine the crystals. After switching from HEPES to a 2-(*N*-morpholino)ethanesulfonic acid (MES) buffer, the first threedimensional crystals appeared in the presence of 4% (w/v) benzamidine hydrochloride (Fig. 6B). These crystals were improved in several fine screens that varied the temperature, pH of the MES buffer and the concentration of citrate, $MgCl_2$, DTT, AMP-PNP and $PknB_{SA\text{-}KD}$ (Fig. 6C). The fine screens were created with the screen-maker and pipetted in a sitting drop setup by the Tecan Freedom EVO. The screen-maker is a collection of Microsoft Excel spreadsheets for customized fine screen design. It complements the robot software and provides additional features such as volume calculations for different viscosities and checks if the screen can technically be pipetted.

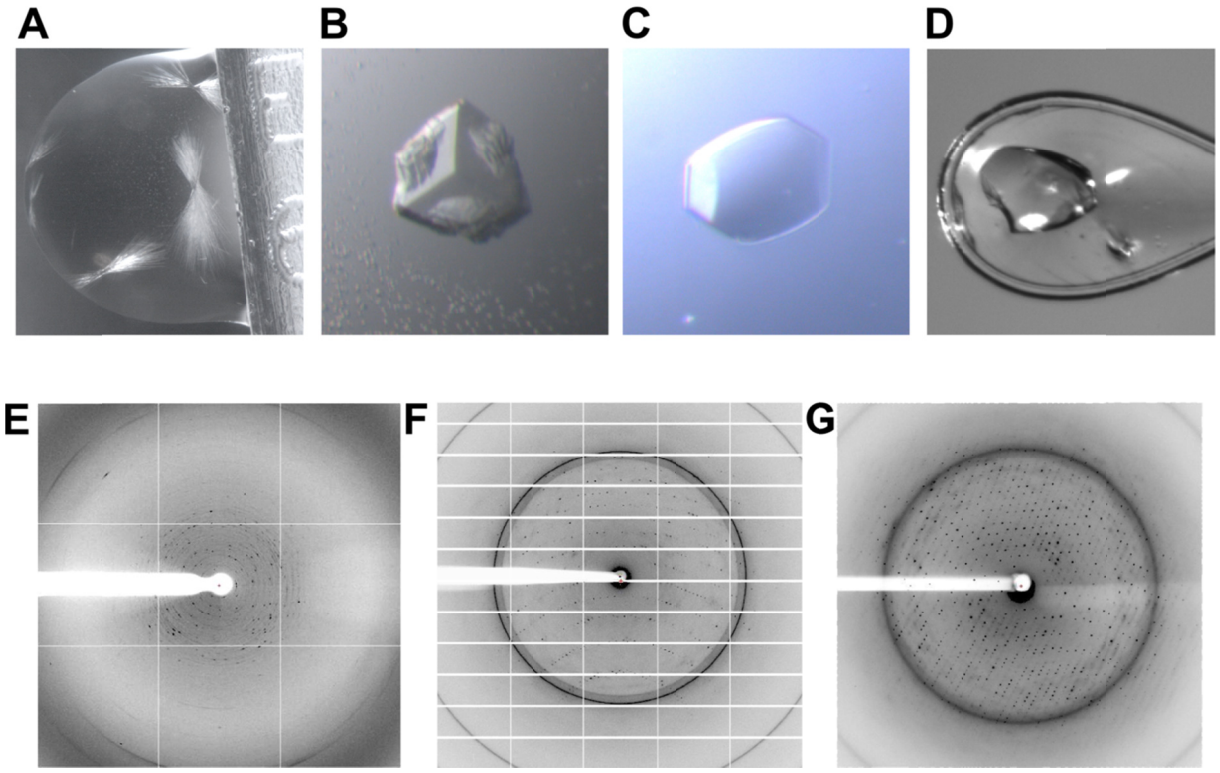

Fig. 6: Crystallization of $PknB_{SA-KD}$. **A:** Needle clusters in conditions of 1.5 M citrate. **B:** Threedimensional, but poorly diffracting crystal in the benzamidine condition of Additive Screen (Hampton Research). **C:** Typical shape of final refined crystals. **D:** Crystal frozen in a loop. **E:** Diffraction pattern of a poorly diffracting crystal (such as shown in pattern B) measured at the ESRF. **F/G:** Diffraction pattern of refined crystals (such as shown in patterns C or D) measured for example at the SLS PX1 or at home source, respectively.

Several other techniques were used to improve crystal quality, such as seeding crystals, varying the temperature, and performing additional additive screens.

It was also tried to obtain co-crystals of $PknB_{SA-KD}$ with target peptides by cocrystallization as well as soaking. Peptides of the substrates of $PknB_{SA-KD}$ (Miller et al., 2010) were used to screen, but no crystals were obtained. Soaking of $PknB_{SA-KD}$ crystals with these peptides likewise was not successful.

The crystals were flash frozen in liquid nitrogen. As the citrate concentration was high enough to be a cryoprotectant by itself, no additional cryoprotectant was necessary. (Fig. 6D). The crystals diffracted to ~ 3.4- 3.2 Å, only a few diffracted better than 3.0 Å. The measurements took place at beam lines PXI-III at SLS, Villigen, Switzerland; MX-14 at BESSY, Berlin, Germany; ID 14.4 and ID 14.1 at the ESRF, Grenoble, France (Fig. 6E-G). The crystal that gave the highest resolution dataset was grown using 8 mg/mL $PknB_{SA-KD}$ in 20 mM HEPES pH 7.5, 100 mM NaCl, 5mM $MgCl_2$, 4 mM AMP-PNP, 2% (w/v) benzamidine hydrochloride, 1 mM DTT. The setup was a sitting drop crystallization experiment at 4 °C

using a crystallization solution of 80 mM MES pH 6.0, 1.3 M sodium citrate (pH 7.0), 2% (w/v) benzamidine hydrochloride and 60 mM $MgCl_2$.

The structure of these crystals and their structural analysis are described in chapter 9.2 ("Structural analysis of *Staphylococcus aureus* serine/threonine kinase PknB"(Rakette et al., 2012) and summarized in chapter 6.3.4.

6.3.4 Structural analysis of *S. aureus* serine/threonine kinase PknB

This chapter is a summary of chapter 9.2:

Structural analysis of *Staphylococcus aureus* serine/threonine kinase PknB

Rakette S, Donat S, Ohlsen K, Stehle T

PLoS One, 2012, **7**, e39136

This work focuses on the crystal structure of the *S. aureus* PknB kinase domain ($PknB_{SA\text{-}KD}$). The structure was compared with structures of eukaryotic serine/threonine kinases and *M. tuberculosis* PknB to analyze the functional details of the kinase.

The $PknB_{SA\text{-}KD}$ was shown to be active in solution. This was established by an activity test. $PknB_{SA\text{-}KD}$ was incubated with γ^{33}-ATP, $MnCl_2$, $MgCl_2$ and myelin basic protein (MBP). After one-dimensional gel electrophoresis, the protein was visualized by autoradiography. The $PknB_{SA\text{-}KD}$ was able to phosphorylate MBP and also performed autophosphorylation.

The crystal structure of $PknB_{SA\text{-}KD}$ was determined at a resolution of 3.0 Å. It was cocrystallized with the ATP analog AMP-PNP and benzamidine. The overall structure is a typical serine/threonine kinase fold. The AMP-PNP is bound in the cleft between the N- and C-lobes , and the kinase is in a closed conformation. The γ-phosphate of AMP-PNP is not visible in the electron density. Residues at both termini and parts of the activation segment are also not present in the electron density. The six chains of the asymmetric unit can be divided into two groups. One group is represented by chains A, B and C, the second group by chains D, E and F. The members of each group are linked *via* non-crystallographic symmetry (NCS) to each other. The two groups differ in the orientation of some loops, crystal contacts and the presence or absence of benzamidine. This ligand is bound only to chains A, B and C. The main-chain B-factor plot shows a lower B-factor for the secondary structure elements and a very high B-factor for loops. The high overall B-factor is a result of the flexible loops, and this flexibility is likely enhanced by inhomogeneous phosphorylation states of the crystallized $PknB_{SA\text{-}KD}$.

In comparison with other serine/threonine kinases in active and inactive states, $PknB_{SA\text{-}KD}$ shows an inactive conformation. The αC-helix in an active conformation of kinases provides a highly conserved salt bridge by a glutamate to a lysine of the β3-strand. This salt bridge is important for the orientation of the phosphates of ATP for enzymatic activity. The αC-helix in

$PknB_{SA-KD}$ is turned away from the phosphate binding site and blocked by an inhibition helix formed by the activation segment direct after the DFG-motif.

Surface conservation analysis with other bacterial serine/threonine revealed highly conserved residues especially at the catalytic important residues. The main part of the surface shows no significant conservation.

For *M. tuberculosis* PknB, a back-to-back dimer formation was observed (Lombana et al., 2010). In $PknB_{SA-KD}$, this dimer was not present in solution as demonstrated by size exclusion chromatography runs and cross-linking experiments. In the crystal structure, a dimer interface similar to the one of *M. tuberculosis* was observed. It is reasonable that this is just a crystallization artifact as this crystal contact only appears between benzamidine binding monomers (chains A, B and C). The benzamidine is bound close to the putative dimer interface. The three other chains (D, E and F) make very different crystal contacts in that area.

$PknB_{SA-KD}$ can only adopt an active conformation when the activation loop changes conformation. The αC-helix can change to an active conformation and form the salt bridge. This could be triggered by phosphorylation in the activation loop, phosphorylation on other parts of the kinase, dimerization or other activation mechanisms.

In conclusion, $PknB_{SA-KD}$ has been crystallized at a resolution of 3.0 Å in an inactive conformation. For an active state of the kinase, several motifs and regions of the kinase have to change their conformation.

6.3.5 Cocrystallization of $PknB_{SA-KD}$ with different nucleotides

The ATP-analog was substituted with all nucleotides shown in Fig. 5, and crystals were set up using the same fine screen for each analog. The crystallization was significantly influenced by changing the ligand. For AMP-PNP most crystals were formed, and the best diffracting crystals were obtained. Fewer crystals grew in the presence of AMP-PCP. Only a few crystals were obtained by cocrystallization together with ATP-γS or α,β-methyleneadenosine 5′-triphosphate (AMP-CPP). ATP, adenosine diphosphat (ADP), adenosine monophosphate (AMP) and cyclic adenosine monophosphate (cAMP) were tested in addition to the non-hydrolyzable ATP analogs. For all these nucleotides a few crystals appeared and could be measured. They showed no improvement over the average AMP-PNP crystals. Conformational changes were not obtained.

The most interesting change could be obtained for cAMP. It is obvious that this is no physiologic relevant ligand and the observed change is just a crystallographic effect. The “tip” of the glycine-rich loop with residues 18-21 was described in to be twisted upwards and away from the phosphates (Rakette et al., 2012). In the crystals containing cAMP, the glycine-rich loop faces more downwards in a more usual conformation. The cAMP is more globular and occupies only the adenosine and sugar binding sites, so the glycine-rich loop has more space to move.

To prove the substrate specificity of $PknB_{SA-KD}$ in the crystallization process, guanosine based nucleotides were used in the same crystallization screen as for the different adenosine based ligands. As expected, $PknB_{SA-KD}$ is specific to adenosine based nucleotides as no crystals were obtained with the guanosine analog.

6.3.6 Influence of ions

$PknB_{SA-KD}$ was shown to be magnesium and manganese dependent (Debarbouille et al., 2009; Donat et al., 2009). $PknB_{SA-KD}$ was crystallized in the presence of magnesium (Rakette et al., 2012). No magnesium ions are visible in the electron density and several residues known to stabilize magnesium in active kinases are not in position. For example, the Lys39-Glu58 salt bridge is not present and Glu58 is not able to stabilize Lys39 for magnesium binding. The electron density for this side chain is very weak and its B-factor indicates high flexibility.

Another fact indicating that no magnesium is bound in the $PknB_{SA-KD}$ structure is that the crystals could also be reproduced without magnesium. The crystal finally chosen for the structure determination just grew in a magnesium containing condition by chance. The *in vitro* activity test performed by S. Donat 2010 (Donat et al., 2009) resulted in the highest activity within a mixture of $MgCl_2$ and $MnCl_2$ in a 1:1 ratio.

6.3.6.1 Influence of cations on $PknB_{SA-KD}$ properties in solution and crystallization

Analytic size exclusion runs were performed. 3 mM $MgCl_2$ or 3 mM $MnCl_2$ were added to $PknB_{SA-KD}$ and incubated at 4 °C for up to 5 days.

The size exclusion run of the sample with $MgCl_2$ resulted in a monomeric peak of $PknB_{SA-KD}$ (Fig. 7). The $MnCl_2$ sample gradually dimerized and finally aggregated. After 5 days, about one third of the protein was aggregated. The crystallization time of $PknB_{SA-KD}$ is several days or weeks, so that crystallization in the presence of $MnCl_2$ may compete with unspecific aggregation processes.

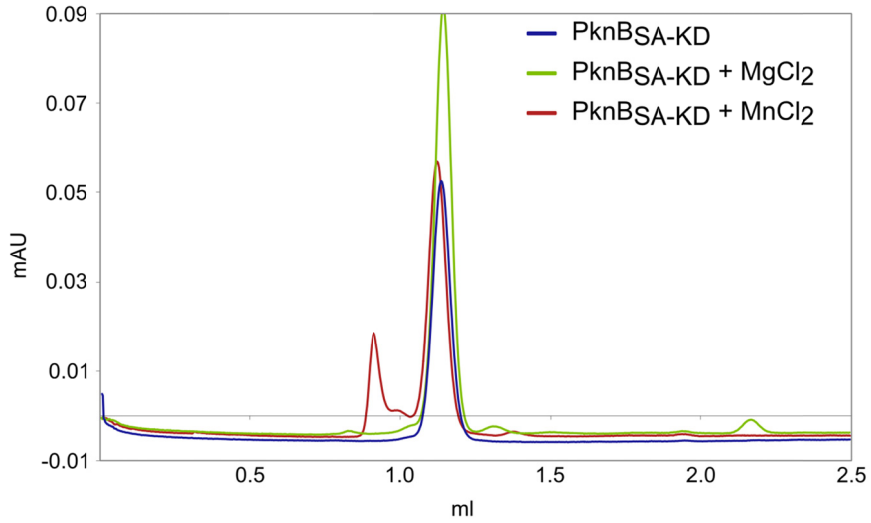

Fig. 7: Influence of ions on multimeric state of $PknB_{SA-KD}$ in analytical size exclusion runs. In presence of $MnCl_2$, $PknB_{SA-KD}$ shows an aggregate peak in the void volume of the column after five days.

Crystallization experiments were performed in conditions containing different concentrations of Mg^{2+}, Mn^{2+} or Ca^{2+} as well as mixtures of Mg^{2+}/Mn^{2+}. No crystals appeared in conditions with calcium. Manganese and manganese/magnesium best conditions resulted in few crystals, but no improvement of the crystals, diffracting to 3.5Å. Crystal packing, space group, electron

density and model are not different from the final $PknB_{SA-KD}$ structure. Even in absence of divalent cations, $PknB_{SA-KD}$ crystallized in complex with AMP-PNP.

6.3.7 Full-length PknB

The full-length PknB was overexpressed and purified *via* nickel affinity chromatography by (Donat et al., 2009). One further attempt was the crystallization of the full-length protein. The success probability is very low due to the multi domain structure of the protein. The structure of the 70 residues between the kinase domain and the transmembrane helix is not known. A full-length structure would show the orientation of $PknB_{SA-KD}$ with respect to the transmembrane domain and the positioning of the linker residues. This would help to understand the external triggered dimerization process.

Full-length PknB was cloned into pET-28b including the N-terminal 6xHis-Tag (this construct was provided by Stefanie Donat (Ohlsen Laboratory, IMIB, University of Würzburg)).

The protein was expressed and purified according to the purification of $PknB_{SA-KD}$. The protein was soluble, but the purity was not sufficient for crystallization as for $PknB_{SA-KD}$.

6.3.7.1 Tryptic digest

This test was performed to determine whether the protein was folded. Moreover, the more resistant the protein is against trypsin, the higher the chance of crystallization due to the lack of exposed flexible loops or linker regions. The purified protein was incubated with trypsin in a 1:1000 ratio in solution or on a nickel-nitrilotriacetic acid agarose (Ni^{2+}-NTA) column overnight. The reaction was stopped by addition of 4x SDS-PAGE sample buffer and heating at 95 °C for 5 minutes. The samples were analyzed by SDS-PAGE (Fig. 8).

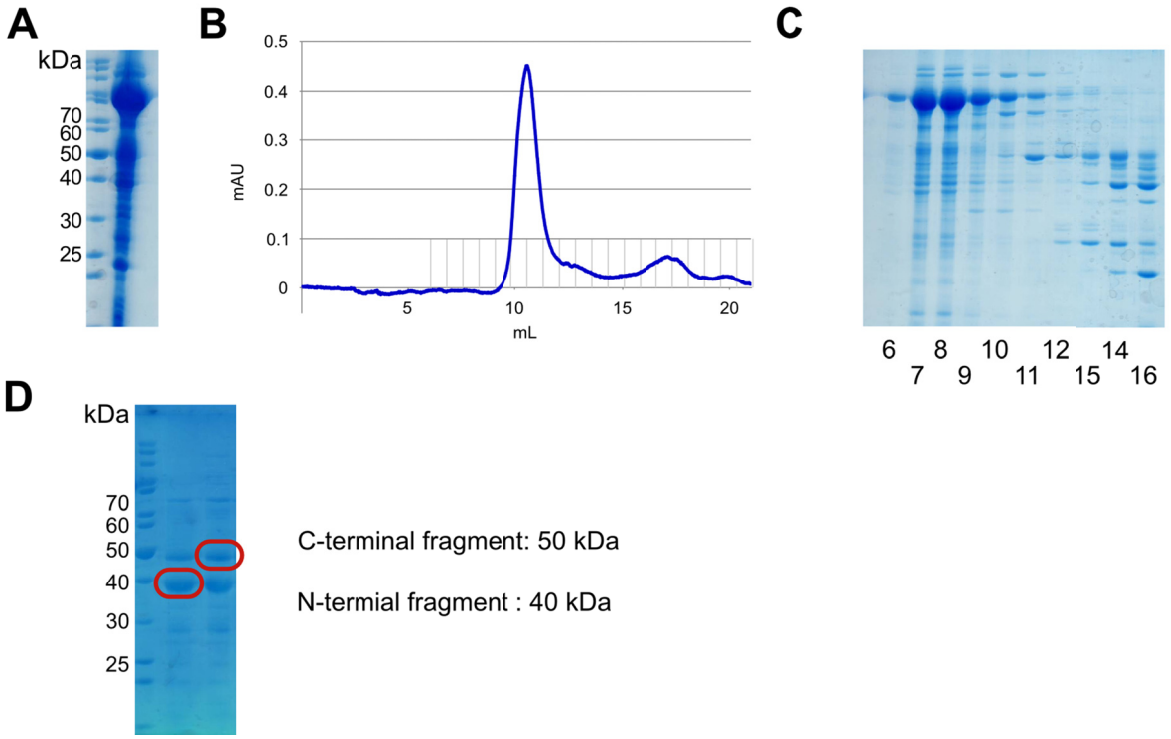

Fig. 8: Full-length PknB. **A:** Pooled protein before size exclusion chromatography run. **B:** Size exclusion chromatography run (Superdex 200; SD200). **C:** Fractions eluted from SD200. **D:** Full-length PknB treated with trypsin on Ni^{2+}-column overnight, bands marked red were analyzed by mass spectrometry.

Full-length PknB is judged to be folded. Only two prominent fragments appeared on SDS-PAGE, one at 40 kDa and one at 50 kDa. The two fragments are quite stable against trypsin, indicating that these domains are both folded proteins (Fig. 8).

To verify the identity of the full-length protein and the digested fragments, SDS-PAGE bands were analyzed by mass spectrometry (Andreas Maurer, Kalbacher Laboratory; IFIB, University of Tübingen), verifying its identity. The 40 kDa fragment contained the N-terminal kinase domain and parts of the linker to the transmembrane region. The 50 kDa fragment was identified to be part of the C-terminus of the protein; it included the PASTA domain, the transmembrane domain and some residues of the linker region.

6.3.7.2 Crystallization of PknB fragments and full-length protein

The full-length protein and both fragments were crystallized with commercials screens available in the lab. Corresponding to $PknB_{SA\text{-}KD}$, AMP-PNP and $MgCl_2$ were added to the protein solution of the full-length protein and the 40 kDa fragment before crystallization. In addition the proteins were crystallized without an ATP analog. The 40 kDa fragment could be

crystallized in conditions similar to $PknB_{SA-KD}$ (Rakette et al., 2012), but no further C-terminal residues were observed in the electron density.

The 50 kDa fragment crystallized in 15 % ethanol, 100 mM CHES at pH 10.5. They diffracted very weakly up to 8Å (Fig. 9). Further crystallization tests were stopped when the structure of the PASTA-domains was published (Paracuellos et al., 2010; Ruggiero et al., 2011).

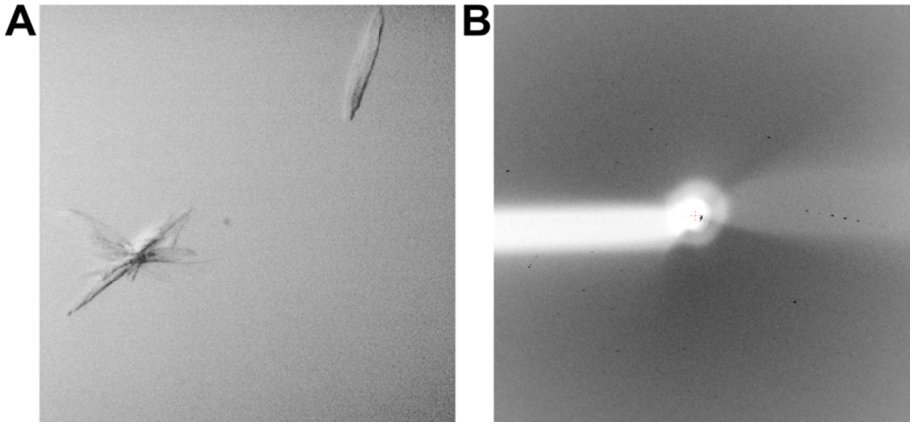

Fig. 9: Crystals of the 50 kDa fragment. A: Crystals in 15 % ethanol, 100 mM CHES at pH 10.5. **B:** Diffraction image from SLS PXIII. The crystal diffracted weakly up to 8Å.

Besides the crystallization of PknB the function of the protein has been analyzed. The role of PknB in *S. aureus* metabolism and the enzymatic function of the protein *in vitro* have been studied in (Donat et al., 2009). A summary of this work is given in chapter 6.3.8 and the full text in chapter 9.3. Additionally, PknB could be detected in the external milieu. Peptide microarrays with human peptides have been performed in (Miller et al., 2010). A summary of this work is given in chapter 6.3.9 and the full text in chapter 9.4.

6.3.8 Transcriptome and functional analysis of the eukaryotic-type serine/threonine kinase PknB in *Staphylococcus aureus*.

This chapter is a summary of the Chapter 9.3:

Transcriptome and functional analysis of the eukaryotic-type serine/threonine kinase PknB in *Staphylococcus aureus*

Donat S, Streker K, Schirmeister T, Rakette S, Stehle T, Liebeke M, Lalk M, Ohlsen K.

J Bacteriol. 2009 Jul;191(13):4056-69. Epub 2009 Apr 17.

In this study, the functional analysis of *S. aureus* PknB was in the main focus. DNA microarray analysis comparing wild-type with a *pknB* deletion mutants were used to identify the processes PknB is involved in. Overexpressed and purified PknB was used for activity tests *in vitro*.

His-tagged PknB was expressed in *E. coli* for testing the phosphorylation activity *in vitro*. The purified protein was incubated with MBP as a surrogate substrate, [γ-^{32}P-]ATP and bivalent cations. The products were visualized after SDS-PAGE by autoradiography. The kinase is able to phosphorylate MBP and perform autophosphorylation. Cations influenced kinase activity. The highest kinase activity was found in the range of 5 to 10 mM for Mg^{2+} or up to 5 mM for Mn^{2+}. At concentrations of 10 mM the kinase was inhibited Mn^{2+}, while Ca^{2+} concentrations had no influence on the activity.

DNA microarray experiments and real-time polymerase chain reaction (RT-PCR) were used to explore the role of PknB in *S. aureus*. The expression of open reading frames (ORFs) in a Δ*pknB* mutant was compared with the 8325 strain. 72 ORFs were repressed, the expression of 185 was increased. The effected genes were involved in nucleotide biosynthesis, cell wall metabolism and central metabolic pathways. Genes encoding for proteins involved in the *de novo* purine and pyrimidine biosynthesis were downregulated (*purK*, *purQ*, *purl*, *purF*, *purM*, *purN*, *purH* and *purD* of purine biosynthesis pathway and *pyrP*, *pyrR*, *pyrB*, *pyrC*, *pyrAA*, *pyrAB*, *pyrF* and *pyrE* of pyrimidine metabolism).

PurA is an adenylosuccinate synthase involved in AMP synthesis. *In vitro* phosphorylation of PurA by PknB resulted in a 1.8 fold decrease of PurA activity. The dependence of the A

nucleotide (AMP, ADP and ATP) concentration on phosphorylation and inhibition of PurA by PknB was proven. The intracellular AMP, ADP and ATP concentrations were higher in the *pknB* mutant than the wild type.

Besides its role in purine biosynthesis, it was shown that PknB also influences autolysis of *S. aureus*. Expression of two regulators of autolysis, *fmtA* and *lytR,* as well as the expression of regulators of the murine hydrolase genes *lrgA* and *lrgB* were induced. Autolysis of the Δ*pknb* mutant and wild type were compared. The percentage of lysed cells after 3.5 h was lower for the Δ*pknb* mutant (58% instead of 86%).

The two-component system VraSR is involved in the β-lactam and glycopeptide resistance of *S. aureus* and plays a role in cell-wall biosynthesis (Kuroda et al., 2003). 9 of the 13 genes of the VraSR system were shown to be upregulated in the Δ*pknb* mutant by microarray experiments. The mutant and the wildtype were tested against several cell-wall active antibiotics. The MraY transferase inhibitor tunicamycin was 32-fold more active for the mutant than the wild type. The MIC (minimum inhibitory concentration) for methicillin in a *pknb*-deletion mutant of the methicillin resistant COL strain was reduced.

RocA and *rocD* encode for proteins involved in the degradation of L- ornithine and L-glutamate. Both genes were induced in the Δ*pknb* mutant. Several genes of the pyruvate metabolism and the citrate cycle were upregulated in the Δ*pknb* mutant.

DNA microarray analysis comparing *pknB* deletion mutants with wild-type strain could identify PknB to be involved in several central metabolic functions such as purine/pyrimidine biosynthesis, cell wall synthesis, glycolysis and the citrate cycle. Comparison of the results with serine/threonine/tyrosine phosphoproteomes of other bacteria showed similarities in modulation of central metabolic functions. The virulence of *S. aureus* was reduced in case of the *pknB* deletion strain in a murine model of kidney infection.

6.3.9 Staphylococcal PknB as the first prokaryotic representative of the proline-directed kinases.

This chapter is a summary of chapter 9.4:

Staphylococcal PknB as the first prokaryotic representative of the proline-directed kinases.

Miller M, Donat S, Rakette S, Stehle T, Kouwen TR, Diks SH, Dreisbach A, Reilman E, Gronau K, Becher D, Peppelenbosch MP, van Dijl JM, Ohlsen K.

PLoS One. 2010 Feb 4;5(2):e9057

Serine/threonine kinases of different bacteria can be secreted by these bacteria directly into the host. Therefore it was investigated weather *S. aureus* PknB can also be found in extracellular media. Additionally, the recognition and phosphorylation of substrates of human serine/threonine kinases by PknB was analyzed. Therefore peptide microarrays and mass spectrometry were used to identify putative target peptide sequences of PknB.

Western blot analysis using polyclonal antibodies against PknB was able to detect full-length PknB in the cell and the growth medium of *S. aureus* NCTC 8325. In comparison, it could not be detected in cellular or growth medium of a Δpknb mutant. The exact way in which PknB is released into the extracellular medium is not known. If the protein was released by cell lysis, the cytoplasmic marker thioredoxin A (TrxA) would be detectable in the growth medium. More PknB than TrxA was detected in the medium, which might suggest that PknB is released by a more specific mechanism than lysis. *S. aureus* is primarily an extracellular pathogen, but it could also be found internalized by human host cells (Ahmed et al., 2001; Dziewanowska et al., 1999; Lammers et al., 1999).

Peptide arrays were incubated with purified PknB and [γ-^{33}P]ATP. 68 potential human substrates for PknB were found, 32 of them are involved in signal transduction and cell communication, 13 in gene regulation, three in immune response and recognition, five in transport processes, ten in cell growth, two in cell metabolism, two in stress responses and one in apoptosis.

A peptide from Activating Factor-2 (ATF-2), which belongs to the basic leucine zipper domain (bZIP) DNA–binding protein family, is the peptide phosphorylated best by PknB. This was confirmed *in vitro* by incubation of ATF-2 with PknB and mass spectrometric analysis. Thr73 was phosphorylated by PknB, which is the known phosphorylation site of the human Vaccina-related Kinase 1 (VRK1) (Nezu et al., 1997; Sevilla et al., 2004; Vega et al., 2003).

Bcl-2 interacting protein Bim was also phosphorylated very efficiently by PknB at Thr56. Bim is part of apoptosis regulation and is phosphorylated at Thr56 by JNK kinase *in vivo* (Lei and Davis, 2003; Putcha et al., 2003; Puthalakath and Strasser, 2002).

A sequence logo of the 15% best-phosphorylated peptides was generated. Serine and threonine were found most frequently in the phosphorylated peptides. The presence of proline next to the phosphorylated residue suggested that PknB is related to the proline-directed eukaryotic kinases. Members of this family are cyclin-dependent protein kinases (CDKs), mitogen-activated protein kinases (MAP kinases) and glycogen synthase kinase-3 (GSK-3). These kinases are involved in cell cycle, regulation, transcription and signal transduction processes.

PknB is able to phosphorylate human peptides such as ATF-2 in vitro. The preference of PknB to phosphorylate next to proline residues was shown by comparing the phosphorylated peptides. Thus PknB can be classified as a proline-directed kinase such as eukaryotic MAP kinases.

6.4 Discussion PknB

The crystal structure of the intracellular kinase domain of PknB was solved at a resolution of 3.0 Å. Most of the discussion concerning the possible activation mechanism, including dimer formation of $PknB_{SA\text{-}KD}$, is described in (Rakette et al., 2012). While the crystal structures of the extracellular PASTA domains have been solved by (Paracuellos et al., 2010; Ruggiero et al., 2011), the transmembrane domain and its linker to the kinase domain are still structurally unknown. This missing part is about 70 amino acids in length. Structural information of this segment would provide insights into the threedimensional orientation of the kinase with respect to the membrane. This orientation can become important for activation of the kinase as it influences the presumed dimer formation. Crystallization of the full-length kinase is challenging due to many flexible regions. Another method such as small angle X-ray scattering (SAXS) could provide insights into the overall conformation of PknB. All methods will have to tackle the problem of the flexibility between PknB domains.

Further approaches to structurally characterize PknB could be either a complex of the kinase domain together with substrate or of the PASTA domains in complex with the ligand. The approach for crystallizing $PknB_{SA\text{-}KD}$ in complex with peptides failed. The crystallized $PknB_{SA\text{-}KD}$ was in an inactive conformation, which likely abolished binding of the peptide in this conformation. Therefore a crystal structure of an active state could provide additional useful insights into PknB function. As the $PknB_{SA\text{-}KD}$ used for activity test and crystallization is known to contain a mixture of different phosphorylation states, the kinase should be in a homogenous state for all further experiments. This could either be done with the purified $PknB_{SA\text{-}KD}$ by incubation with phosphatases such as shrimp alkaline phosphatase (SAP), by changing the construct or by changing the expression conditions of $PknB_{SA\text{-}KD}$. The $PknB_{SA\text{-}KD}$ was expressed for 24 hours. During this long expression time, $PknB_{SA\text{-}KD}$ can be phosphorylated by *E. coli* kinases or/and autophosphorylation by active $PknB_{SA\text{-}KD}$. Expression times of only a few hours should be tested. The yield of purified $PknB_{SA\text{-}KD}$ after 24 hours expression is very high, so shorter expression may also result in satisfying yields. The phosphorylation state of full-length PknB should also be tested before further experiments. The activation mechanism of PknB is still not known. Dimer formation appears to be a possible trigger for activation of PknB. Crosslinking experiments of $PknB_{SA\text{-}KD}$ did not identify dimers of $PknB_{SA\text{-}KD}$ in solution (Rakette et al., 2012). Therefore, similar experiments with a longer construct or the full-length PknB can be a way to define the oligomeric state of *S. aureus* PknB.

7 THE MULTIPLE PEPTIDE RESISTANT FACTOR – MPRF

7.1 MprF - Introduction

7.1.1 Cationic antimicrobial peptides

Phosphatidylglycerol (PG) and diphosphatidylglycerol (cardiolipin) are typical components of bacterial membranes. Both compounds are negatively charged and are thus contributing to the net negative membrane charge. Cationic antimicrobial peptides (CAMPs) play a role in the defense against microbes by the innate immune system (Hancock and Rozek, 2002). These peptides are 10-50 amino acids in length, and they are often folded into amphipathic structures by forming a cationic and a hydrophobic part (Bowdish et al., 2005). These CAMPs target bacterial membranes by electrostatic interactions. After binding to the bacterial membrane, CAMPs can insert into the membrane bilayer and form transmembrane pores or disrupt the membrane. In addition, the CAMPs can be involved in mechanisms of internal killing such as the activation of bacterial autolysins, and they have immunomodulatory properties (Brogden, 2005; Hancock and Sahl, 2006; Peschel and Sahl, 2006).

In addition to PG, membranes of *S. aureus* and other gram-positive bacteria also contain the modified compound *lysyl*-phosphatidylglycerol (Lys-PG) (Fig. 10). In this compound lysine is covalently linked to the terminal hydroxyl group of glycerol *via* the carboxyl group of the amino acid. This modification changes the net charge of the phospholipid to be positive. The Lys-PG changes the charge of the bacterial membrane and so reduces the affinity of CAMPs to the bacterial cell wall (Ernst and Peschel, 2011).

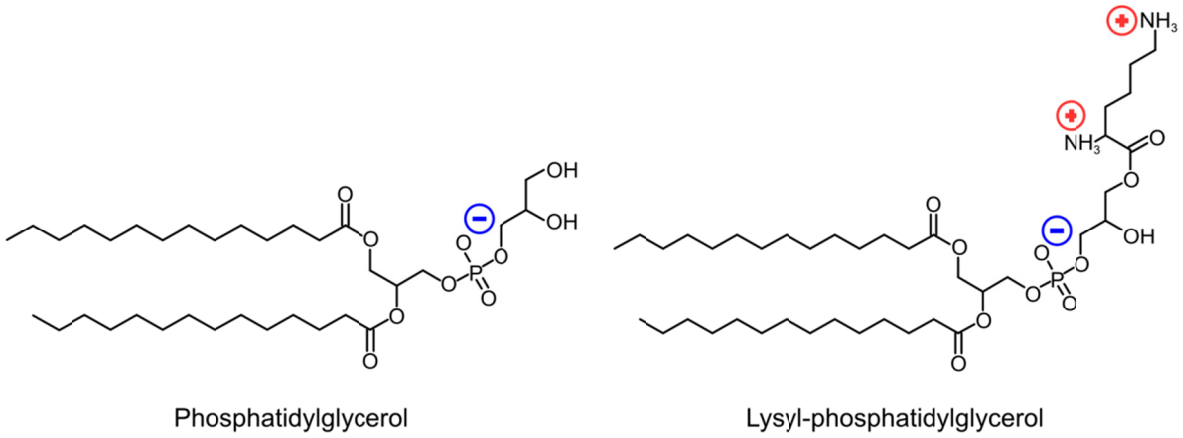

Fig. 10: Phosphatidylglycerol and lysyl-phosphatidylglycerol. Phosphatidylglycerol (left) provides one negative charge; Lys-PG (right) provides a positive net charge. The figure is adapted from Ernst and Peschel, 2011.

7.1.2 Domain structure of MprF

The multiple peptide resistant factor (MprF) was identified to play a crucial role in Lys-PG synthesis (Peschel et al., 2001). Orthologs of MprF can be found in both gram positive and gram negative bacteria (Roy and Ibba, 2008). No structure of MprF or structure of an ortholog of MprF is available. Sequence analysis with the SOSUI program (engine ver.1.11; http://bp.nuap.nagoya-u.ac.jp/sosui/) predicts MprF to consist of a large hydrophobic N-terminal part containing 14 transmembrane segments (TMSs) and a hydrophilic intracellular part at its C-terminus (Fig. 11) (Ernst et al., 2009).

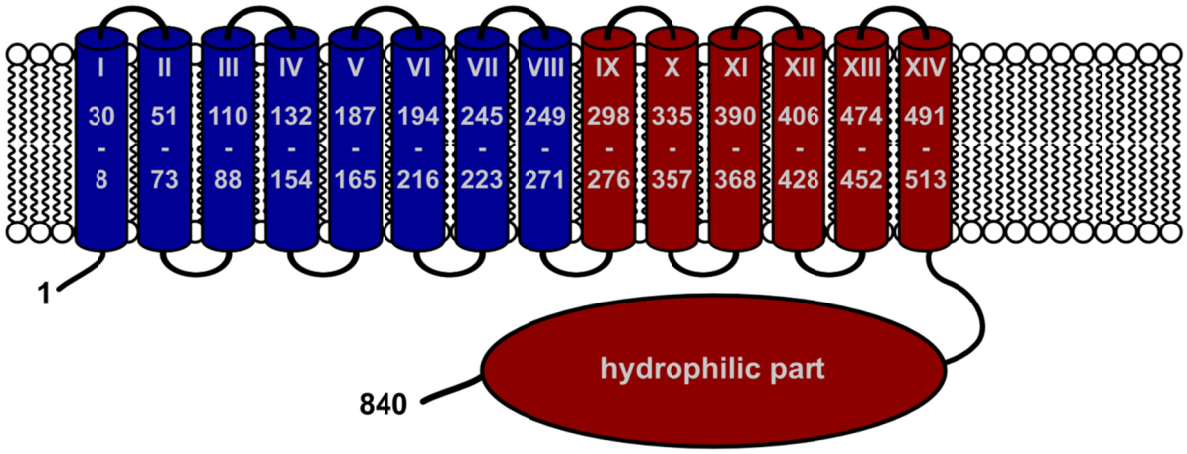

Fig. 11: Domain prediction of MprF. The N-terminal eight TMSs form the flippase domain, whereas the last 6 TMSs plus the soluble intracellular part constitute the synthase of MprF. The figure is adapted from Ernst et al., 2009.

7.1.3 Function of MprF

The enzymatic function of MprF can be described in two steps. The first is the synthesis of Lys-PG by the synthase part of MprF. The synthase adds lysine provided by lys-tRNA to PG. The C-terminal six TMSs and the C-terminal hydrophilic part were necessary for synthase function *in vivo* (Ernst et al., 2009).

The second step in MprF function is the transfer of Lys-PG from the inner to the outer leaflet of the membrane. This flippase activity is harbored by the eight N-terminal TMSs (Ernst and Peschel, 2011). Truncated MprF constructs, lacking these TMSs, were able to produce Lys-PG, but most of the Lys-PG was found in the inner leaflet and the CAMP resistance was lost (Ernst et al., 2009). CAMP resistance could only be observed for the full MprF protein or when both domains were coexpressed as separate proteins (Ernst et al., 2009). The function of MprF is shown schematically in Fig. 12.

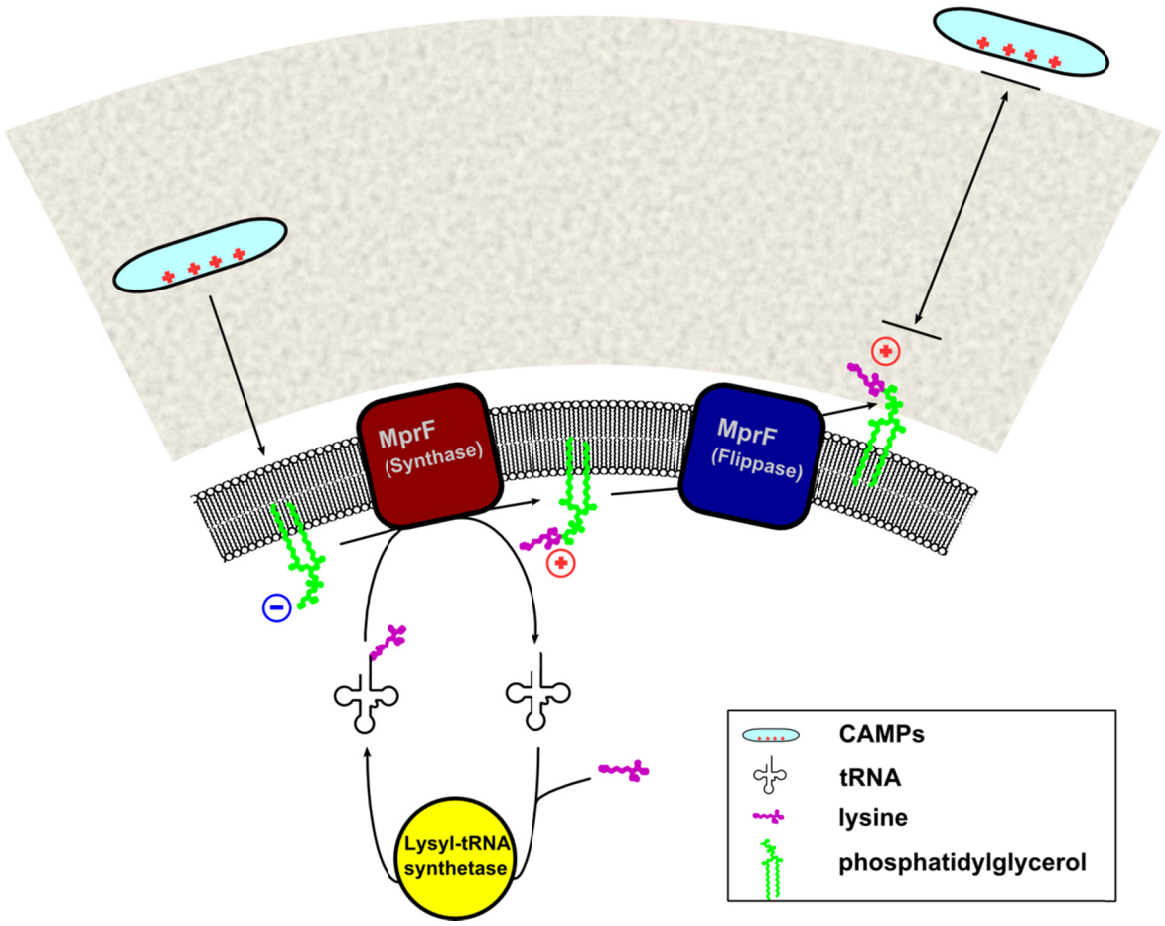

Fig. 12: Schematic overview of MprF function. Lysine provided by lys-tRNA is transferred to phosphatidylglycerol. This Lys-PG is flipped to in the outer PG layer of the bacterial membrane. The resulting net change of the membrane charge inhibits CAMPs from binding to the membrane. The figure is adapted from Ernst et al., 2009.

7.2 MprF - Aims

The aim of this work was to achieve an understanding of the function of *S. aureus* MprF by analyzing its protein structure. No crystal structure of MprF of any organism is available nor are there crystal structures of close homologs. MprF is known to be a membrane protein, so the crystallization of only the soluble part was the dominant strategy and the primary aim of this project. As first step a soluble and homogenous protein part of MprF had to be purified. As MprF is a *S. aureus* virulence factor, it is also a possible drug target as effective inhibition of MprF can help to lower the CAMP resistance of *S. aureus*. The structure of the synthase domain would give helpful insights into understanding *S. aureus* MprF function. An additional, much more challenging approach would be the purification and crystallization of full-length MprF including all TMSs.

7.3 MprF - Materials and Methods

7.3.1 MprF constructs and cloning

S. aureus MprF residues 510-840 cloned in the vector pBAD served as starting point for further constructs. This construct (number 1 in Table 2) was provided by Dirk Kraus (Peschel Laboratory, IMIT, University of Tübingen).

Table 2: List of MprF constructs

	Name	Residues	Vector	Affinity-tag	Cleavage site	Antibiotic
1	510_HIS	510-840	pBAD	6xHis	---	Ampicillin
2	511_GST_T	511-840	pGEX-4T-3	GST	Thrombin	Ampicillin
3	515_GST_T	515-840	pGEX-4T-3	GST	Thrombin	Ampicillin
4	519_GST_T	519-840	pGEX-4T-3	GST	Thrombin	Ampicillin
5	523_GST_T	523-840	pGEX-4T-3	GST	Thrombin	Ampicillin
6	528_GST_T	528-840	pGEX-4T-3	GST	Thrombin	Ampicillin
7	523_GST_P	523-840	pGEX-6P-2	GST	PreScission protease	Ampicillin
8	528_GST_P	528-840	pGEX-6P-2	GST	PreScission protease	Ampicillin
9	528_HIS_T	528-840	pET-28-b	6xHis	Thrombin	Kanamycin
10	642_HIS_T	642-840	pET-28-b	6xHis	Thrombin	Kanamycin
11	MprF-12	437-840	pET-28-b	6xHis	Thrombin	Kanamycin
12	MprF-10	363-840	pET-28-b	6xHis	Thrombin	Kanamycin
13	MprF-8	274-840	pET-28-b	6xHis	Thrombin	Kanamycin

The commercially available vectors used were pET28b, pGEX4T3 and pGEX6P2. The pET28b vector contributes an N-terminal 6xHis-tag with a thrombin cleavage site. The vector additionally encodes a second C-terminal 6xHis-tag. This second tag was eliminated in constructs 9 and 10 with the introduction of a stop codon. Both pGEX vectors contribute an N-terminal gluthatione S-transferase (GST) fusion protein followed by a protease cleavage motif. In case of pGEX4T3, the protease is thrombin, in case of pGEX6T2 it is PreScission protease. The linker region between the protease cleavage site and the multiple cloning sites differs by two residues in length.

The primers used for cloning and the introduced restriction sites are listed in Table 3. Constructs 11-13 were provided by Christoph M. Ernst (Peschel Laboratory; IMIT, University of Tübingen).

Table 3: Primers for MprF constructs

MprF_840_rev	5'-AGTCCGCTCGAGTTATTTGTGACGTATTACACGCATTA-3'
MprF_511_GST_T_fw	5'-ACACGCGGATCCGATTATCAATTTAGCAAAGTA-3'
MprF_515_GST_T_fw	5'-ACACGCGGATCCAGCAAAGTACGTATTTCTTCTA-3'
MprF_519_GST_T_fw	5'-ACACGCGGATCCATTTCTTCTAAAATTGAAGATTG-3'
MprF_523_GST_T_fw	5'-ACACGCGGATCCATTGAAGATTGCGAGG-3'
MprF_528_GST_T_fw	5'-ACACGCGGATCCGAGATTATTAATCAGTACGGC-3'
MprF_523_GST_P_fw	5'-CTAGCTAGCATGATTGAAGATTGCGAGGAGATTATTAATC-3'
MprF_528_GST_P_fw	5'-ACACGCGGATCCGAGATTATTAATCAGTACGGC-3'
MprF_528_HIS_T_fw	5'-ACACGCGGATCCGAGATTATTAATCAGTACGGC-3'
MprF_642_HIS_T_fw	5'-CTAGCTAGCGGATTTAGAGCGACTTTAAATAAATTC-3'

The final plasmids were transformed with the heat-shock method in the *E. coli* strain NovaBlue for plasmid production, and into *E. coli* strain BL21(DE3) for protein expression. The transformed bacteria were grown at 37 °C in Luria Bertani (LB) media containing the vector specific antibiotic in the vector depending concentration. At an optical density (OD) at 600 nm of 0.5, the temperature was lowered to 20 °C and 1 mM isopropyl β-D-1-thiogalactopyranoside (IPTG) was added. The bacteria were harvested by centrifugation after 24 h at 4000 g for 5 min and stored as pellets at -80 °C.

7.3.2 MprF purification

Unless mentioned differently, all steps of protein purification were performed on ice or at 4 °C, and all used buffers were based on HEPES pH 7.4 (listed in Table 4). Bacteria pellets were resuspended in lysis buffer by gentle pipetting and lysed by micro homogenization using an Emulsiflex C3 system. The lysate was cleared by centrifugation at 19,500 g for 45 min and filtration through a 0.45 µm membrane.

The first purification step was affinity chromatography. GST-tagged proteins were loaded on a GST-trap column, washed with lysis buffer and eluted by addition of reduced glutathione. His-tagged proteins were either applied onto immobilized metal ion affinity chromatography (IMAC) columns loaded with nickel. In cases of weak binding, the lysate was directly incubated with Ni^{2+}-NTA beads and gently stirred overnight. Then, a column was packed from the pre-bound resin, which was then used in the same way as the prepacked columns. All IMAC columns were first washed with IMAC buffer A and then eluted with an imidazole gradient from 20 mM up to concentrations of 500 mM imidazole.

Table 4: Buffers used in MprF purification (EDTA: ethylenediaminetetraacetic acid; PMSF: phenylmethanesulfonyl fluoride)

	HEPES buffers pH 7.4		triethanolamine buffers pH 8.5	
Lysis buffer	20 mM	imidazole	20 mM	imidazole
	150 mM	sodium chloride	150 mM	lithium chloride
	20 mM	HEPES	100 mM	triethanolamine
	1 mM	PMSF	0.5 mM	EDTA
			1 mM	PMSF
IMAC buffer A	20 mM	imidazole	20 mM	imidazole
	150 mM	sodium chloride	150 mM	lithium chloride
	20 mM	HEPES	100 mM	triethanolamine
			0.5 mM	EDTA
IMAC buffer B	500 mM	imidazole	500 mM	imidazole
	150 mM	sodium chloride	150 mM	lithium chloride
	20 mM	HEPES	100 mM	triethanolamine
			0.5 mM	EDTA
GST-trap elution buffer	150 mM	sodium chloride		
	20 mM	HEPES		
	10 mM	GSH		
Ion exchange buffer A	20 mM	sodium chloride	20 mM	triethanolamine
	20 mM	HEPES	0.5 mM	EDTA
Ion exchange buffer B	500 mM	sodium chloride	50 mM	lithium chloride
	20 mM	HEPES	20 mM	triethanolamine
			0.5 mM	EDTA
			1 M	sodium chloride
Size exclusion buffer	150 mM	sodium chloride	50 mM	lithium chloride
	20 mM	HEPES	50 mM	triethanolamine
			0.5 mM	EDTA

An optional purification step was ion exchange chromatography (IEX) on quaternary-ammonium-sepharose columns (HiTrap Q). After the columns were loaded in low salt buffers (ion exchange buffer A), the elution was done by using a salt gradient to ion exchange buffer B.

To cleave affinity tags for crystallization, protease digests were either performed in solution by using the manufacturer's suggested protease amount or directly on the affinity column. In case of the digest in solution, the cleaved protein sample was separated from tags and

uncleaved protein by reapplying it to the affinity column and collecting the flowthrough. Protein cleaved on column was eluted with lysis buffer.

The last step of purification was size exclusion chromatography, using either SD75 or SD200 columns. The protein was concentrated using amicron ultra spin concentrators and filtered through 0.22 µm spin filters before size exclusion chromatography. In case of insufficient purity of the sample, several rounds of size exclusion chromatography were performed.

The purity of the protein was monitored by SDS-PAGE. CD-spectroscopy was used to analyze the folding of the protein in solution at room temperature.

7.4 MprF – Results

7.4.1 Constructs without TMSs

7.4.1.1 MprF_510_HIS

The MprF_510_HIS construct was used in this work only for initial expression tests and as template deoxyribonucleic acid (DNA) for other constructs. The expression of the protein was verified by Western blot analysis (data not shown).

7.4.1.2 MprF_511_GST_T

The protein was expressed and purified in a first step by using a GST-trap, shown in Fig. 13.

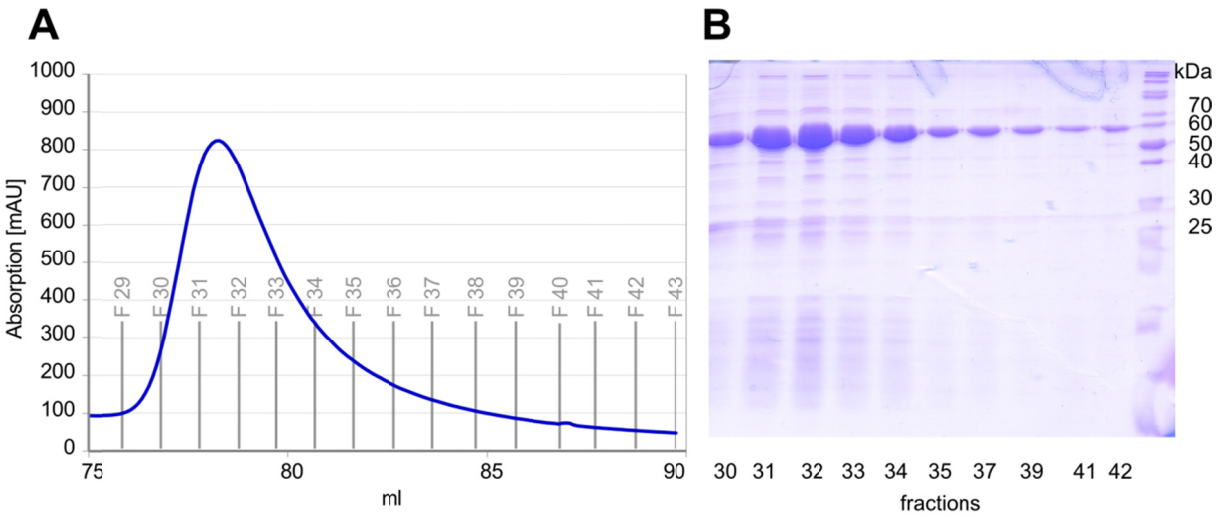

Fig. 13: Purification of MprF_511_GST. A: Elution of MprF_511_GST_T from GST-Trap with GSH containing buffer. **B:** SDS-PAGE of selected elution-peak fractions

Thrombin cleavage of the affinity tag led to partial precipitation of the protein; the cleavage was never complete. Different cleavage conditions were tested, such as the addition of detergents, glycerol, DTT, urea, calcium chloride, change of the pH to higher and lower values or cleavage on column. Some of the approaches are shown in Fig. 14. None of these strategies significantly improved cleavage. In all cases, a mixture of MprF_511_GST, both with and without tag, and GST was obtained.

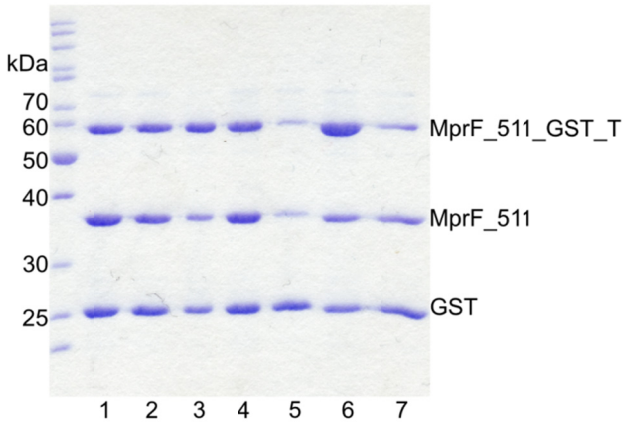

Fig. 14: Different experimental approaches for thrombin digest. The protein was originally in 20 mM HEPES, 150 mM NaCl. 1: + 10 % glycerol; 2: + 50 mM imidazole; 3: reference without additive; 4: + 1 mM DTT; 5: + 1 % Triton X100; 6: + 1 M NaCl; 7: + 90 mM HEPES pH 8.0.

7.4.1.3 MprF_515_GST_T

The first purification step of MprF_515_GST_T *via* GST-trap yielded less protein than MprF_511_GST_T. In addition, the protein was less pure than MprF_511_GST_T. However, the thrombin digest worked better. The protein could be completely cleaved to MprF_515 and GST. Size exclusion chromatography showed a big peak of aggregated protein in the void volume.

To determine whether the protein was partially folded and therefore resistant against proteases, it was incubated either with trypsin (in a 1:1000 ratio) or with chymotrypsin (in a 1:1000 ratio) for several hours. The digest was stopped by the addition of SDS-PAGE sample buffer and heating at 95 °C for 5 min. A second band in the SDS-PAGE below the 515 band appeared after the tryptic digest, Fig. 15.

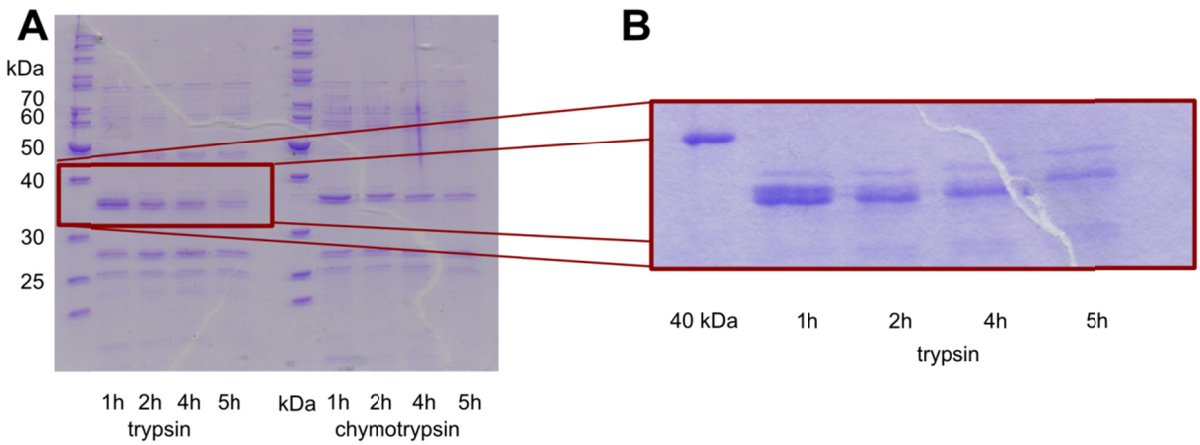

Fig. 15: Tryptic and chymotryptic digest of MprF_515_GST_T. A: Digests with trypsin and chymotrypsin of MprF_515 at different time points. **B:** Closer view of the MprF_515 band. The crack arose from drying the SDS-PAGE onto a filter paper.

As the N-terminal residue of the soluble domain is not exactly known, a possible explanation could be that this size shift was a result of terminal truncation by trypsin. The next constructs were designed by shortening the protein on the N–terminal end at possible trypsin cleavage sites.

7.4.1.4 MprF_519_GST_T, MprF_523_GST_T and MprF_528_GST_T

All three proteins were eluted from GST-trap and digested with thrombin on column overnight. For all three proteins, the thrombin digest failed. Cleavage in solution failed as well. Thrombin cleavages, thrombin cleavages in presence of 50 mM urea and trypsin digests (trypsin in a ratio of 1:1000) have been compared in a further approach. The MprF_528_GST_T construct was stable against trypsin for several hours (Fig. 16).

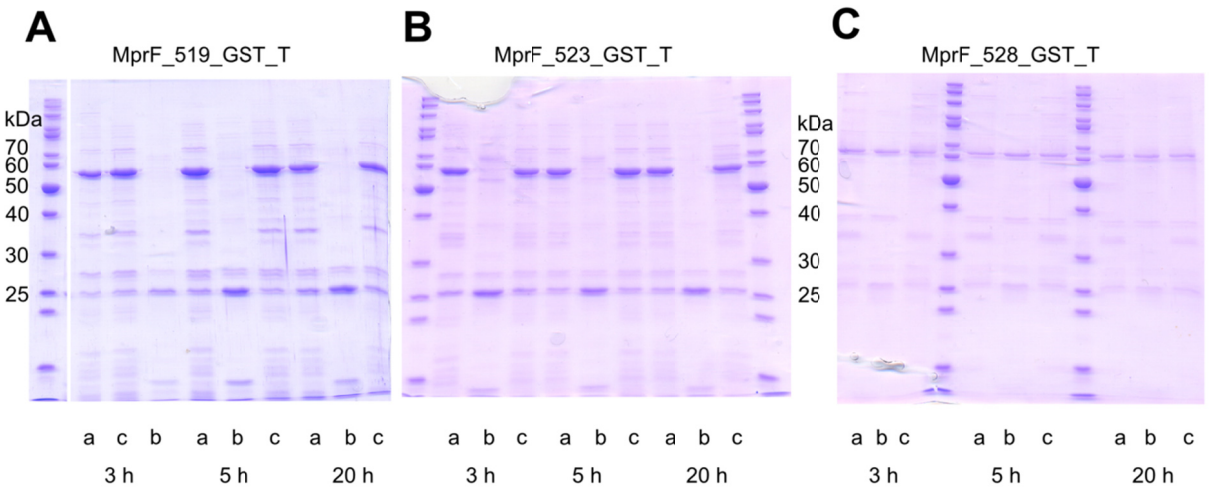

Fig. 16: Digests of MprF_519-GST_T (A), MprF_523_GST_T (B) and MprF_528_GST_T (C). in rows a 50 mM urea and 15 U thrombin were added, in rows b trypsin was added in a 1:1000 ratio, in rows c 15 U of thrombin were added.

Trypsin usually is able to cleave proteins after lysine and arginine residues, thrombin after arginine. So trypsin is able to cleave proteins at the same cleavage site as thrombin. The resistance of MprF_528_GST_T against trypsin shows that the thrombin cleavage site is most likely sterically protected against the proteases because of a short linker sequence between the folded domain and the protease cleavage site (Fig. 17).

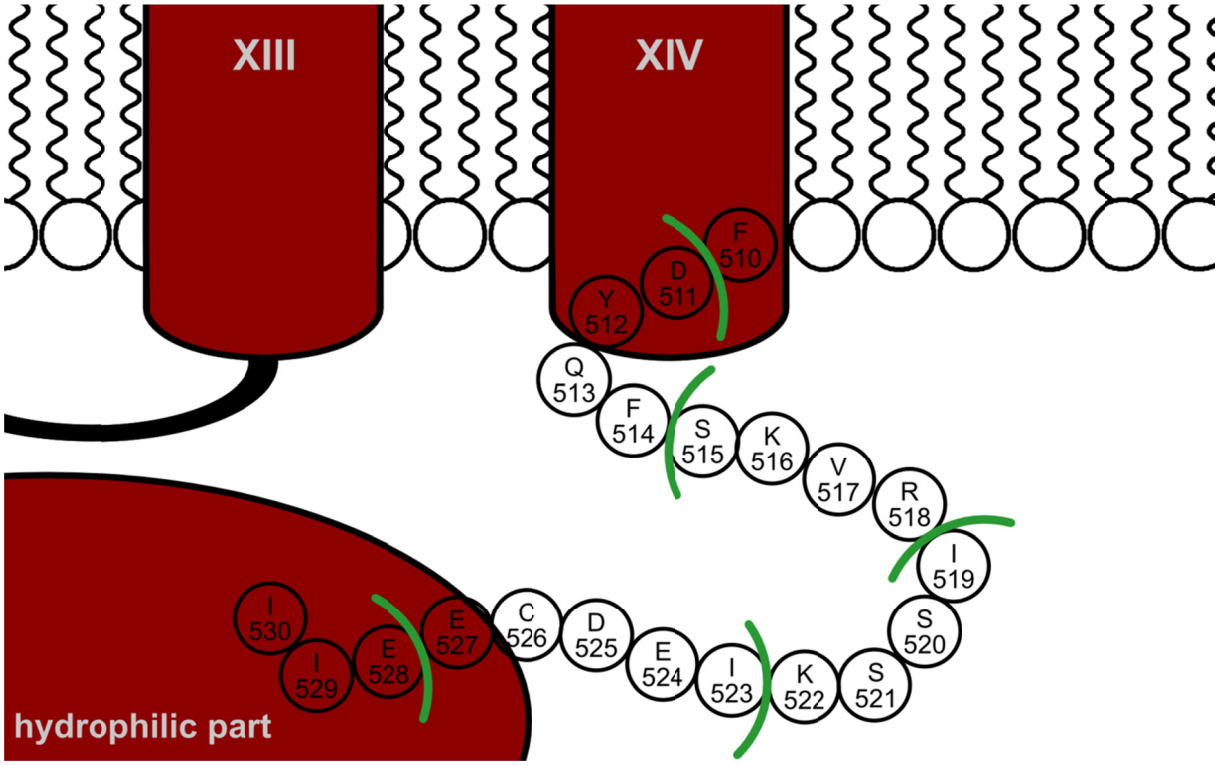

Fig. 17 Linker region between TM14 and the hydrophilic part. This figure is a closer view of Fig. 11. The residues number and sequence of this linker region is in the circles. The green lines indicate the different N-terminal ends of the constructs.

7.4.1.5 MprF_523_GST_P and Mprf_528_GST_P

One strategy to improve cleavage was the change of the protease to PreScission protease. The cleavage site of the vector pGEX_6P2 introduces three more amino acids between the protease site and MprF, making the cleavage site better accessible for the protease. Mprf_523_GST_P could be digested on column overnight. However size exclusion chromatography revealed that MprF_523 aggregates. The cleavage of MprF_528_GST_P was incomplete, and the protein precipitated after cleavage.

7.4.1.6 MprF_528_HIS_T

The MprF_528 construct is stable against trypsin ad therefore seems to be folded. However, the GST-tag is flexible linked to the protein and may prevent crystallization. Thus, the Mprf_528_HIS_T construct was designed. If the 6xHis-tag is not cleavable either, it will have less influence to crystallization than the much larger GST. However the Mprf_528_HIS_T protein was only marginally soluble; denatured purification and refolding were tested. The refolding protocol used was adapted from the protocol "Purifying challenging proteins" (GE Healthcare, 2007). In addition to several refolding efforts, the expression temperature was lowered by using Stratagene Arctic Express *E. coli*. The bacteria are able to express protein at much lower temperatures than *E. coli* Bl21(DE3). Expression tests were performed at 12 °C. Neither refolding nor lower temperature could bring the protein in solution in sufficient amounts. In a new purification approach, the lysis was done in the presence of lysozyme. MprF-528_HIS_T could then be purified *via* Ni^{2+}-affinity chromatography. The fractions 11 and 12 precipitated, fraction 13 was loaded on a SD200 size exclusion chromatography column. The protein eluted in the void volume, indicating again formation of aggregates (Fig. 18).

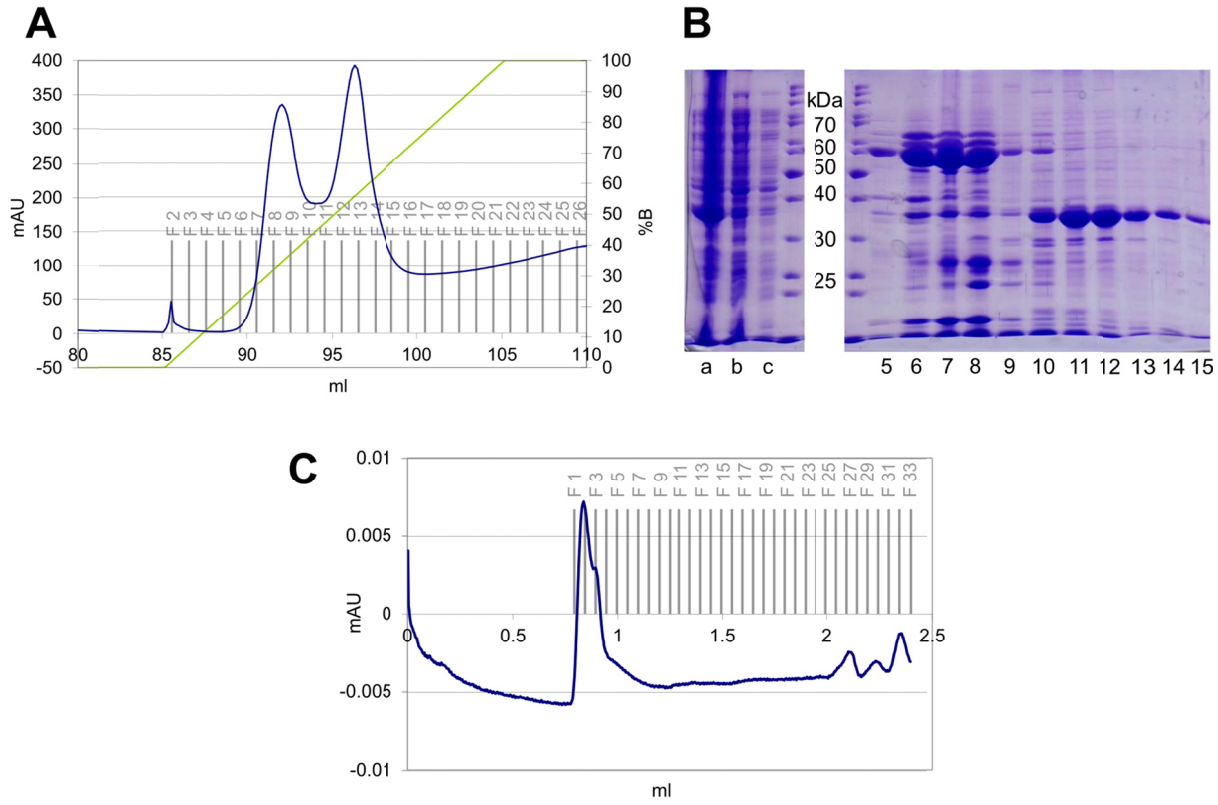

Fig. 18: Purification of Mprf_528_HIS_T. A: Elution of Ni^{2+}-affinity column, UV-absorption is shown in blue, the concentration of buffer B in green. **B:** SDS-Page of fractions 5-15 from A; lane a was the lysate (soluble and insoluble part), b soluble part after lysis, c the flowthrough during loading the Ni-column. **C:** Analytical SD200 size exclusion run of fraction 13 from A.

To identify the influence of the buffer system on MprF_528_HIS_T solubility, a sparse matrix approach to the solubilization of overexpressed proteins was tested (Lindwall et al., 2000). The resuspended bacterial pellet was split into 31 fractions after washing. Each fraction was lysed by sonication in a different buffer and a sample of each was loaded onto SDS-PAGE before and after centrifugation (Fig. 19).

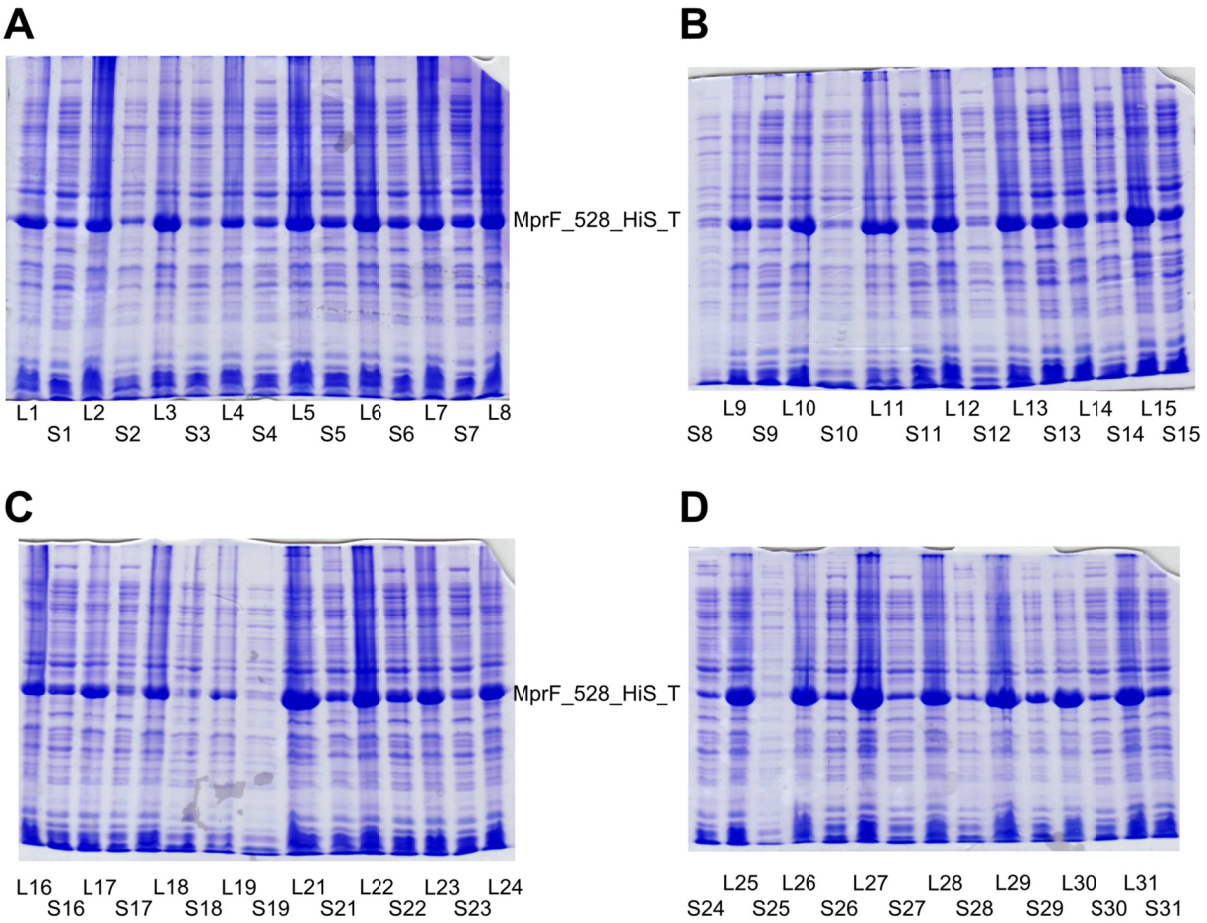

Fig. 19: Solubilitytest of MprF_528_HIS_T. Lanes labeled with L are lysates (soluble and insoluble part), lanes labeled S are soluble supernatants after centrifugation.

The best buffer for solubilization were judged to be buffer 10: 100 mM triethanolamine, 50 mM lithium chloride (LiCl), 5 mM ethylenediaminetetraacetic acid (EDTA) at pH 8.5. For Ni^{2+}-affinitychromatgraphy, the EDTA had to be reduced to 0.5 mM. The protein could be cleaved by thrombin after IMAC (Fig. 20) and was further purified by IEX and size exclusion chromatography. The protein was analyzed by size exclusion chromatography and showed to form aggregates (data not shown).

Purified, but aggregated MprF_528_His_T was used for further trypsin digest approaches. A 22 kDa band appeared in the SDS-PAGE; this band was stable against trypsin (Fig. 20). Mass spectrometry analysis (by Andreas Maurer, Kalbacher Laboratory; IFIB, University of Tübingen) identified it to be MprF residues 642-830.

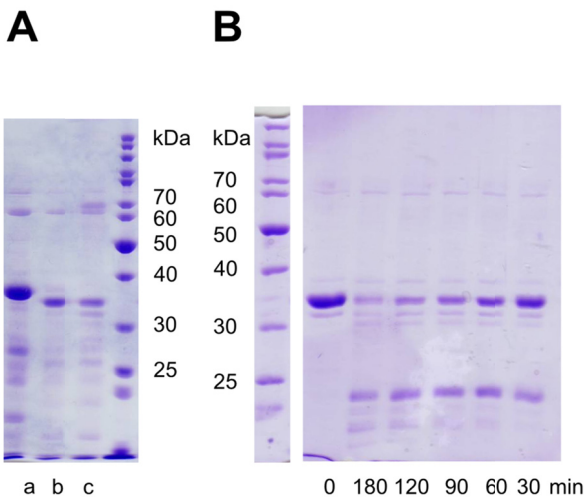

Fig. 20: MprF_528_HIS_T thrombin and trypsin digest. A: Thrombin digest, lane a: without thrombin, b: cleavage at 4 °C, c: cleavage at 20 °C. **B:** Trypsin digest in a 1: 10,000 trypsin to protein ratio.

7.4.1.7 MprF_642_HIS_T

Mprf_642_HIS_T was expressed, lysed, loaded onto a Ni^{2+}-column and cleaved overnight on column with thrombin. After IEX, the protein was applied to a size exclusion column and eluted in the void volume as a mixture together with other impurities of *E. coli* proteins.

As the resulting protein would only be a small part of the soluble part of the synthase, further efforts on this construct were stopped.

7.4.2 Constructs with TMSs

7.4.2.1 Mprf-8, MprF-10 and MprF-12

The step by step shortening of the soluble part of the synthase domain emphasized that this might not be the best way to successfully get purified protein useful for crystallization. Longer constructs containing the synthase domain and up to 6 predicted transmembrane helices were tested. The three designed constructs were MprF-8, Mprf-10 and MprF-12 (Table 2). The number in their names indicates how many N-terminal TMSs are missing in the proteins. MprF-12 contains the intracellular soluble domain and only two TMSs out of 14, for example.

To find a useful lysis buffer, the bacterial pellet was split and washed in buffer systems based on HEPES at pH 7.0 or tris(hydroxymethyl)aminomethane (Tris) at pH 8.0. Both resulting

pellets were fractionated into 10 reaction tubes, each was resuspended in 1 ml buffer plus additive and lysed by sonification. Several detergents and β-mercaptoethanol were tested as additives (Table 5).

Table 5: Lysistest buffer composition for MprF-8, MprF-10, MprF-12

	20 mM HEPES pH 7.0 150 mM NaCl	20 mM Tris pH 8.0 150 mM NaCl
No additive	A	B
5 mM β- mercaptoethanol	A2	B2
1% Tween 80	A3	B3
0.1 % Tween 80	A4	B4
1% Triton X-100	A5	B5
0.1 % Triton X-100	A6	B6
1 mM CHAPS	A7	B7
10 mM CHAPS	A8	B8
1% Tween 20	A9	B9
0.1 % Tween 20	A10	B10

SDS-PAGE samples of the soluble supernatant and the mixture of soluble and insoluble fraction were collected and analyzed. All three constructs could be identified by mass spectrometry to be the correct (Bands analyzed are marked in red in Fig. 21). SDS-PAGE revealed the best expression levels for MprF-12. HEPES buffer with added β–mercaptoethanol (buffer A2 in Table 5) was judged to be the best buffer and was used as a basis for further purification (Fig. 21).

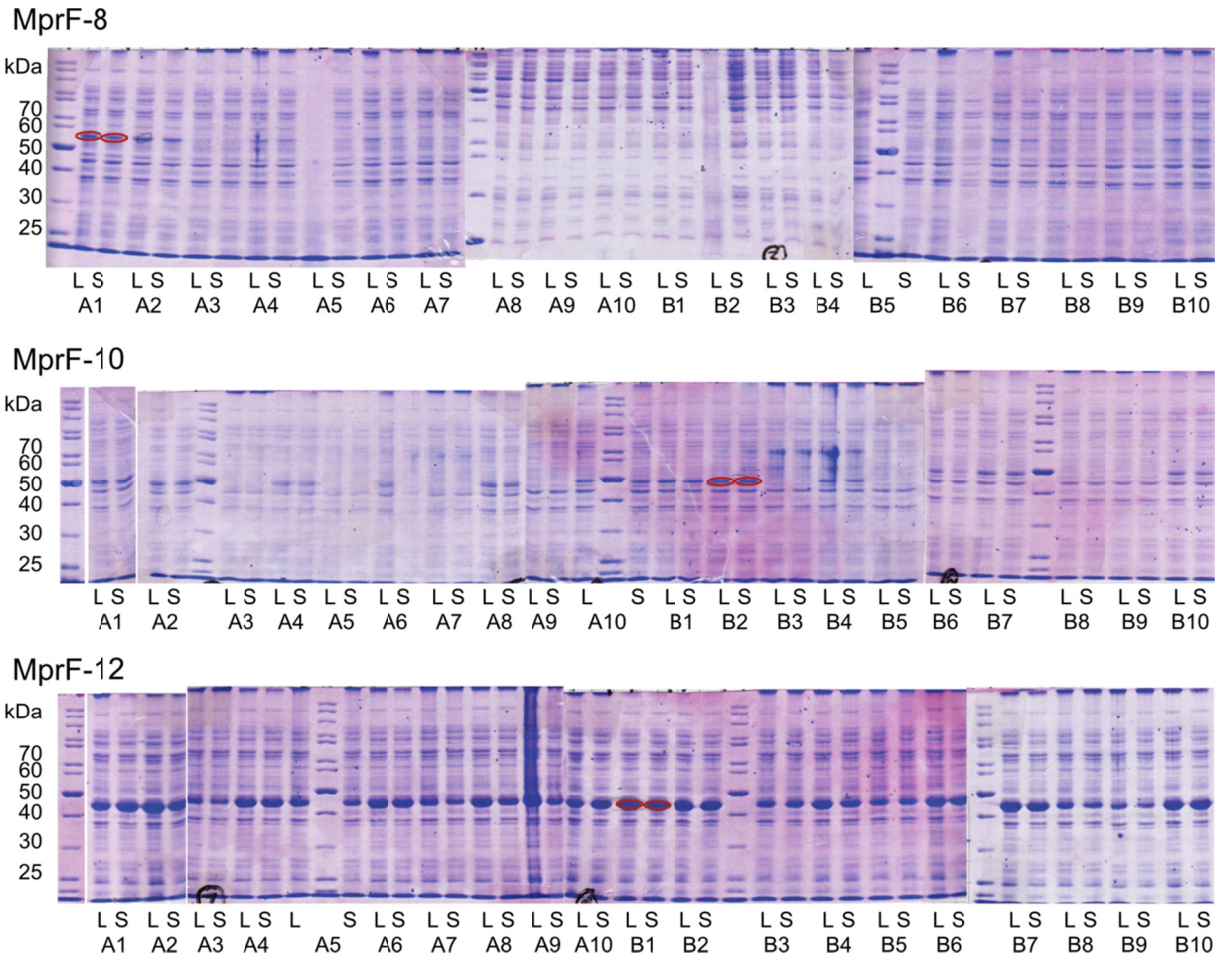

Fig. 21 Lysistest of MprF constructs with TMSs. For all three constructs lysate L (soluble and insoluble fraction) and the supernatant S after centrifugation were loaded for each buffer of Table 5.

The binding of the protein to the Ni^{2+}-column was very weak. Longer loading steps with reduced flow, batch loading and different additives such as Tween 20 or urea did not improve binding. The protein was further purified by IEX and size exclusion chromatography. The purified protein did not elute in the void volume, in contrast to the constructs before. CD-spectroscopy indicated a folded protein that was stable against 1:1000 trypsin for at least 2 hours by only shifting only to a ~5 kDa smaller size. Initial crystallization tests resulted in small, poorly diffracting crystals. The purified protein was again analyzed by mass spectrometry (Andreas Maurer, Kalbacher Laboratory; IFIB, University of Tübingen). The measured SDS-PAGE band was identified to be *E. coli* EF-Tu. After sequencing the band from the lysis test by mass spectrometry again, it was found that both proteins, EF-Tu and Mprf-12, have the same size and are coexpressed. During the different purification steps, EF-Tu was purified, while MprF-12 was lost.

7.5 MprF - Discussion

The domain structure of MprF was predicted computationally (Ernst et al., 2009). Several mutation studies showed the influence of mutations to the functionality of the protein (Ernst et al., 2009). These results helped to correlate the parts with function. No crystal structure is available for MprF or orthologous proteins of other organisms. The efforts to purify and crystallize the synthase domain all have the same problem, that the domain boundaries of the intracellular soluble domain are not known. The different constructs designed for purification tried to pinpoint these boundaries, but they were never proven conclusively. For example, the two last suggested TMSs clearly play a role in the activity of the synthase (Ernst et al., 2009). It is possible that these hydrophobic helices are not really transmembrane helices. They could also be located in a hydrophobic region of the intracellular part of the synthase. Alternatively, one or more of the loops connecting the TMSs can be part of the soluble domain or provide an important interaction to this domain. The purification of the construct containing these two helices in addition to the intracellular part (MprF-12) is not feasible. The protein was expressed in *E. coli*, but it has the same size as EF-Tu, an *E. coli* elongation factor, in SDS-PAGE. The main issue during purification is detection of Mprf-12 and the discrimination from EF-Tu. This cannot be done by SDS-PAGE, but only by mass spectrometry or Western Blot experiments. The purification of a synthase construct containing only the suggested soluble part failed as well. The proteins were prone to aggregation or the affinity tag was not cleavable, suggesting the possible linker region between the last TMS and the soluble domain to be short and folded close to the domain. Protease treatment was highly sensitive to the length of this linker domain. Shortening by only few amino acids prevented the digest, perhaps due to steric hindrance.

Several new strategies for MprF crystallization are envisioned. One approach is the change from an N-terminal to a C-terminal His-tag and elongation of the tag from six to eight histidine residues. The full-length MprF will also be tried to be expressed and purified. As this protein will be very challenging to crystallize, the protein must be analyzed biophysically and biochemically. Limited proteolysis can help to identify compactly packed areas or even domains for further construct design. Another approach would be the switch to a thermophile source organism coding for a homologous protein. This protein could also be used for domain mapping or even be crystallized. MprF construct design would clearly benefit from such a structure.

8 REFERENCES

Aguilar, J., Urday-Cornejo, V., Donabedian, S., Perri, M., Tibbetts, R., and Zervos, M. (2010). *Staphylococcus aureus* meningitis: case series and literature review. Medicine (Baltimore) 89, 117-125.

Ahmed, S., Meghji, S., Williams, R.J., Henderson, B., Brock, J.H., and Nair, S.P. (2001). *Staphylococcus aureus* fibronectin binding proteins are essential for internalization by osteoblasts but do not account for differences in intracellular levels of bacteria. Infect Immun 69, 2872-2877.

Bakal, C.J., and Davies, J.E. (2000). No longer an exclusive club: eukaryotic signalling domains in bacteria. Trends Cell Biol 10, 32-38.

Barthe, P., Mukamolova, G.V., Roumestand, C., and Cohen-Gonsaud, M. (2010). The structure of PknB extracellular PASTA domain from *Mycobacterium tuberculosis* suggests a ligand-dependent kinase activation. Structure 18, 606-615.

Bohach, G.A., Fast, D.J., Nelson, R.D., and Schlievert, P.M. (1990). Staphylococcal and streptococcal pyrogenic toxins involved in toxic shock syndrome and related illnesses. Crit Rev Microbiol 17, 251-272.

Bowdish, D.M., Davidson, D.J., Scott, M.G., and Hancock, R.E. (2005). Immunomodulatory activities of small host defense peptides. Antimicrob Agents Chemother 49, 1727-1732.

Bradford, M.M. (1976). A rapid and sensitive method for the quantitation of microgram quantities of protein utilizing the principle of protein-dye binding. Anal Biochem 72, 248-254.

Brogden, K.A. (2005). Antimicrobial peptides: pore formers or metabolic inhibitors in bacteria? Nat Rev Microbiol 3, 238-250.

CDC (2002). *Staphylococcus aureus* resistant to vancomycin--United States, 2002. MMWR Morb Mortal Wkly Rep 51, 565-567.

Debarbouille, M., Dramsi, S., Dussurget, O., Nahori, M.A., Vaganay, E., Jouvion, G., Cozzone, A., Msadek, T., and Duclos, B. (2009). Characterization of a

serine/threonine kinase involved in virulence of *Staphylococcus aureus*. J Bacteriol 191, 4070-4081.

Deftereos, S.P., Michailidou, E., Karagiannakis, G.K., Grigoriadi, S., and Prassopoulos, P. (2009). Hematogenous infantile infection presenting as osteomyelitis and septic arthritis: a case report. Cases J 2, 8293.

Donat, S., Streker, K., Schirmeister, T., Rakette, S., Stehle, T., Liebeke, M., Lalk, M., and Ohlsen, K. (2009). Transcriptome and functional analysis of the eukaryotic-type serine/threonine kinase PknB in *Staphylococcus aureus*. J Bacteriol 191, 4056-4069.

Dziewanowska, K., Patti, J.M., Deobald, C.F., Bayles, K.W., Trumble, W.R., and Bohach, G.A. (1999). Fibronectin binding protein and host cell tyrosine kinase are required for internalization of *Staphylococcus aureus* by epithelial cells. Infect Immun 67, 4673-4678.

Edwards, A.M., Massey, R.C., and Clarke, S.R. (2012). Molecular mechanisms of *Staphylococcus aureus* nasopharyngeal colonization. Mol Oral Microbiol 27, 1-10.

Ernst, C.M., and Peschel, A. (2011). Broad-spectrum antimicrobial peptide resistance by MprF-mediated aminoacylation and flipping of phospholipids. Mol Microbiol 80, 290-299.

Ernst, C.M., Staubitz, P., Mishra, N.N., Yang, S.J., Hornig, G., Kalbacher, H., Bayer, A.S., Kraus, D., and Peschel, A. (2009). The bacterial defensin resistance protein MprF consists of separable domains for lipid lysinylation and antimicrobial peptide repulsion. PLoS Pathog 5, e1000660.

GE Healthcare, B.-S. (2007). Purifying challenging Proteins, Vol 28-9095-31 AA (Uppsala).

Gordon, E., Mouz, N., Duee, E., and Dideberg, O. (2000). The crystal structure of the penicillin-binding protein 2x from *Streptococcus pneumoniae* and its acyl-enzyme form: implication in drug resistance. J Mol Biol 299, 477-485.

Hancock, R.E., and Rozek, A. (2002). Role of membranes in the activities of antimicrobial cationic peptides. FEMS Microbiol Lett 206, 143-149.

Hancock, R.E., and Sahl, H.G. (2006). Antimicrobial and host-defense peptides as new anti-infective therapeutic strategies. Nat Biotechnol 24, 1551-1557.

Hunter, T. (1995). Protein kinases and phosphatases: the yin and yang of protein phosphorylation and signaling. Cell 80, 225-236.

Kuroda, M., Kuroda, H., Oshima, T., Takeuchi, F., Mori, H., and Hiramatsu, K. (2003). Two-component system VraSR positively modulates the regulation of cell-wall biosynthesis pathway in *Staphylococcus aureus*. Mol Microbiol 49, 807-821.

Lammers, A., Nuijten, P.J., and Smith, H.E. (1999). The fibronectin binding proteins of *Staphylococcus aureus* are required for adhesion to and invasion of bovine mammary gland cells. FEMS Microbiol Lett 180, 103-109.

Lei, K., and Davis, R.J. (2003). JNK phosphorylation of Bim-related members of the Bcl2 family induces Bax-dependent apoptosis. Proc Natl Acad Sci U S A 100, 2432-2437.

Lindwall, G., Chau, M., Gardner, S.R., and Kohlstaedt, L.A. (2000). A sparse matrix approach to the solubilization of overexpressed proteins. Protein Eng 13, 67-71.

Lombana, T.N., Echols, N., Good, M.C., Thomsen, N.D., Ng, H.L., Greenstein, A.E., Falick, A.M., King, D.S., and Alber, T. (2010). Allosteric activation mechanism of the *Mycobacterium tuberculosis* receptor Ser/Thr protein kinase, PknB. Structure 18, 1667-1677.

Lowy, F.D. (1998). *Staphylococcus aureus* infections. N Engl J Med 339, 520-532.

Madigan, M.T.M., John M.; Stahl, David A.; Clark, David P. (2012). Brock Biology of Microorganisms, 13 edn (Pearson Education, Inc.).

Miller, M., Donat, S., Rakette, S., Stehle, T., Kouwen, T.R., Diks, S.H., Dreisbach, A., Reilman, E., Gronau, K., Becher, D., et al. (2010). Staphylococcal PknB as the first prokaryotic representative of the proline-directed kinases. PLoS One 5, e9057.

Nezu, J., Oku, A., Jones, M.H., and Shimane, M. (1997). Identification of two novel human putative serine/threonine kinases, VRK1 and VRK2, with structural similarity to vaccinia virus B1R kinase. Genomics 45, 327-331.

Ogston, A. (1882). Micrococcus Poisoning. J Anat Physiol 17, 24-58.

Ogston, A. (1884). Classics in infectious diseases. "On abscesses". Alexander Ogston (1844-1929). Rev Infect Dis 6, 122-128.

Ohlsen, K., and Donat, S. (2010). The impact of serine/threonine phosphorylation in *Staphylococcus aureus*. Int J Med Microbiol 300, 137-141.

Ortiz-Lombardia, M., Pompeo, F., Boitel, B., and Alzari, P.M. (2003). Crystal structure of the catalytic domain of the PknB serine/threonine kinase from *Mycobacterium tuberculosis*. J Biol Chem 278, 13094-13100.

Otto, M. (2010). Looking toward basic science for potential drug discovery targets against community-associated MRSA. Med Res Rev 30, 1-22.

Paracuellos, P., Ballandras, A., Robert, X., Kahn, R., Herve, M., Mengin-Lecreulx, D., Cozzone, A.J., Duclos, B., and Gouet, P. (2010). The extended conformation of the 2.9-A crystal structure of the three-PASTA domain of a Ser/Thr kinase from the human pathogen *Staphylococcus aureus*. J Mol Biol 404, 847-858.

Pereira, S.F., Goss, L., and Dworkin, J. (2011). Eukaryote-like serine/threonine kinases and phosphatases in bacteria. Microbiol Mol Biol Rev 75, 192-212.

Peschel, A., Jack, R.W., Otto, M., Collins, L.V., Staubitz, P., Nicholson, G., Kalbacher, H., Nieuwenhuizen, W.F., Jung, G., Tarkowski, A., et al. (2001). *Staphylococcus aureus* resistance to human defensins and evasion of neutrophil killing via the novel virulence factor MprF is based on modification of membrane lipids with l-lysine. J Exp Med 193, 1067-1076.

Peschel, A., and Sahl, H.G. (2006). The co-evolution of host cationic antimicrobial peptides and microbial resistance. Nat Rev Microbiol 4, 529-536.

Putcha, G.V., Le, S., Frank, S., Besirli, C.G., Clark, K., Chu, B., Alix, S., Youle, R.J., LaMarche, A., Maroney, A.C., et al. (2003). JNK-mediated BIM phosphorylation potentiates BAX-dependent apoptosis. Neuron 38, 899-914.

Puthalakath, H., and Strasser, A. (2002). Keeping killers on a tight leash: transcriptional and post-translational control of the pro-apoptotic activity of BH3-only proteins. Cell Death Differ 9, 505-512.

Rakette, S., Donat, S., Ohlsen, K., and Stehle, T. (2012). Structural Analysis of *Staphylococcus aureus* Serine/Threonine Kinase PknB. PLoS One 7, e39136.

Ranjbar, B., and Gill, P. (2009). Circular dichroism techniques: biomolecular and nanostructural analyses- a review. Chem Biol Drug Des 74, 101-120.

Roy, H., and Ibba, M. (2008). RNA-dependent lipid remodeling by bacterial multiple peptide resistance factors. Proc Natl Acad Sci U S A 105, 4667-4672.

Ruggiero, A., Squeglia, F., Marasco, D., Marchetti, R., Molinaro, A., and Berisio, R. (2011). X-ray structural studies of the entire extracellular region of the serine/threonine kinase PrkC from *Staphylococcus aureus*. Biochem J 435, 33-41.

Sevilla, A., Santos, C.R., Vega, F.M., and Lazo, P.A. (2004). Human vaccinia-related kinase 1 (VRK1) activates the ATF2 transcriptional activity by novel phosphorylation on Thr-73 and Ser-62 and cooperates with JNK. J Biol Chem 279, 27458-27465.

Vega, F.M., Gonzalo, P., Gaspar, M.L., and Lazo, P.A. (2003). Expression of the VRK (vaccinia-related kinase) gene family of p53 regulators in murine hematopoietic development. FEBS Lett 544, 176-180.

Yeats, C., Finn, R.D., and Bateman, A. (2002). The PASTA domain: a beta-lactam-binding domain. Trends Biochem Sci 27, 438.

Young, T.A., Delagoutte, B., Endrizzi, J.A., Falick, A.M., and Alber, T. (2003). Structure of *Mycobacterium tuberculosis* PknB supports a universal activation mechanism for Ser/Thr protein kinases. Nat Struct Biol 10, 168-174.

9 APPENDIX

9.1 Structural features determining the activation of eukaryotic serine/threonine protein kinase domains

Minireview: Structural features determining the activation of eukaryotic serine/threonine kinase domains

S. Rakette, T. Stehle

Manuscript in preparation

Reversible phosphorylation is a key mechanism for organisms to regulate a wide range of molecular processes in response to a changing environment. Phosphorylation of specific amino acids can change the characteristics of the target proteins and influence their activity (Pereira, Goss et al. 2011). This reversible process of phosphorylation is regulated by kinases and their antagonists, the phosphatases.

Among the homologous group of proteins, the eukaryotic protein kinases form the largest superfamily (Hunter 1995). They can be divided into the subgroups of serine/threonine kinases (STK) and tyrosine kinases. The three-dimensional structure of the STK kinase domain will be in the focus of this text.

Structure of the kinase domain

The kinase domains of serine/threonine kinases show a conserved fold with highly conserved motifs. Twelve subdomains are forming two lobes with a catalytic cleft in between (Hanks and Hunter 1995).

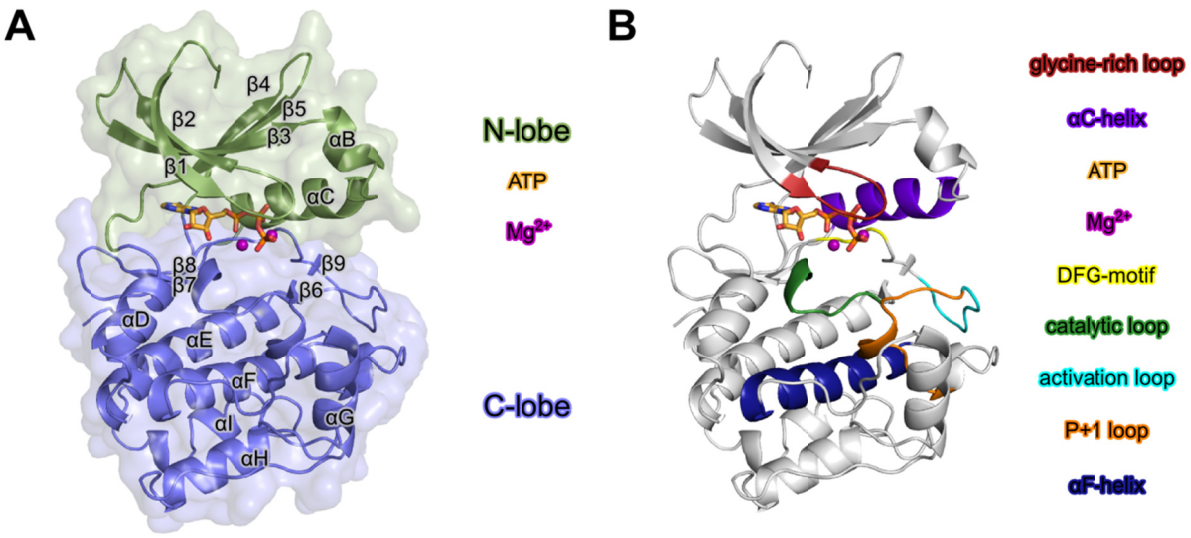

Fig. 1: Overview of conserved kinase domain structural elements. A: Secondary structure elements of kinases are labeled on the example PKA (PDB-ID: 1ATP)**.** The N-lobe is colored green, the C-lobe blue. In the cleft between the two lobes ATP and two magnesium ions are bound (ATP is shown in stick representation and the magnesium ions as magenta spheres). **B:** Overview of the location of motifs and loops important for enzymatic activity.

The smaller N-lobe is localized at the N-terminus of the kinase domain. The C-terminal C-lobe forms the larger part of the kinase domain (Fig. 1A). As an example for a eukaryotic STK, the protein kinase A (PKA, protein data base (PDB) entry: 1ATP) (Zheng, Trafny et al. 1993) will be the model and provide the residue numbers in the following description of structural details.

Open and closed conformation

The two lobes of kinases are connected in a flexible manner. Only one loop of the N-lobe, the loop between the αC-Helix and β4, extends to the C-lobe (Taylor and Kornev 2011). The orientation of the two lobes with respect to each other changes by domain movements during the catalytic cycle. In the open conformation the cleft between the two lobes is larger and no ATP is bound to the kinase. Upon ATP binding to the kinase, the N-lobe approaches the C-lobe. The difference in the orientation of the two states is highlighted by the comparison of an open and a closed conformation of PKA (Fig. 2) (Taylor and Kornev 2011).

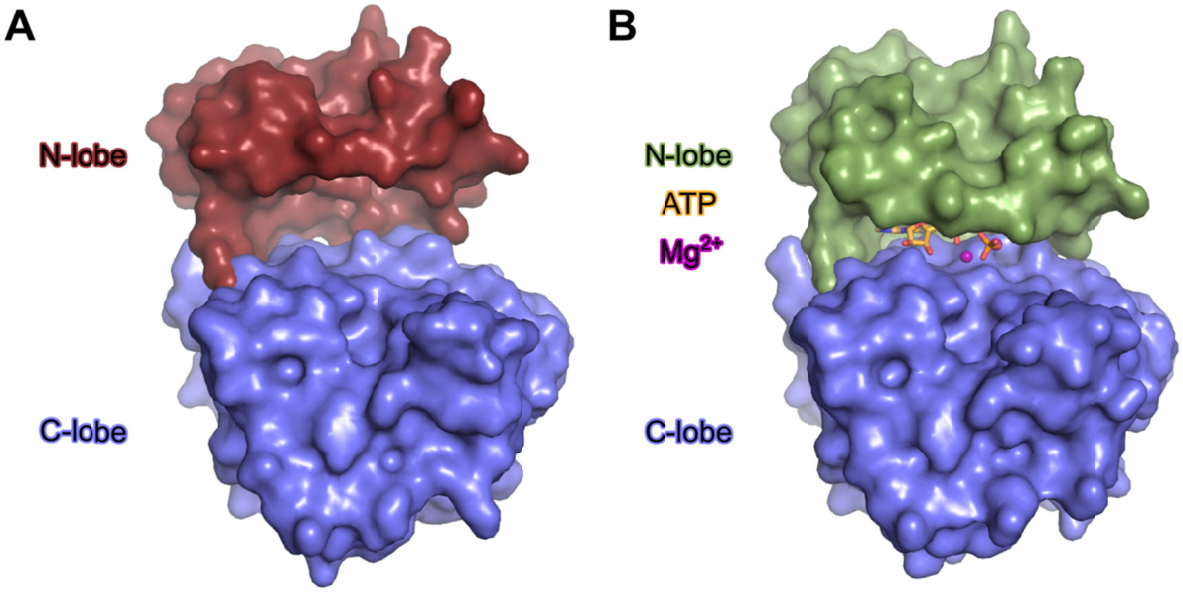

Fig. 2: Open and closed conformation of PKA. A: The surface of PKA in an open conformation is shown. No ATP is bound. The N-lobe is colored red, the C-lobe blue. The PDB-ID of this Structure is 1CMK (Zheng, Knighton et al. 1993). **B:** The closed conformation of PKA (PDB-ID: 1ATP) is shown. The N-lobe, in green, covers the bound ATP (stick representation). The cleft between N-lobe and C-lobe (blue) is much smaller.

N-lobe

The N-lobe is formed by a five stranded β-sheet and one conserved α-helix, the αC-helix (Fig. 1). The second α-helix of the N-lobe, the αB-helix, is not present in all kinase structures (Hanks and Hunter 1995). Several motifs in the β-sheet are highly conserved and important for the kinase to bind ATP.

One of these motifs is the phosphate-binding loop (P-loop) between β1 and β2 (colored red in Fig. 1B) (Saraste, Sibbald et al. 1990; Bossemeyer 1994). It is also named glycine-rich loop according to its amino acid sequence, the consensus sequence is GXGX□GXV (in which X stands for an arbitrary amino acid and □ for a hydrophobic residue, usually tyrosine or phenylalanine) (Huse and Kuriyan 2002; Ortiz-Lombardia, Pompeo et al. 2003; Taylor and Kornev 2011). The loop covers the ATP and anchors the phosphates. The last residue of the consensus glycine-rich loop sequence (valine) makes a hydrophobic contact to the nucleobase of ATP.

The second conserved motif of the N-lobe is the AXK-motif, which is localized in β3. The strictly conserved lysine (Lys72) makes contacts to the phosphates of ATP and forms a very important salt bridge to the strictly conserved glutamate (Glu91) localized in the αC-helix (Taylor and Kornev 2011).

The αC-helix (colored purple in Fig.1B) is in contact with both lobes. The loop between β4 and the αC-helix brings the C-terminus of the helix in contact to the C-lobe; the main part of the αC-helix is part of the N–lobe. In the active state of kinases, the αC-helix is close to the activation loop (Taylor and Kornev 2011). Only in this orientation, the previously described lysine-glutamate salt bridge can be formed.

C-lobe

The C-lobe is composed by mainly α-helices and two β-sheets. One of these sheets, the β6/β9 sheet, is missing in several kinase structures due to changes in the activation segment. The other β-sheet (β7/β8) flanks the magnesium binding loop, which contains the universally conserved DFG-motif (colored yellow in Fig. 1B). The aspartate of this motif makes contacts to the phosphates of ATP. These contacts can be direct or mediated by magnesium ions. The DFG-motif itself is stabilized by an internal hydrogen bond between the aspartate and the glycine. The second hydrogen bond stabilizing the DFG-motif is formed between the glycine and the amide nitrogen two amino acid after the DFG-motif (DFG+2) (Kornev, Haste et al. 2006; Pereira, Goss et al. 2011).

The DFG-motif and the APE-motif (or SPE-motif in some kinases) are flanking the activation segment including the activation loop and the P+1 loop, which are directly linked to each other (colored cyan and orange in Fig. 1B, respectively) (Johnson, Noble et al. 1996). The activation loop is a very flexible region. Many kinases are activated by phosphorylation or autophosphorylation of one or more serine or threonine residue in this loop.

The catalytic loop (colored green in Fig. 1B), including the conserved HXD-motif, is localized between β6 and β7. Parts of the motif are able to interact with the activation loop. In RD-kinases, the X of the HXD-motif is an arginine. This arginine forms a salt bridge to a phosphorylated residue of the activation loop and thus stabilizes this loop. The aspartate of HXD orientates the hydroxyl acceptor group of the peptide substrate (Kornev, Haste et al. 2006; Pereira, Goss et al. 2011). In some kinases (such as PKA), the histidine of this motif is replaced with a tyrosine.

The P+1 loop is an essential part of the contact between the kinase and its substrate. It is located at the C-terminus of the activation loop and contacts the residue of the peptide substrate after the phosphorylation site, the so called P+1 residue (Kornev and Taylor 2010; Pereira, Goss et al. 2011).

The αF-helix is the central hydrophobic helix in the C-lobe. Two hydrophobic spines are anchored to the αF-helix. It also provides hydrophobic contacts to many other motifs of the C-lobe such as the catalytic loop, the P+1 loop and the activation segment (Taylor and Kornev 2011).

Active and inactive conformations of kinases

Kinases can be in an active "on" or inactive "off" state. By switching between these states, the kinases undergo large conformal changes especially in the activation segment. One criterion for distinguishing whether a kinase is active is the formation of the regulatory spine (R-spine). A kinase with a broken, discontinuous R-spine is never in an active conformation. In contrast, the older distinction between open and closed conformation is no criterion for activity as active kinases can adopt open and closed conformations (Taylor and Kornev 2011).

Hydrophobic spines

Two sets of non-continuous hydrophobic residues constitute additional motifs in kinases. They were identified by using local spatial pattern (LPS) alignment methods (Kornev, Haste et al. 2006; Kornev, Taylor et al. 2008). The hydrophobic residues form two spines in kinases. Both spines comprise residues of N- and C-lobe and connect the two lobes (Fig. 3).

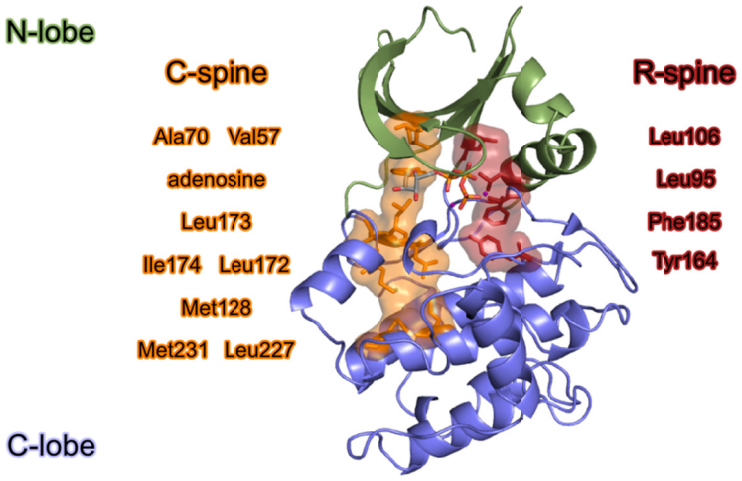

Fig. 3: Locations of the two hydrophobic spines. The residues of the R-spine are shown in red, residues of the C-spine and the adenosine ring of ATP in orange. Both spines connect the N-lobe (green) and the C-lobe (blue). The figure is adapted from Kornev, Taylor et al. 2008 and Taylor and Kornev 2011.

The shorter spine is termed the regulatory spine (R-spine). It consists of only four residues and is only formed in active kinases. The middle residues of this spine are part of the αC-helix and the activation loop, both very mobile parts of the kinase. The spine is formed by Leu106, which is part of the β4 strand in the N-lobe, Leu95 of the αC-Helix, Phe185 of the DFG motif in the activation loop and Tyr164, the residue replacing the histidine of the HRD-motif in PKA (Fig. 3). The peptide backbone of Tyr164 is anchored to the central αF-helix by the conserved Asp220. As displacements of the αC-helix or the activation segment in inactive kinases disrupt the spine, the R-spine is only formed in active kinases (Taylor and Kornev 2011).

The second spine is the catalytic spine (C-spine). In addition to residues of both lobes, the adenine ring of ATP completes this spine. In the N-lobe residues Val57, bordering the glycine-rich loop, and Ala70 of the AXK-motif in the β3-strand are involved in forming the C-spine. Ala70 and Val57 of the N-lobe and Leu173 of the C-lobe are docking to the adenine ring of ATP from both sides. The neighboring residues of Leu173 in the β7-strand, Leu172 and Ile174, interact with the Met128 in the αD-helix. Met128 engages with Leu227 and Met231 on the αF- helix, anchoring the C-spine to this helix (Taylor and Kornev 2011).

Position of the DFG-motif

In inactive kinases, the activation segment can be displaced from its active position. The phenylalanine of the DFG-motif is flipped into the ATP binding site and occupies the position of the adenosine ring of ATP in the C-spine. This inactive orientation is called "DFG-out" (Taylor and Kornev 2011). However, the orientation of the DFG-motif alone is a necessary, but not a sufficient criterion for the active state of a kinase. The DFG-motif has to be in an "in" orientation for the active state of a kinase, but a kinase with a "DFG-in" orientation is not automatically in an active conformation. Other parts of the kinase can still be in inactive conformations.

Orientation of the αC-helix

The orientation of the αC-helix plays a crucial role in kinase activation. In inactive kinases, the helix can be in an "out" conformation. This conformation of the αC-helix can be caused by a displacement of the activation segment. The activation loop can then form an additional helix after the DFG-motif. This inhibition helix prevents the αC-helix from adopting an active "in" conformation; Leu95 is not in its position to form the R-spine. Thus, the R-spine is broken and the small β-sheet between β6 and β9 cannot be formed. In addition the strictly conserved Lys72-Glu91 salt bridge to coordinate the correct orientation and fixation of the phosphates is not formed (Fig. 4). One examples for a kinase in an inactive state is the structure of c-Src kinase (PDB-ID: 2SRC, (Xu, Doshi et al. 1999)).

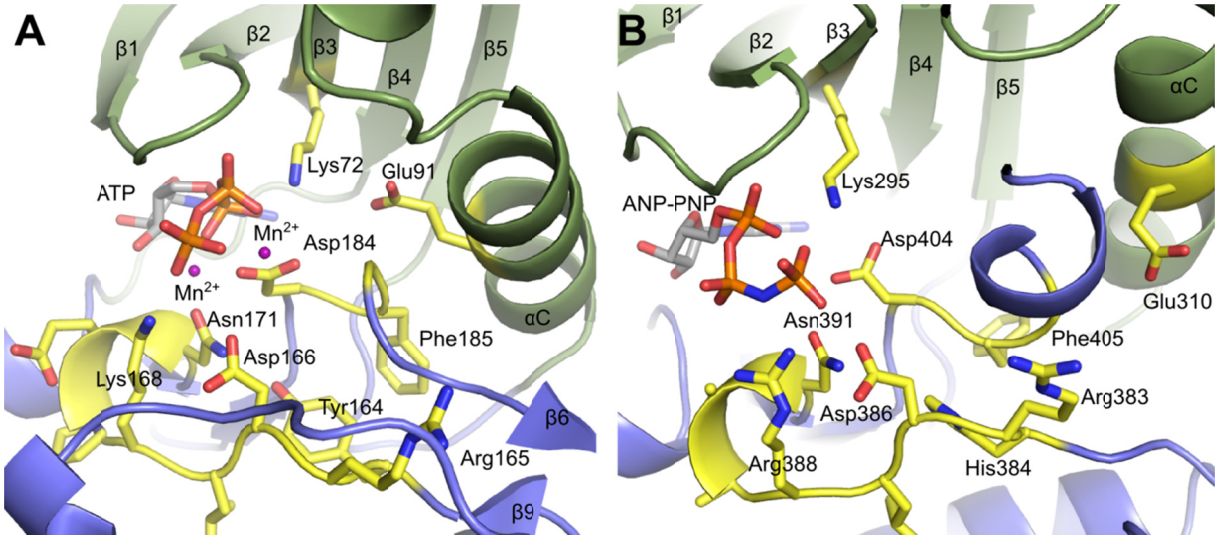

Fig. 4: Comparison of active and inactive kinases. Detailed view of the active site of kinases. The N-lobe is shown in green, the C-lobe in blue. In (A), the active PKA (PDB-ID:1ATP) is shown in complex with ATP and manganese. In (B) the same area as in (A) of the inactive kinase c-Src (PDB-ID: 2SRC) in complex with the ATP analog Adenosine 5′-(β,γ-imido)triphosphate (ANP-PNP).

Activation mechanisms of kinases

Several mechanisms for activation of kinases are known. These mechanisms can either directly affect the previously described structure elements of the kinase domain by its phosphorylation or dephosphorylation or dimerization. Alternatively, they can effect more global conformational changes of the entire protein. These changes then induce the active conformation of the kinase domain. This form of activation can be induced by modification of additional subunits or domain outside of the kinase domain, response to second messengers (Johnson, Noble et al. 1996).

Phosphorylation

Phosphorylation of residues in the activation loop is a common activation mechanism of kinases. The number of phosphorylated residues in the active loop necessary for activity differs among kinases. The insulin receptor kinase (IRK), for example, needs to be phosphorylated at three tyrosine residues in the activation loop for the movement from the "DFG-out" conformation to the active state (Fig. 5) (Hubbard, Mohammadi et al. 1998; Huse and Kuriyan 2002). In PKA only one residue in the activation loop has to be phosphorylated for activation of the kinase. In this case, phosphorylated Thr197 forms an ion pair with Arg165 of the HRD-motif (Knighton, Zheng et al. 1991; Huse and Kuriyan 2002).

Phosphorylation can also be involved in the inhibition of kinases. The SH2 domain of Src family members is engaged to the phosphorylated Tyr527 in the C-terminal tail of the kinase. This positions the SH3 domain so that it interacts with the N-lobe and stabilizes the αC-helix in an inactive "out" conformation (Fig. 5) (Huse and Kuriyan 2002; Cowan-Jacob, Fendrich et al. 2005).

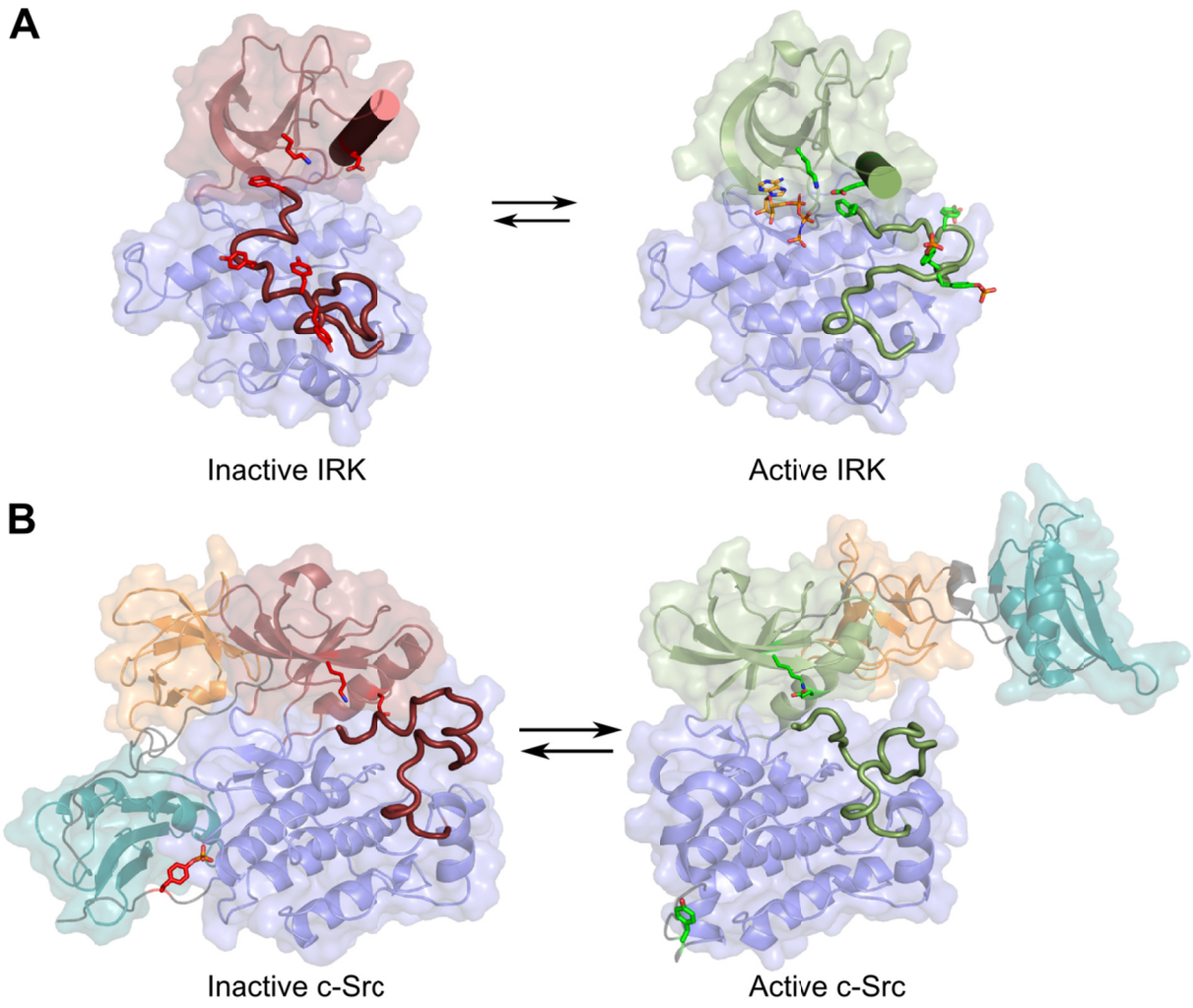

Fig. 5 Influence of phosphorylation on kinase activity. In all panels the phosphorylated residues and the conserved lysine and glutamate are highlighted in stick representation. The activation loop is highlighted in red in inactive conformations and in green in active conformations. **A:** Phosphorylation of IRK brings the activation loop into an active conformation (right panel). The phenylalanine of the DFG-motif is shown in stick representation; the αC-helix is highlighted as a tube. (PDB-IDs: 1IRK, 1IR3) **B:** Phosphorylation of c-Src at Tyr527 stabilizes the inactive conformation (left panel) by linking to the SH2 domain. The SH2 domain is colored in cyan, SH3 in orange (PDB_IDs: 2SRC, 1Y57). The figure is adapted from Huse and Kuriyan 2002.

Dimer formation

In the activation process of kinases the formation of dimers can play an important role. Dimerization can be induced by binding of ligands to sensor domains such as the binding of peptidoglycan to the PASTA domain of *M. tuberculosis* PknB (Shah, Laaberki et al. 2008; Barthe, Mukamolova et al. 2010). Two molecular models were proposed. In the first one the ligand binds to the PASTA domains and promotes the formation of a front-to-front dimer of the catalytic kinase domain. The catalytic domain is activated by *trans*-phosphorylation. The asymmetric front-to-front dimer interface is involving the activation loop and the αG-helix (Alber 2009; Barthe, Mukamolova et al. 2010). An alternative model for activation is

dimerization-dependent autophosphorylation. When a ligand is bound do the PASTA domain, this promotes the formation of a back-to-back dimer of the kinase domains. Dimerization primes the kinase domains to adopt active conformations and carry out interdimer *trans*-phosphorylation (Alber 2009; Barthe, Mukamolova et al. 2010). Studies on the kinase domain of *M. tuberculosis* PknB showed that dimer formation stimulated autophosphorylation (Lombana, Echols et al. 2010). The back-to-back dimerization of the unphosphorylated kinase domain seemed to activate the kinase and leads to intermolecular autophosphorylation. The resulting phosphorylated active kinase remains active even when the extracellular signal dissipates (Lombana, Echols et al. 2010).

The kinase domain of serine/threonine protein kinases undergoes large conformational changes by switching between inactive and active states. These conformational changes occur in several motifs of the kinase. To discriminate whether a kinase structure is in an active or inactive state, a detailed structural analysis has to be performed.

References

Alber, T. (2009). "Signaling mechanisms of the *Mycobacterium tuberculosis* receptor Ser/Thr protein kinases." Current opinion in structural biology **19**(6): 650-657.

Barthe, P., G. V. Mukamolova, et al. (2010). "The structure of PknB extracellular PASTA domain from *Mycobacterium tuberculosi*s suggests a ligand-dependent kinase activation." Structure **18**(5): 606-615.

Bossemeyer, D. (1994). "The glycine-rich sequence of protein kinases: a multifunctional element." Trends in biochemical sciences **19**(5): 201-205.

Cowan-Jacob, S. W., G. Fendrich, et al. (2005). "The crystal structure of a c-Src complex in an active conformation suggests possible steps in c-Src activation." Structure **13**(6): 861-871.

Hanks, S. K. and T. Hunter (1995). "Protein kinases 6. The eukaryotic protein kinase superfamily: kinase (catalytic) domain structure and classification." The FASEB journal : official publication of the Federation of American Societies for Experimental Biology **9**(8): 576-596.

Hubbard, S. R., M. Mohammadi, et al. (1998). "Autoregulatory mechanisms in protein-tyrosine kinases." The Journal of biological chemistry **273**(20): 11987-11990.

Hunter, T. (1995). "Protein kinases and phosphatases: the yin and yang of protein phosphorylation and signaling." Cell **80**(2): 225-236.

Huse, M. and J. Kuriyan (2002). "The conformational plasticity of protein kinases." Cell **109**(3): 275-282.

Johnson, L. N., M. E. Noble, et al. (1996). "Active and inactive protein kinases: structural basis for regulation." Cell **85**(2): 149-158.

Knighton, D. R., J. H. Zheng, et al. (1991). "Crystal structure of the catalytic subunit of cyclic adenosine monophosphate-dependent protein kinase." Science **253**(5018): 407-414.

Kornev, A. P., N. M. Haste, et al. (2006). "Surface comparison of active and inactive protein kinases identifies a conserved activation mechanism." Proceedings of the National Academy of Sciences of the United States of America **103**(47): 17783-17788.

Kornev, A. P. and S. S. Taylor (2010). "Defining the conserved internal architecture of a protein kinase." Biochimica et biophysica acta **1804**(3): 440-444.

Kornev, A. P., S. S. Taylor, et al. (2008). "A helix scaffold for the assembly of active protein kinases." Proceedings of the National Academy of Sciences of the United States of America **105**(38): 14377-14382.

Lombana, T. N., N. Echols, et al. (2010). "Allosteric activation mechanism of the *Mycobacterium tuberculosis* receptor Ser/Thr protein kinase, PknB." Structure **18**(12): 1667-1677.

Ortiz-Lombardia, M., F. Pompeo, et al. (2003). "Crystal structure of the catalytic domain of the PknB serine/threonine kinase from *Mycobacterium tuberculosis*." The Journal of biological chemistry **278**(15): 13094-13100.

Pereira, S. F., L. Goss, et al. (2011). "Eukaryote-like serine/threonine kinases and phosphatases in bacteria." Microbiology and molecular biology reviews : MMBR **75**(1): 192-212.

Saraste, M., P. R. Sibbald, et al. (1990). "The P-loop--a common motif in ATP- and GTP-binding proteins." Trends in biochemical sciences **15**(11): 430-434.

Shah, I. M., M. H. Laaberki, et al. (2008). "A eukaryotic-like Ser/Thr kinase signals bacteria to exit dormancy in response to peptidoglycan fragments." Cell **135**(3): 486-496.

Taylor, S. S. and A. P. Kornev (2011). "Protein kinases: evolution of dynamic regulatory proteins." Trends in biochemical sciences **36**(2): 65-77.

Xu, W., A. Doshi, et al. (1999). "Crystal structures of c-Src reveal features of its autoinhibitory mechanism." Molecular cell **3**(5): 629-638.

Zheng, J., D. R. Knighton, et al. (1993). "Crystal structures of the myristylated catalytic subunit of cAMP-dependent protein kinase reveal open and closed conformations." Protein science : a publication of the Protein Society **2**(10): 1559-1573.

Zheng, J., E. A. Trafny, et al. (1993). "2.2 A refined crystal structure of the catalytic subunit of cAMP-dependent protein kinase complexed with MnATP and a peptide inhibitor." Acta crystallographica. Section D, Biological crystallography **49**(Pt 3): 362-365.

9.2 Structural analysis of *Staphylococcus aureus* serine/threonine kinase PknB

Structural analysis of *Staphylococcus aureus* serine/threonine kinase PknB

Rakette S, Donat S, Ohlsen K, Stehle T

PLoS One, 2012, **7**, e39136

OPEN ACCESS Freely available online

PLoS one

Structural Analysis of *Staphylococcus aureus* Serine/Threonine Kinase PknB

Sonja Rakette[1], Stefanie Donat[2], Knut Ohlsen[2], Thilo Stehle[1,3]*

1 Interfaculty Institute of Biochemistry, University of Tübingen, Tübingen, Germany, **2** Institute for Molecular Infection Biology, University of Würzburg, Würzburg, Germany, **3** Department of Pediatrics, Vanderbilt University School of Medicine, Nashville, Tennessee, United States of America

Abstract

Effective treatment of infections caused by the bacterium *Staphylococcus aureus* remains a worldwide challenge, in part due to the constant emergence of new strains that are resistant to antibiotics. The serine/threonine kinase PknB is of particular relevance to the life cycle of *S. aureus* as it is involved in the regulation of purine biosynthesis, autolysis, and other central metabolic processes of the bacterium. We have determined the crystal structure of the kinase domain of PknB in complex with a non-hydrolyzable analog of the substrate ATP at 3.0 Å resolution. Although the purified PknB kinase is active in solution, it crystallized in an inactive, autoinhibited state. Comparison with other bacterial kinases provides insights into the determinants of catalysis, interactions of PknB with ligands, and the pathway of activation.

Citation: Rakette S, Donat S, Ohlsen K, Stehle T (2012) Structural Analysis of *Staphylococcus aureus* Serine/Threonine Kinase PknB. PLoS ONE 7(6): e39136. doi:10.1371/journal.pone.0039136

Editor: Inari Kursula, Helmholtz Centre for Infection Research, Germany

Received December 19, 2011; **Accepted** May 18, 2012; **Published** June 11, 2012

Funding: This work was supported by Collaborative Research Grant SFB-TR34 from the Deutsche Forschungsgemeinschaft via grants to KO and TS. The funders had no role in study design, data collection and analysis, decision to publish, or preparation of the manuscript.

Competing Interests: The authors have declared that no competing interests exist.

* E-mail: thilo.stehle@uni-tuebingen.de

Introduction

The gram-positive bacterium *Staphylococcus aureus* is a serious human pathogen that is responsible for an increasing number of illnesses and deaths each year [1]. The bacterium colonizes the nose and skin of humans and can cause illnesses ranging from skin infections [2] to life-threatening diseases such as endocarditis, bacteremia, pneumonia, meningitis, osteomyelitis, sepsis and the toxic shock syndrome [3,4,5,6]. Successful treatment of *S. aureus* infections remains a challenge as drug-resistant strains, such as methicillin-resistant and vancomycin-resistant *S. aureus* (MRSA and VRSA, respectively), are gaining prominence. Furthermore, the emergence of community-acquired *S. aureus* strains forms a rapidly emerging public health problem [7]. In order to develop new strategies to combat these bacteria, a better understanding of the organisms and the functions of its components is needed.

To overcome stressful conditions imposed by its host, *S. aureus* has developed various protective and offensive responses such as the sensing of environmental stimuli and the activation and inactivation of response regulators. This is generally achieved through cascades of phosphorylation reactions in the host, which in turn points to a key role of protein kinases in staphylococcal persistence. Protein kinases regulate a multitude of processes and signal transduction pathways in prokaryotes and eukaryotes [8]. A subgroup, the serine/threonine kinases (STKs), was originally thought to only be present in eukaryotic cells. However, in recent years STKs have also been identified in bacteria [9,10], and these have been classified as eukaryotic-type serine/threonine kinases [11]. While many microorganisms encode for several eukaryotic-type STKs, *S. aureus* encodes only for one such protein, which has been termed PknB, PrkC or Stk1 by different research groups [11,12,13] and will be referred to as PknB here. PknB was originally identified through a transposon mutagenesis approach and is conserved in all *S. aureus* strains [14]. The kinase is composed of an N-terminal, cytosolic kinase domain, a central transmembrane domain, and three C-terminal, extracellular PASTA (penicillin-binding protein and serine/threonine kinase associated) domains (Fig. 1). PASTA domains are constructed from about 65–70 amino acids and are thought to bind beta-lactam compounds as well as peptidoglycans [15,16]. The number of PASTA domains present in eukaryotic-type STKs can vary. *S. aureus* PknB and *B. subtilis* PrkC have both three PASTA domains, while the PknB of *M. tuberculosis* contains four such repeats [11,12,17].

PknB is of particular relevance for *S. aureus* survival and pathogenesis as it helps to regulate purine biosynthesis, autolysis, and other central metabolic processes of the bacterium and is involved in antibiotic resistance [12,18,19]. Moreover, recent data show that PknB can also act on human cellular proteins, and that these potential targets are involved in apoptosis, immune responses, transport, and metabolism [20]. The recently discovered secretion of PknB may also help the bacterium to evade intracellular killing and facilitate its growth [20]. Proper function of PknB is important for full expression of *S. aureus* pathogenesis, and it is also likely that phosphorylation levels controlled by PknB are essential in controlling bacterial survival within the host [21].

Structural information on *S. aureus* PknB is so far limited to the three PASTA domains that constitute the extracellular portion of the protein [11,17]. Structural analyses of PknB homologs, such as PknB from *M. tuberculosis* [22,23,24,25,26] have provided insights into the overall fold of the cytosolic kinase domain and its interactions with ligands. However, it is well established that kinases adopt similar folds but differ in subtle ways in order to achieve their specificity. Here, we report a structural analysis of

Figure 1. Domain structure of *S. aureus* PknB. The kinase region ($PknB_{SA\text{-}KD}$) is shown in orange. TM: transmembrane domain, PASTA: penicillin-binding protein and serine/threonine kinase associated domains.
doi:10.1371/journal.pone.0039136.g001

the kinase domain of *S. aureus* PknB in complex with a non-cleavable ATP analog, adenosine 5′-(β, γ-imido)-triphosphate (AMP-PNP). Comparison with other bacterial STKs provides insights into the determinants of PknB catalysis, its state of activation, and its interactions with potential ligands.

Materials and Methods

Cloning, expression and purification

DNA encoding the kinase domain of *S. aureus* PknB ($PknB_{SA\text{-}KD}$) (residues 1–291) of *S. aureus* strain 8352 (GenBank accession number BAB42315) was amplified by PCR, and NdeI and XhoI cleavage sites and an additional stop codon were introduced. After digestion with NdeI and XhoI, the PCR product was inserted into the pET28b vector (Novagen), which includes an N-terminal His_6-tag followed by a thrombin cleavage site, for protein expression in *E. coli* strain BL21-DE3. Transformed bacteria were grown in LB medium supplemented with 30 μg/ml kanamycin at 37°C to an optical density of 0.3 at 600 nm. After lowering the temperature to 20°C, the bacteria were induced by addition of 1 mM isopropyl-β-thiogalactopyranoside. After 24 hours of expression, bacteria were harvested by centrifugation and resuspended in 20 mM HEPES, 150 mM NaCl, 20 mM imidazole and 1 mM phenylmethanesulfonyl fluoride at pH 7.4. The sonified lysate was clarified by centrifugation and filtered. The solution was loaded onto a HisTrap column (GE Healthcare), which was then washed with lysis buffer. The His-tagged $PknB_{SA\text{-}KD}$ was eluted with a linear imidazole gradient ranging from 10 to 500 mM. After reducing the imidazole concentration by alternating concentration and dilution steps, the protein was cleaved with thrombin (1 U/mg protein; GE Healthcare) for 24 h at 20°C. Cleavage was followed with a second Ni^{2+}-affinity run to remove thrombin and uncleaved $PknB_{SA\text{-}KD}$. The 33.1 kDa $PknB_{SA\text{-}KD}$ was concentrated and purified by gel filtration (Superdex 75, GE Healthcare) in 20 mM HEPES, 150 mM NaCl at pH 7.4 (Fig. S1A). SDS-PAGE confirmed the purity of the product (Fig. S1B). Mass spectrometry analysis was used to verify the identity of $PknB_{SA\text{-}KD}$, and circular dichroism spectroscopy (CD-spectroscopy, Jasco J -720) confirmed that it was folded (Fig. S1C). $PknB_{SA\text{-}KD}$ was used at a concentration of 0.2 mg/mL in 2.5 mM HEPES, 18.75 mM NaCl at pH 7.4 for CD-spectroscopy measurements at room temperature.

Table 1. Data collection and refinement statistics.

Parameter	Value
Data collection	
Beam line	X06SA, SLS
Wavelength (Å)	1.0000
Space group	C2
Cell dimensions	
a, *b*, *c* (Å)	221.51, 127.55, 70.28
α, β, γ (°)	90.00, 89.96, 90.00
Resolution (Å)	45.0–3.0 (3.08–3.00)[α]
R_{meas}	4.8 (46.0)[α]
I/σI	17.99 (2.68)[α]
Completeness (%)	99.1 (99.5)[α]
Unique reflections	38,868 (2,889)[α]
Redundancy	3.39 (3.38)[α]
Wilson B ($Å^2$)	95.43
Refinement	
Resolution (Å)	43.5–3.0
R_{work}/R_{free}	0.2149/0.2464 (0.3403/0.3962)[α]
No. of atoms	12,609
Protein	12,420
Ligands	189
B-factors ($Å^2$)	
Protein	97.1
Benzamidine/AMP-PNP	87.9/105.1
r.m.s.[β] deviations	
Bond lengths (Å)	0.005
Bond angles (°)	0.918
Ramachandran plot	
Most favored regions (%)	95.7
Allowed regions (%)	4.3
Disallowed regions (%)	0.0

[α]Values in parentheses are for highest resolution shell.
[β]r.m.s., root mean square.
doi:10.1371/journal.pone.0039136.t001

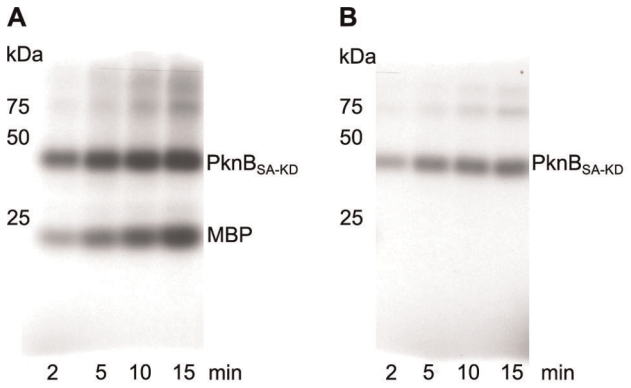

Figure 2. Activity test of $PknB_{SA\text{-}KD}$. $PknB_{SA\text{-}KD}$ (25 ng) was incubated either with myelin basic protein (MBP; 1 μg) (A) or alone (B) together with γ^{33}-ATP, $MnCl_2$ and $MgCl_2$ for the time indicated. Position and size (kDa) of molecular weight markers are indicated on the left side. Phosphorylation of MBP (A) and autophosphorylation (B) are visualized by autoradiography using direct-exposure film. The phosphorylation rate is increasing as a function of time in both experiments, demonstrating that the purified $PknB_{SA\text{-}KD}$ protein is active.
doi:10.1371/journal.pone.0039136.g002

The path length was 0.1 cm, and data were acquired at a scanning speed 100 nm/min with a data pitch of 0.5 nm.

Chemical cross-linking

Purified $PknB_{SA\text{-}KD}$ was incubated with different concentrations of glutaraldehyde for 15 min at room temperature. The reaction was stopped by adding 4xSDS-protein buffer and incubating the mixture at 95°C for 5 minutes. Identical procedures were carried out with the 22 kDa adenovirus type 21 fiber knob (Ad21), which forms trimers and served as a positive control, and with the 25kDa chymotrypsinogen A (Sigma-Aldrich), which is monomeric and served as the negative control.

Protein kinase assay

In vitro phosphorylation of 25 µg/mL $PknB_{SA\text{-}KD}$ was performed for the indicated time at 37°C with 1 µg/mL myelin basic protein (MBP, Sigma, Deisenhofen, Germany) and 4 µCi γ^{33}-ATP/µl in 20 µl reaction buffer containing 50 mM HEPES (pH 7.5), 1 mM DTT, 0.01% Brij35, 3 mM $MnCl_2$ and 3 mM $MgCl_2$. In each case, the reaction was stopped by adding 4xSDS-protein buffer. One-dimensional gel electrophoresis was performed and finally, radioactive proteins were visualized by autoradiography using direct-exposure film.

Protein crystallization and structure determination

The final solution used for crystallization contained 8 mg/mL $PknB_{SA\text{-}KD}$, 5 mM $MgCl_2$, 4 mM AMP-PNP (tetralithium salt hydrate), 2% (w/v) benzamidine hydrochloride and 1 mM dithiothreitol in 20 mM HEPES, 150 mM NaCl at pH 7.4. Crystals were grown with the sitting drop vapor diffusion method by mixing equal amounts of protein solution and crystallization solution (80 mM 2-(N-morpholino)ethanesulfonic acid pH 6.0, 1.3 M sodium citrate (pH 7.0), 2% (w/v) benzamidine hydrochloride and 60 mM $MgCl_2$ at 4°C. Crystals appeared after several days and grew to a maximum size of 150 µm diameter. Crystallization trials using mixtures of $MnCl_2$ and $MgCl_2$ or $MnCl_2$ could not improve the crystal quality. They belong to space group C2 and contain six kinase domains in their asymmetric unit. The crystals were mounted on a loop and flash frozen in liquid nitrogen prior to data collection.

X-ray diffraction experiments were performed at the X06SA beam line of the Swiss Light Source, Paul Scherrer Institut, Villigen, Switzerland. Data extending to 3.0 Å resolution were recorded using the PILATUS detector and processed with XDS [27]. Initial phases were determined with PHASER [28] using the *M. tuberculosis* PknB structure as search model (Protein data bank (PDB) ID: 1O6Y [23]). The search model was modified by truncating side chains that differed in sequence from the *S. aureus* protein, and by removing loops and bound ligands. Molecular replacement yielded one solution containing six copies that gave rise to a sensible crystal packing. The initial model was then improved through alternating steps of model building in Coot [29] and refinement in Phenix [30]. The refinement parameters included simulated annealing, Ramachandran refinement, and non-crystallographic symmetry (NCS) restraints. Eight groups per chain were defined in the NCS refinement, excluding the most flexible loops. The fragments of chains A, B and C, which were similar to each other, were defined as NCS-linked groups, and the same was done for chains D, E and F. Electron density for AMP-PNP appeared in all six chains during the course of the refinement, allowing the incorporation of the ligand into the model. The final structure has good quality, with R_{work} and R_{free} values [31] of 21.49 and 24.64%, respectively. Geometric restraints for the AMP-PNP ligand were calculated using the PRODRG server [32]. Data and refinement statistics are given in Table 1. Atomic coordinates und structure factors have been deposited in the PDB (http://www.pdb.org) under the accession code 4EQM.

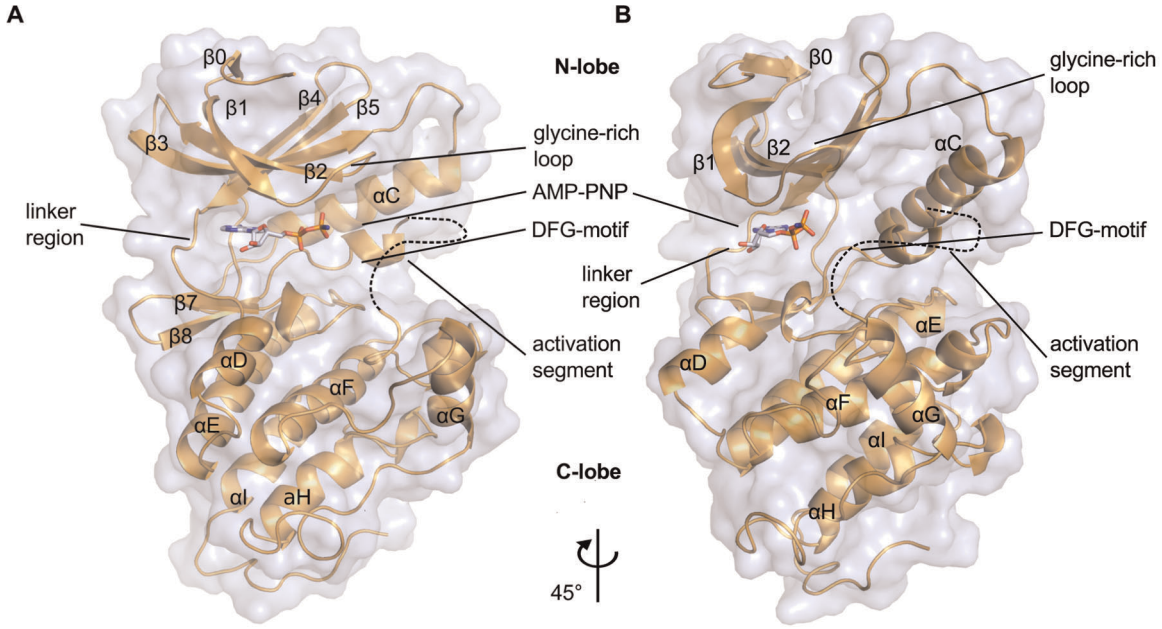

Figure 3. Overall structure of $PknB_{SA\text{-}KD}$ in complex with AMP-PNP. The two views differ by a rotation of 45° around a vertical axis. The AMP-PNP ligand is located in the cleft between the N- and the C-lobe. Due to its high flexibility, the terminal phosphate group of AMP-PNP is not visible in the electron density and is therefore not shown here.
doi:10.1371/journal.pone.0039136.g003

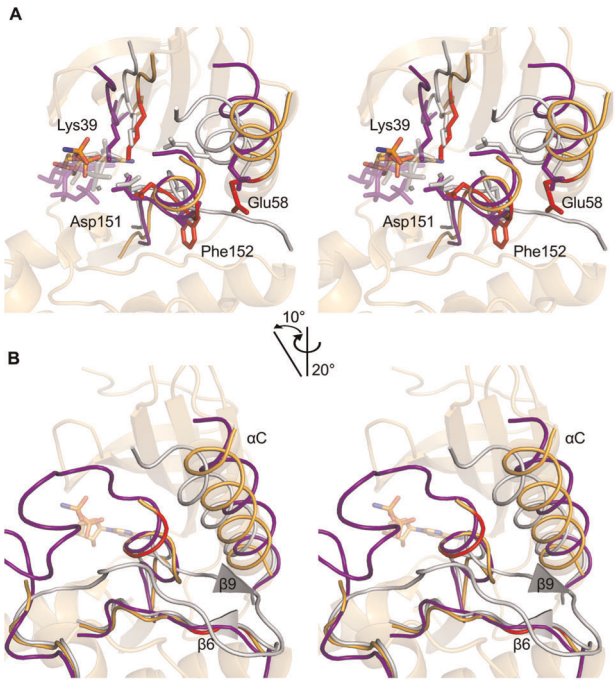

Figure 4. Stereo views of the activation site of $PknB_{SA\text{-}KD}$. (A). The PknB structure is shown in light orange. It was superimposed onto the kinase structures of active PKA (grey, PDB ID: 1ATP [35]) and inactive c-Src (purple, PDB ID: 2SRC [36]) using C-lobe residues 100–250. The highly conserved residues Lys39, Glu58, Asp151 and Phe152 of $PknB_{SA\text{-}KD}$ are highlighted as red sticks. The latter two residues are part of the DFG-motif. Corresponding residues Lys72, Glu91, Asp184 and Phe185 of PKA, as well as the backbone of PKA and ATP, are colored in grey. Corresponding residues Lys295, Glu310, Asp404 and Phe405 of c-Src, as well as the backbone of c-Src and ATP, are colored in purple. Mn^{2+} ions in the PKA structure are shown as small gray spheres. (B). Close-up view of the β-sheet formed by β6 and β9 in active kinases such as PKA. The colors are the same as in A. The β-sheet in PKA is represented with triangles as the β-strands only consist of two residues each. The red part of $PknB_{SA\text{-}KD}$ represents residues Ile129, Val130, Lys156 and Ala157, which are the residues that would form strands β6 and β9 in the active protein.
doi:10.1371/journal.pone.0039136.g004

Results

Activity assay

The functional activity of the kinase domain of *S. aureus* PknB ($PknB_{SA\text{-}KD}$) was tested by an *in vitro* phosphorylation assay. $PknB_{SA\text{-}KD}$ is able to phosphorylate other proteins such as myelin basic protein (MBP) in an efficient manner (Fig. 2A). The target protein MBP was previously used as a surrogate substrate for activity tests of the full-length PknB [12] and of *Mycobacterium tuberculosis* PknB [33]. Additionally, $PknB_{SA\text{-}KD}$ is able to perform autophosphorylation (Fig. 2B).

Overall Structure

$PknB_{SA\text{-}KD}$ exhibits the typical kinase fold, with N- and C-lobes creating a central ligand binding region that serves to accommodate the substrate or its analog AMP-PNP (Fig. 3). The N-lobe comprises residues 1 to 90 and contains a six-stranded, antiparallel β-sheet (strands β0-β5) that packs against the αC-helix. The C-lobe is composed of six α-helices and a small two-stranded β-sheet (strands β7-β8). Many kinases contain two additional strands, β6 and β9, which form a second β-sheet in the C-lobe. This small sheet is absent in $PknB_{SA\text{-}KD}$ due to the conformation of the activation segment (Fig. 4). The two lobes in $PknB_{SA\text{-}KD}$ are connected *via* the linker region (residues 87–92) and *via* a loop that leads from the C-terminus of the αC-helix to the β4 strand (Fig. 3A, B). Although present in the crystallized $PknB_{SA\text{-}KD}$, residues 284 to 291 at the C-terminus are not well defined by electron density and could not be built. We conclude that the kinase domain of *S. aureus* PknB includes residues 1–282 (Fig. 1), in contrast to the computer aided residue assignment for the kinase region in Donat et. al, 2009 [12] (residues 10–268) and the longer $PknB_{SA\text{-}KD}$ sequence used for crystallization. As is the case in many kinase structures, high flexibility of the activation loop (residues 160–171) results in this segment not being traceable in the electron density maps. The six $PknB_{SA\text{-}KD}$ structures present in the asymmetric unit (molecules A to F, respectively) differ in several surface-exposed loops as a result of non-identical crystal contacts. The molecules can be divided into two homogeneous groups; molecules A, B and C bind benzamidine in a similar location and form similar crystal contacts. However, these features are not conserved in molecules D, E and F. The electron density for molecules A, B and C is more detailed in most regions, allowing unambiguous assignment of most side chains orientations. By contrast, the electron density for chains D, E and F is less well defined, and the density for the ATP-binding site is also somewhat different in these three chains. The β-phosphates of AMP-PNP are arranged in a different orientation in chains D-F compared with chains A-C. The main chain B-factor plot (Fig. S2) shows overall agreement of the B-factor distribution in all six chains. Residues forming a secondary structure element have significantly lower B-factors compared to residues in flexible loop regions. This flexibility is also reflected in the high overall B-factor. The B-factor differences between the chains A, B and C are small, the same is true for chains D, E and F. It is likely that variation in $PknB_{SA\text{-}KD}$ phosphorylation contribute to the observed differences in electron density. Unless specified otherwise, molecule A will be used to discuss the salient features of $PknB_{SA\text{-}KD}$.

AMP-PNP binding

The ATP analog AMP-PNP is bound in the cleft separating the two lobes of the kinase (Fig. 3). The adenine ring projects deep inside the cleft, into a pocket that is largely hydrophobic. Two hydrogen bonds, contributed by the backbone amide of Ile90 and the backbone oxygen of Glu88, anchor the adenine ring (Fig. S3). The ribose and phosphate moieties of AMP-PNP do not make equivalent contacts in the different chains, and these contacts are therefore probably not significant. Furthermore, the γ-phosphate group is not visible in the electron density maps, suggesting that the lack of contacts with $PknB_{SA\text{-}KD}$ increases its flexibility.

$PknB_{SA\text{-}KD}$ is in an inactive conformation

In order to determine whether the structure of $PknB_{SA\text{-}KD}$ is in an active or an inactive conformation, we have compared it with the following kinase structures: (i) PknB of *M. tuberculosis*, which is the first reported structure of a bacterial STK (PDB ID: 1O6Y [23] and 1MRU [24]; (ii) cAMP-dependent protein kinase A (PKA) in an open conformation (PDB ID: 1CTP [34]); (iii) a closed, active PKA structure with bound ATP (PDB ID: 1ATP [35]); and (iv) human c-Src, a tyrosine kinase in the autoinhibited conformation (PDB ID: 2SRC [36]). A structure-based sequence alignment was generated for all five kinases using ClustalW [37], Espript [38], Strap [39] (Fig. 5), and superpositions were performed by aligning residues 100–250 of the C-lobe of $PknB_{SA\text{-}KD}$ with the other structures. Although there is no crystal structure available for it, we also included the sequence of the *B. subtilis* protein kinase C (PrkC) in our analysis because of its

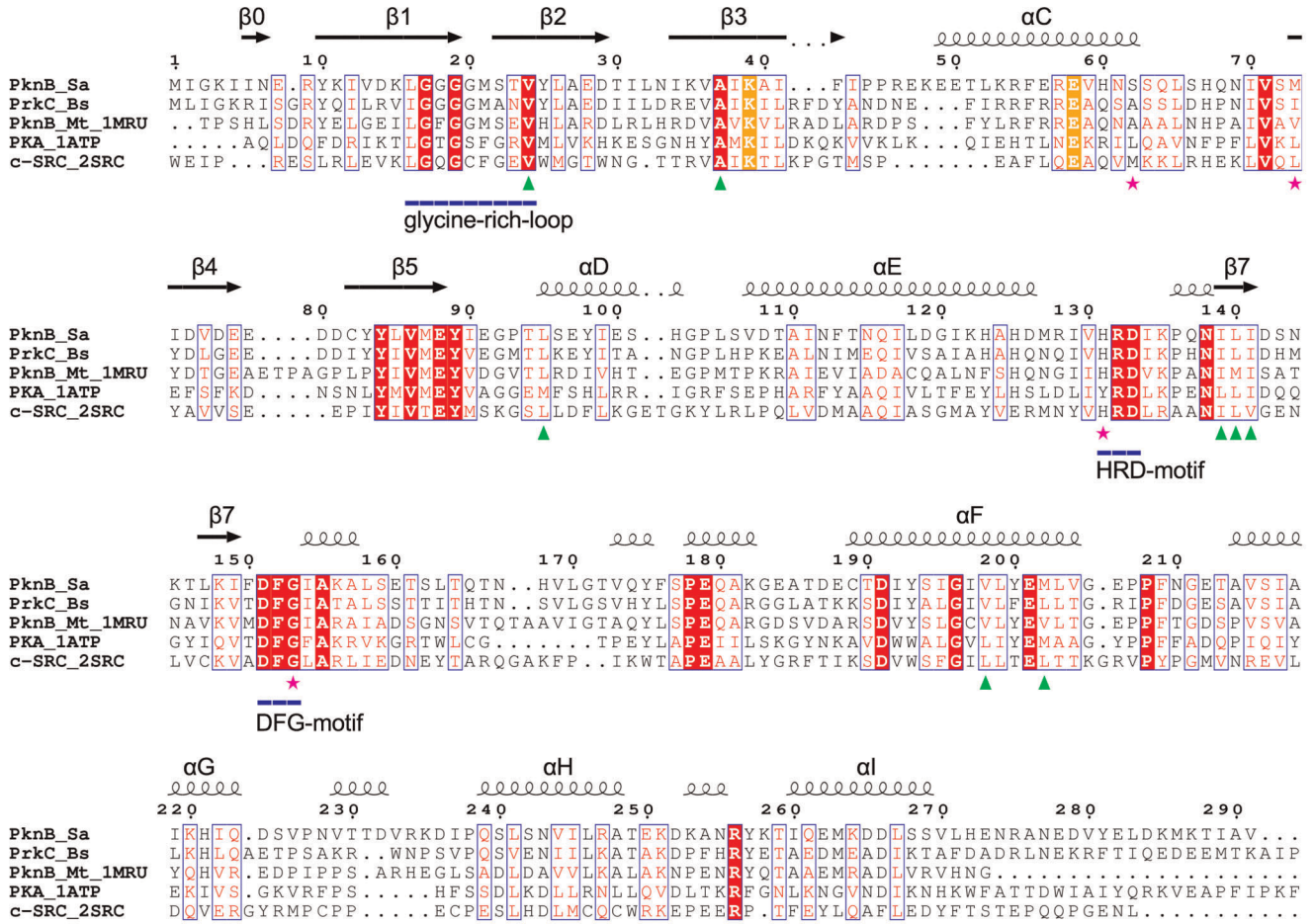

Figure 5. Structure-based sequence alignment. Structure-based sequence alignment of the *S. aureus* PknB kinase domain with the kinase domains of *B. subtilis* PrkC (no structure available), *M. tuberculosis* PknB (PDB ID: 1MRU [24]), murine cAMP dependent Protein Kinase A (PDB ID: 1ATP [35]; PDB ID: 1CTP [34]) and human tyrosine protein kinase c-Src (PDB ID: 2SRC [36]). The secondary structure of $PknB_{SA\text{-}KD}$ is shown above the alignment and the numbering of the sequences corresponds to *S. aureus* as well. The HRD- and DFG-motifs and the glycine-rich loop are underlined in blue. The highly conserved residues Lys39 and Glu58 are marked in orange. Green triangles indicate the residues of the C-spine; magenta stars mark residues of the R-spine.
doi:10.1371/journal.pone.0039136.g005

especially high homology to the *S. aureus* PknB sequence and the fact that both kinases have three extracellular PASTA domains.

Our analysis highlights several highly conserved residues that are important for kinase function: the glycine-rich loop, the DFG-motif, the position of the αC-helix, and the catalytic and regulatory spines (C-spine and R-spine, respectively). Representative F_{obs}-F_{calc} omit electron density maps of the ATP binding regions in chains A and D are shown in Figs. S3A and S3B, respectively. F_{obs}-F_{calc} omit electron density maps of the DFG-motif and the inhibition helix of chain A, the AMP-PNP and its surroundings, and the αF-helix of chains A and D are shown in Fig. S4A–D. The glycine-rich loop positions the γ-phosphate of ATP in an orientation that facilitates phosphoryl transfer during catalysis [40]. The DFG-motif is near the activation segment (Fig. 3). The C- and R-spines are sets of non-contiguous hydrophobic residues that line the interior of a kinase and stabilize its active, closed conformation (Fig. 6A, B) [40,41,42,43].

a. Stabilization of the phosphates. Connecting strands β1 and β2 in the N-lobe, the glycine-rich loop has a consensus sequence of $GX_1GX_2\phi GX_3V$, with ϕ denoting a hydrophobic residue (usually tyrosine or phenylalanine) and X indicating any amino acid [23,44,45]. Since it serves to stabilize the phosphates of ATP, this loop is also sometimes referred to as phosphate binding loop or P-loop [45]. In the active state of kinases, the glycine-rich loop faces the terminal phosphates of ATP, positioning the γ-phosphate for the transfer reaction [46,47,48]. In contrast, the glycine-rich loop faces away from ATP in open and inactive kinases such as PKA (in PDB ID: 1CTP [34]) (Figs. S3, S5). While the glycine-rich loop is strictly conserved in PKA, c-Src, and many other kinases, its consensus sequence is altered to $GX_1GGMX_2X_3V$ in $PknB_{SA\text{-}KD}$ and the two other bacterial kinases included in our comparison. Moreover, the X_1 residue is also a glycine in both *B. subtilis* PrkC and $PknB_{SA\text{-}KD}$. The increased number of directly linked glycines would likely render the loop more flexible in both proteins. The comparison of the structures shows that the glycine-rich loop in $PknB_{SA\text{-}KD}$ is in a conformation that differs from those observed in both active and inactive kinases (see above) (Figs. S3, S5). Its "tip" (residues 18 to 20) is twisted upwards, facing away from the phosphates. However, its "base" (residues 22–25) is still in a position similar to those observed in active kinases.

In active kinases, the phosphates of ATP are stabilized in the cleft between the two lobes. The motif involved in binding phosphates on the C-lobe side is the DFG-motif. Protein kinases

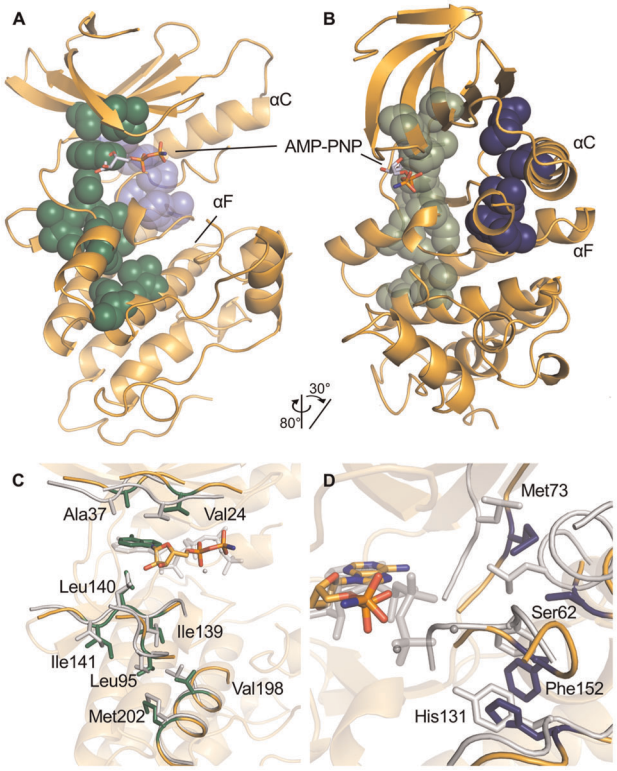

Figure 6. The C- and R-spine regions of PknB$_{SA-KD}$. (A, B). Overview of the location of the two spines in PknB$_{SA-KD}$. The C-spine is colored in green, the R-spine in the background in blue. The two views differ by the indicated rotation to provide a better view of the orientation and location of the R-spine. (C). Detailed view of the residues belonging to the C-spine of PknB$_{SA-KD}$ and the adenine of AMP-PNP as part of the spine are shown in green. The residues of the C-spine of PKA in a closed state (PDB ID: 1ATP [35]) are shown for comparison. (D). Detailed view of the R-spine residues of PknB$_{SA-KD}$ in blue. Corresponding residues of PKA are shown in grey. While the spine is formed in PKA, it is interrupted by the Ser62 and placed away from ideal position in PknB$_{SA-KD}$. The structure of PKA in panels C and D was aligned with PknB$_{SA-KD}$ C-lobe residues 100–250.
doi:10.1371/journal.pone.0039136.g006

stabilize the phosphates of bound ATP with magnesium ions, which in turn are ligated to an aspartic acid in the DFG-motif (residues 151–153 in PknB$_{SA-KD}$). In active kinases, the DFG-motif also features an internal hydrogen bond between the aspartic acid and the glycine, and a second hydrogen bond between the glycine and the amide nitrogen of residue DFG+2 (Ala155 in PknB$_{SA-KD}$) [41]. The DFG-motif of PknB$_{SA-KD}$ lacks internal hydrogen bonds, and no magnesium ion is visible in the vicinity of Asp151. It is clearly not in an active conformation and does not stabilize the phosphate groups of AMP-PNP.

A salt bridge is located close to the DFG-motif in active kinases. To enable an active kinase conformation, the αC-helix must be oriented such that a salt bridge between the strictly conserved residues Glu58 and Lys39 can be formed. Lys39 lies in the β3-strand of the N-lobe and helps to stabilize the α- and β-phosphates of ATP [46,47,48]. Structural comparison with other active kinases shows that the αC-helix of PknB$_{SA-KD}$ is not in a closed conformation (Fig. 4 and Fig. S4B). The helix is rotated away from the active site, and Glu58 does not form a salt bridge with Lys39.

b. The C- and R-spines. These spines stabilize the active, closed conformation of a kinase and contain residues from both lobes of the kinase. The C-spine attaches the active site to the αF-helix, connecting the two lobes *via* the adenine ring system. It lines the rear of the adenosine-binding pocket and stabilizes the closed, active conformation of protein kinases. In PknB$_{SA-KD}$, the C-spine is formed by residues Val24, Ala37 in the N-lobe and residues Ile139, Leu140, Ile141, Leu95, Val198 and Met202 in the C-lobe (Fig. 6A, C). The C-spine of PknB$_{SA-KD}$ and the bound adenine ring superimpose well with those of the closed, active PKA structure (Fig. 6C).

The R-spine also serves to stabilize the active conformation of protein kinases [40,41,42,43]. In PknB$_{SA-KD}$, the putative residues for the spine are Met73, Ser62, His131 and Phe152. The latter residue is part of the DFG-motif. Asp191 is stabilizing the backbone of His131, thereby anchoring the spine to the αF-helix. Ser62 lies in the αC-helix and is located four residues C-terminal to the highly conserved Glu58. Since the DFG-motif and the αC-helix are not in an active conformation, the R-spine cannot be fully formed in PknB$_{SA-KD}$ (Fig. 6B, D).

c. Inhibition helix. In order to assume an active state, the αC-helix of PknB$_{SA-KD}$ would have to change its position (Fig. 4). This is however not possible in our structure because the space into which the αC-helix would have to rotate is already occupied by the activation segment located directly after the DFG-motif (Fig. 4). In active kinases the activation loop makes close contacts to the C-lobe [40] and forms the β-sheet between strands β6 and β9 (Fig. 4B). The activation segment of PknB$_{SA-KD}$ interacts with the N-lobe and the αC-helix. The activation segment forms a short helix directly after the DFG-motif and blocks the area for the αC-helix to assume an active conformation. The putative residues of β9 are part of the inhibition helix and far away from β6, so that the β-sheet cannot be formed. The absence of the β6/β9 sheet is also a marker for an inactive conformation of PknB$_{SA-KD}$ (Fig. 4B). The PknB$_{SA-KD}$ αC-helix is stabilized by a hydrophobic interface similar to the one found in the structures of CDK2 and c-Src in their autoinhibited conformations [36,49,50]. The interface is formed by several residues in the αC-helix, strands β3 and β4, and the activation segment.

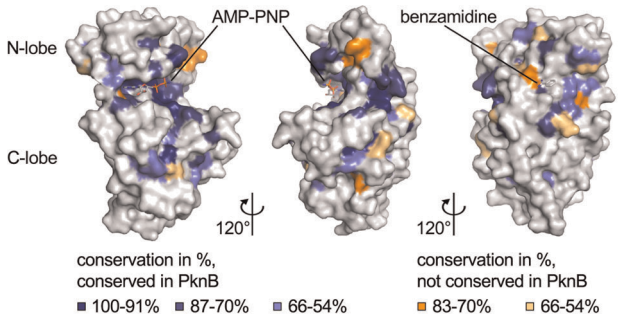

Figure 7. Analysis of conservation of PknB residues. Surface representation of PknB$_{SA-KD}$. The three views differ by rotations of 120° and 240°, respectively, around a vertical axis. The coloring is based on an alignment of 24 bacterial STKs (Fig. S6). Blue indicates highly conserved residues (100–91% conservation in dark blue, 87–70% conservation in blue, and 66–54% light blue). Residues that are highly conserved in most kinases but are different in PknB$_{SA-KD}$ are colored in orange (83–70% conservation in orange, 66–54% conservation in light orange). In the right panel, the benzamidine bound to PknB$_{SA-KD}$ in three of the six chains of the asymmetric unit is shown as a stick model. The benzamidine is not visible in the other two panels.
doi:10.1371/journal.pone.0039136.g007

Analysis of surface conservation

In order to identify conserved features and compare them with homologous proteins, the PknB$_{SA-KD}$ sequence was aligned with

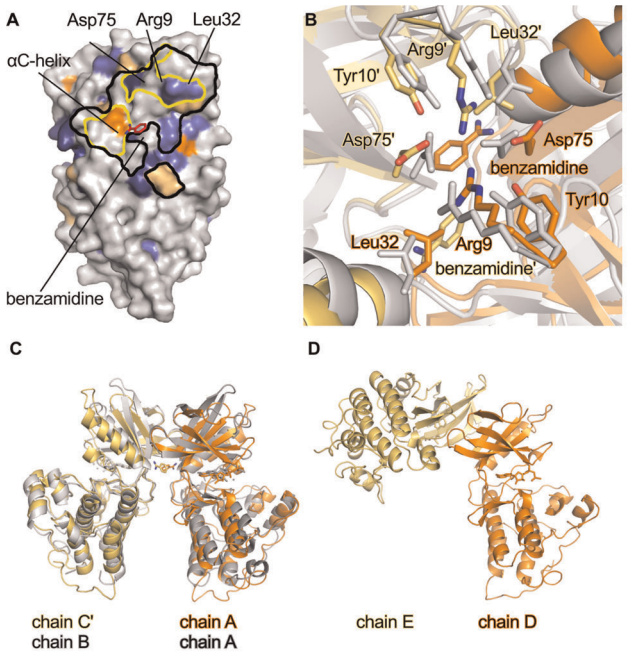

Figure 8. Analysis of $PknB_{SA\text{-}KD}$ crystal contacts. (A). Footprint of contacts between a symmetry mate of molecule C (C′) and molecule A in the crystals. Molecule A is shown in surface representation. Areas within black lines indicate crystal contacts with molecule C′ (distance <4.5 Å). Areas within yellow lines indicate the residues involved in dimer formation [22]. The surface conservation is shown as in Fig. 7, and the benzamidine is bound to chain A of $PknB_{SA\text{-}KD}$ is shown as a red stick model. Molecule pairs B/B′ and C′/A form similar crystal contacts. (B). Detailed view into the dimer interface formed by the A/C′ dimer. Chains A and C′ of $PknB_{SA\text{-}KD}$ are shown in orange and yellow, respectively. Chains A and B of dimeric *M. tuberculosis* PknB (PDB ID: 1MRU [24]) are in grey. Residues Arg9, Tyr10, Leu32 and Asp75, which are involved in dimer formation, are represented with sticks. These residues were also used for superimposing the two dimers. (C). Overview of the orientation of the dimer of *M. tuberculosis* PknB and $PknB_{SA\text{-}KD}$. The colors are the same as in panel B. The N-lobes of $PknB_{SA\text{-}KD}$ chain A and *M. tuberculosis* PknB chain A were superposed. (D). Crystal contact involving chains D and E in $PknB_{SA\text{-}KD}$. The orientation of chain D is the same as that of chain A in panel C.
doi:10.1371/journal.pone.0039136.g008

representatives of several bacterial STKs (Fig. S6). For our analysis, we selected the bacterial STKs recently analyzed by Pereira *et al.* [10]. All analyzed kinases exhibit strong conservation in the prototypical regions required for catalytic function, such as the DFG-, HRD- and SPE-motifs and the glycine-rich loop. In order to depict the location and distribution of conserved residues, we mapped them onto the surface of $PknB_{SA\text{-}KD}$ (Fig. 7). As expected, residues important for the catalytic function of the kinase are highly conserved (highlighted blue in Fig. 7). These residues cluster in the ATP-binding site, the glycine-rich loop, and the DFG-, HRD- and SPE-motifs. However, a small number of residues are highly conserved in most other kinases but differ from the consensus sequence in PknB (highlighted orange in Fig. 7). The remaining surface of $PknB_{SA\text{-}KD}$ is remarkably devoid of conserved residues.

Discussion

We report here the crystal structure of the catalytically competent kinase region of *S. aureus* PknB. In its physiological context, the kinase is attached to the bacterial cell wall *via* a membrane anchor, and it phosphorylates substrates in response to stimuli that engage the extracellular PASTA domains. Activity assays demonstrate that purified $PknB_{SA\text{-}KD}$ is able to phosphorylate substrates efficiently. However, an analysis of structural parameters that define the active states of protein kinases clearly demonstrates that $PknB_{SA\text{-}KD}$ has crystallized in an inactive conformation. Although it does bind the ATP analog AMP-PNP, this substrate is not bound in a conformation that would enable catalysis. The AMP-PNP triphosphate moiety is not contacted by either a magnesium ion or residues from the glycine-rich loop or the DFG-motif. As $PknB_{SA\text{-}KD}$ is catalytically active in solution, it is conceivable that it exists in different conformations, corresponding to active and inactive states, in solution, perhaps owing to different states of phosphorylation. Hence, crystallization likely selected the inactive state.

Dimer formation

An attractive scenario for PknB activation could be based on dimer formation, and dimerization has in fact been implicated in the regulation of the activity of the *M. tuberculosis* PknB kinase domain. In that case, the kinase domain forms dimers that are stabilized by a salt bridge between Arg9 in one monomer and Asp75 of another monomer [22,51]. Although $PknB_{SA\text{-}KD}$ consistently eluted as a monomer in gel filtration experiments in solution (Fig. S1A), it is conceivable that low-affinity dimerization of $PknB_{SA\text{-}KD}$ could occur at higher concentration. This hypothesis was evaluated by chemical crosslinking experiments using glutaraldehyde (Fig. S7). No crosslinked dimer of $PknB_{SA\text{-}KD}$ was obtained under any of the tested conditions, while a control protein known to form trimers could be successfully cross-linked under identical conditions. Additionally, inspection of the crystal packing can sometimes provide clues about the possible existence of oligomers. We find that three of the six $PknB_{SA\text{-}KD}$ molecules present in the crystals form nearly identical dimers with their symmetry mates (A–C′, B–B′, C–A′), and the arrangement of these putative dimers resembles the *M. tuberculosis* PknB dimer (Fig. 8). It is therefore conceivable that activation of *S. aureus* PknB also involves dimerization. We note, however, that the putative $PknB_{SA\text{-}KD}$ dimer interface contains benzamidine, a compound that was present in the crystallization solution and that was required to obtain good-quality crystals. The observed dimer may therefore be a crystallization artifact. Moreover, the three remaining molecules in the crystals (chains D, E, F) do not form similar dimers.

It is of course possible that dimerization of the kinase region is linked to its phosphorylation status, and that the copies of $PknB_{SA\text{-}KD}$ present in the crystals have different states of phosphorylation, thus impacting their dimerization properties.

Another, perhaps more likely, scenario could link dimerization to the extracellular PASTA domains, which could alter their association state in response to signal binding [11,17].

Inhibition helix

Although it represents an inactive conformation of the kinase, the $PknB_{SA\text{-}KD}$ crystal structure nevertheless provides insights into a pathway of activation. In order to activate $PknB_{SA\text{-}KD}$, the αC-helix would need to significantly change its location by rotating into the binding site. Such a rotation, however, is not possible in our crystal structure because the space that would accommodate the rotated αC-helix is already occupied by the activation segment, which forms a short helix directly following the DFG-motif (Fig. 4 and Fig. S4A). The activation loop of active kinases makes close contacts with the C-lobe, whereas in $PknB_{SA\text{-}KD}$ it interacts with the N-lobe and the αC-helix.

The activation segment would have to be displaced to allow for the formation of an active PknB conformation. This could be triggered by autophosphorylation in the activation segment. Thr164 could play a key role in this conformational change. Structural alignments with inactive c-Src kinase reveal a similar orientation of the activation segment, with an autoinhibition helix blocking the inward rotation of the αC-helix [36,52] (Fig. 4). In this case, c-Src can be activated through the phosphorylation of residue Tyr416, which is the residue equivalent to Thr164 in PknB.

A dissolving of the inactive state of the activation segment could conceivably trigger a downward movement of the glycine-rich loop to stabilize the β- and γ-phosphates of the ATP. Due to weak electron density as a result of flexibility, it is not possible to model the activation segment. However, difference electron density in this region suggests that parts of the activation loop lie next to the glycine-rich loop, preventing interaction of the glycine-rich loop with phosphates.

In conclusion, our structural study provides improved understanding of the function of eukaryotic like serine/threonine kinases in bacteria at the molecular level. Future work will aim at the identification of substrates of PknB, the molecular mechanisms of substrate selection and the role of autophosphorylation for the activity of the kinase. In particular, the role of ligand-dependent dimerization of extracellular PASTA domains for activation of PknB remains to be clarified. Moreover, recent work provided evidence that PknB is embedded in the tight regulatory network controlling virulence of *S. aureus*. The structural information presented in this study may serve as a basis for further investigations of the molecular mechanisms determining pathogenesis of the major human pathogen *S. aureus*.

Supporting Information

Figure S1 Biochemical and biophysical analysis of purified $PknB_{SA\text{-}KD}$. A. Size-exclusion chromatography run on Superdex 75 (PC 3.2/30). The elution profile of $PknB_{SA\text{-}KD}$ is shown in red in comparison to standard proteins. B. SDS-PAGE of purified $PknB_{SA\text{-}KD}$. C. CD-spectrum of purified $PknB_{SA\text{-}KD}$.
(TIF)

Figure S2 B-factor plot for the six chains of $PknB_{SA\text{-}KD}$ present in the asymmetric unit. Secondary structure elements are aligned below the plot, with α-helices colored in blue and β-strands colored in orange. The red line indicates the overall B-factor average for all six chains.
(TIF)

Figure S3 Stereo view into the AMP-PNP binding site. The depicted map is an omit map (F_{obs}-F_{calc}) of the ligand, contoured at 3.0 σ and drawn with a radius of 5Å around AMP-PNP. Panels A and B show omit maps of the AMP-PNP bound to chains A and D, respectively.
(TIF)

Figure S4 Stereo views of representative omit maps of $PknB_{SA\text{-}KD}$. All panels show F_{obs}-F_{calc} omit electron density maps contoured at 1.0 σ. In panel A the omit map for the DFG-motif and the inhibition helix is shown. Panel B shows the phosphate binding region. Panels C and D show the omit map for the αF-helix for chain A in panel C and chain D in panel D. Maps were drawn with radii of 3Å (panels A, C and D) and 8Å (panel B) around the depicted coordinates. The larger radius for panel B was chosen to show that no extra density that would account for a magnesium ion exists in the vicinity of the AMP-PNP ligand.
(TIF)

Figure S5 Orientation of the glycine-rich loop. All kinases were aligned with the C-lobe of $PknB_{SA\text{-}KD}$ (residues 100–250). The $PknB_{SA\text{-}KD}$ structure is drawn in orange. The closed PKA structure is shown in green (PDB ID: 1ATP [35]), and the open PKA structure is shown in red (PDB ID: 1CTP [34]). The kinase domain of c-Src (PDB ID: 2SRC [36]) is shown in purple.
(TIF)

Figure S6 Alignment of selected kinases and analysis of conservation. The kinases were selected according to [10]. Five kinases were omitted due to lack of DFG-, SPE-, HRD-motif or the N-lobe. The color code is identical to that used in Fig 7. Blue indicates highly conserved residues (100–91% conservation in dark blue 88–74% in blue and 69–54% light blue). Residues highly conserved but different in $PknB_{SA\text{-}KD}$ are colored in orange (88–71% in orange, 69–54% in light orange). The selected kinases are (Uniprot-ID in parentheses): *Staphylococcus aureus*, PknB (Q7A5Z8); *Bacillus subtilis*, PrkC (O34507); *Corynebacterium glutamicum*, PknA (Q8NU97); *Corynebacterium glutamicum*, PknB (Q8NU98); *Corynebacterium glutamicum*, PknG (Q6M299); *Corynebacterium glutamicum*, PknL (Q6M3Q8); *Mycobacterium tuberculosis*, PknA (P65726); *Mycobacterium tuberculosis*, PknB (P0A5S4); *Mycobacterium tuberculosis*, PknD (O05871); *Mycobacterium tuberculosis*, PknE (P72003); *Mycobacterium tuberculosis*, PknF (P72003); *Mycobacterium tuberculosis*, PknG (P65728); *Mycobacterium tuberculosis*, PknH (Q11053); *Mycobacterium tuberculosis*, PknI (P65730); *Mycobacterium tuberculosis*, PknJ (P65732); *Mycobacterium tuberculosis*, PknK (P95078); *Mycobacterium tuberculosis*, PknL (O53510); *Myxococcus xanthus*, Pkn4 (Q95478); *Myxococcus xanthus*, Pkn8 (Q9XBP6); *Myxococcus xanthus*, Pkn14 (Q93NE3); *Pseudomonas aeruginosa*, PpkA (Q9I758); *Streptococcus pneumonia*, StkP (Q8KY50).
(TIF)

Figure S7 Chemical cross-linking of $PknB_{SA\text{-}KD}$ and controls with glutaraldehyde. Shown is an SDS-PAGE analysis of the crosslinking experiment. Untreated (ut) protein was loaded on the gel next to each protein as controls. The small bands in $PknB_{SA\text{-}KD}$ lanes indicate a weak impurity of $PknB_{SA\text{-}KD}$ at 80 kDa.
(TIF)

Acknowledgments

We thank the beam line staff at the Swiss Light Source for assistance with data collection.

Author Contributions

Conceived and designed the experiments: SR SD KO TS. Performed the experiments: SR SD. Analyzed the data: SR SD KO TS. Wrote the paper: SR SD KO TS.

References

1. Klevens RM, Morrison MA, Nadle J, Petit S, Gershman K, et al. (2007) Invasive methicillin-resistant *Staphylococcus aureus* infections in the United States. JAMA: the journal of the American Medical Association 298: 1763–1771.
2. Hansra NK, Shinkai K (2011) Cutaneous community-acquired and hospital-acquired methicillin-resistant *Staphylococcus aureus*. Dermatologic therapy 24: 263–272.
3. Bohach GA, Fast DJ, Nelson RD, Schlievert PM (1990) Staphylococcal and streptococcal pyrogenic toxins involved in toxic shock syndrome and related illnesses. Critical reviews in microbiology 17: 251–272.
4. Lowy FD (1998) *Staphylococcus aureus* infections. The New England journal of medicine 339: 520–532.

5. Deftereos SP, Michailidou E, Karagiannakis GK, Grigoriadi S, Prassopoulos P (2009) Hematogenous infantile infection presenting as osteomyelitis and septic arthritis: a case report. Cases journal 2: 8293.
6. Aguilar J, Urday-Cornejo V, Donabedian S, Perri M, Tibbetts R, et al. (2010) *Staphylococcus aureus* meningitis: case series and literature review. Medicine 89: 117–125.
7. Otto M (2010) Looking toward basic science for potential drug discovery targets against community-associated MRSA. Medicinal research reviews 30: 1–22.
8. Hunter T (1995) Protein kinases and phosphatases: the yin and yang of protein phosphorylation and signaling. Cell 80: 225–236.
9. Kennelly PJ (2002) Protein kinases and protein phosphatases in prokaryotes: a genomic perspective. FEMS microbiology letters 206: 1–8.
10. Pereira SF, Goss L, Dworkin J (2011) Eukaryote-like serine/threonine kinases and phosphatases in bacteria. Microbiology and molecular biology reviews: MMBR 75: 192–212.
11. Ruggiero A, Squeglia F, Marasco D, Marchetti R, Molinaro A, et al. (2011) X-ray structural studies of the entire extracellular region of the serine/threonine kinase PrkC from *Staphylococcus aureus*. The Biochemical journal 435: 33–41.
12. Donat S, Streker K, Schirmeister T, Rakette S, Stehle T, et al. (2009) Transcriptome and functional analysis of the eukaryotic-type serine/threonine kinase PknB in *Staphylococcus aureus*. Journal of bacteriology 191: 4056–4069.
13. Lomas-Lopez R, Paracuellos P, Riberty M, Cozzone AJ, Duclos B (2007) Several enzymes of the central metabolism are phosphorylated in *Staphylococcus aureus*. FEMS microbiology letters 272: 35–42.
14. De Lencastre H, Wu SW, Pinho MG, Ludovice AM, Filipe S, et al. (1999) Antibiotic resistance as a stress response: complete sequencing of a large number of chromosomal loci in *Staphylococcus aureus* strain COL that impact on the expression of resistance to methicillin. Microbial drug resistance 5: 163–175.
15. Yeats C, Finn RD, Bateman A (2002) The PASTA domain: a beta-lactam-binding domain. Trends in biochemical sciences 27: 438.
16. Gordon E, Mouz N, Duee E, Dideberg O (2000) The crystal structure of the penicillin-binding protein 2x from *Streptococcus pneumoniae* and its acyl-enzyme form: implication in drug resistance. Journal of molecular biology 299: 477–485.
17. Paracuellos P, Ballandras A, Robert X, Kahn R, Herve M, et al. (2010) The extended conformation of the 2.9-A crystal structure of the three-PASTA domain of a Ser/Thr kinase from the human pathogen *Staphylococcus aureus*. Journal of molecular biology 404: 847–858.
18. Truong-Bolduc QC, Hooper DC (2010) Phosphorylation of MgrA and its effect on expression of the NorA and NorB efflux pumps of *Staphylococcus aureus*. Journal of bacteriology 192: 2525–2534.
19. Tamber S, Schwartzman J, Cheung AL (2010) Role of PknB kinase in antibiotic resistance and virulence in community-acquired methicillin-resistant *Staphylococcus aureus* strain USA300. Infection and immunity 78: 3637–3646.
20. Miller M, Donat S, Rakette S, Stehle T, Kouwen TR, et al. (2010) Staphylococcal PknB as the first prokaryotic representative of the proline-directed kinases. PloS one 5: e9057.
21. Debarbouille M, Dramsi S, Dussurget O, Nahori MA, Vaganay E, et al. (2009) Characterization of a serine/threonine kinase involved in virulence of *Staphylococcus aureus*. Journal of bacteriology 191: 4070–4081.
22. Lombana TN, Echols N, Good MC, Thomsen ND, Ng HL, et al. (2010) Allosteric activation mechanism of the *Mycobacterium tuberculosis* receptor Ser/Thr protein kinase, PknB. Structure 18: 1667–1677.
23. Ortiz-Lombardia M, Pompeo F, Boitel B, Alzari PM (2003) Crystal structure of the catalytic domain of the PknB serine/threonine kinase from *Mycobacterium tuberculosis*. The Journal of biological chemistry 278: 13094–13100.
24. Young TA, Delagoutte B, Endrizzi JA, Falick AM, Alber T (2003) Structure of *Mycobacterium tuberculosis* PknB supports a universal activation mechanism for Ser/Thr protein kinases. Nature structural biology 10: 168–174.
25. Mieczkowski C, Iavarone AT, Alber T (2008) Auto-activation mechanism of the *Mycobacterium tuberculosis* PknB receptor Ser/Thr kinase. The EMBO journal 27: 3186–3197.
26. Wehenkel A, Fernandez P, Bellinzoni M, Catherinot V, Barilone N, et al. (2006) The structure of PknB in complex with mitoxantrone, an ATP-competitive inhibitor, suggests a mode of protein kinase regulation in mycobacteria. FEBS letters 580: 3018–3022.
27. Kabsch W (2010) Xds. Acta crystallographica Section D, Biological crystallography 66: 125–132.
28. McCoy AJ, Grosse-Kunstleve RW, Adams PD, Winn MD, Storoni LC, et al. (2007) Phaser crystallographic software. Journal of applied crystallography 40: 658–674.
29. Emsley P, Lohkamp B, Scott WG, Cowtan K (2010) Features and development of Coot. Acta crystallographica Section D, Biological crystallography 66: 486–501.
30. Adams PD, Afonine PV, Bunkoczi G, Chen VB, Davis IW, et al. (2010) PHENIX: a comprehensive Python-based system for macromolecular structure solution. Acta crystallographica Section D, Biological crystallography 66: 213–221.
31. Brunger AT (1992) Free R value: a novel statistical quantity for assessing the accuracy of crystal structures. Nature 355: 472–475.
32. Schuttelkopf AW, van Aalten DM (2004) PRODRG: a tool for high-throughput crystallography of protein-ligand complexes. Acta crystallographica Section D, Biological crystallography 60: 1355–1363.
33. Av-Gay Y, Jamil S, Drews SJ (1999) Expression and characterization of the *Mycobacterium tuberculosis* serine/threonine protein kinase PknB. Infection and immunity 67: 5676–5682.
34. Karlsson R, Zheng J, Xuong N, Taylor SS, Sowadski JM (1993) Structure of the mammalian catalytic subunit of cAMP-dependent protein kinase and an inhibitor peptide displays an open conformation. Acta crystallographica Section D, Biological crystallography 49: 381–388.
35. Zheng J, Trafny EA, Knighton DR, Xuong NH, Taylor SS, et al. (1993) 2.2 A refined crystal structure of the catalytic subunit of cAMP-dependent protein kinase complexed with MnATP and a peptide inhibitor. Acta crystallographica Section D, Biological crystallography 49: 362–365.
36. Xu W, Doshi A, Lei M, Eck MJ, Harrison SC (1999) Crystal structures of c-Src reveal features of its autoinhibitory mechanism. Molecular cell 3: 629–638.
37. Thompson JD, Higgins DG, Gibson TJ (1994) CLUSTAL W: improving the sensitivity of progressive multiple sequence alignment through sequence weighting, position-specific gap penalties and weight matrix choice. Nucleic acids research 22: 4673–4680.
38. Gouet P, Courcelle E, Stuart DI, Metoz F (1999) ESPript: analysis of multiple sequence alignments in PostScript. Bioinformatics 15: 305–308.
39. Gille C, Frommel C (2001) STRAP: editor for STRuctural Alignments of Proteins. Bioinformatics 17: 377–378.
40. Taylor SS, Kornev AP (2011) Protein kinases: evolution of dynamic regulatory proteins. Trends in biochemical sciences 36: 65–77.
41. Kornev AP, Haste NM, Taylor SS, Eyck LF (2006) Surface comparison of active and inactive protein kinases identifies a conserved activation mechanism. Proceedings of the National Academy of Sciences of the United States of America 103: 17783–17788.
42. Kornev AP, Taylor SS (2010) Defining the conserved internal architecture of a protein kinase. Biochimica et biophysica acta 1804: 440–444.
43. Kornev AP, Taylor SS, Ten Eyck LF (2008) A helix scaffold for the assembly of active protein kinases. Proceedings of the National Academy of Sciences of the United States of America 105: 14377–14382.
44. Bossemeyer D (1994) The glycine-rich sequence of protein kinases: a multifunctional element. Trends in biochemical sciences 19: 201–205.
45. Saraste M, Sibbald PR, Wittinghofer A (1990) The P-loop–a common motif in ATP- and GTP-binding proteins. Trends in biochemical sciences 15: 430–434.
46. Huse M, Kuriyan J (2002) The conformational plasticity of protein kinases. Cell 109: 275–282.
47. Cox S, Radzio-Andzelm E, Taylor SS (1994) Domain movements in protein kinases. Current opinion in structural biology 4: 893–901.
48. Johnson LN, Noble ME, Owen DJ (1996) Active and inactive protein kinases: structural basis for regulation. Cell 85: 149–158.
49. Hubbard SR (1999) Src autoinhibition: let us count the ways. Nature structural biology 6: 711–714.
50. Jeffrey PD, Russo AA, Polyak K, Gibbs E, Hurwitz J, et al. (1995) Mechanism of CDK activation revealed by the structure of a cyclinA-CDK2 complex. Nature 376: 313–320.
51. Alber T (2009) Signaling mechanisms of the *Mycobacterium tuberculosis* receptor Ser/Thr protein kinases. Current opinion in structural biology 19: 650–657.
52. Schulze-Gahmen U, De Bondt HL, Kim SH (1996) High-resolution crystal structures of human cyclin-dependent kinase 2 with and without ATP: bound waters and natural ligand as guides for inhibitor design. Journal of medicinal chemistry 39: 4540–4546.

9.2.1 Supplemental figures- Structural analysis of *Staphylococcus aureus* serine/threonine kinase PknB

Figure S1 Biochemical and biophysical analysis of purified $PknB_{SA\text{-}KD}$. A. Size-exclusion chromatography run on Superdex 75 (PC 3.2/30). The elution profile of $PknB_{SA\text{-}KD}$ is shown in red in comparison to standard proteins. B. SDS-PAGE of purified $PknB_{SA\text{-}KD}$. C. CD-spectrum of purified $PknB_{SA\text{-}KD}$.

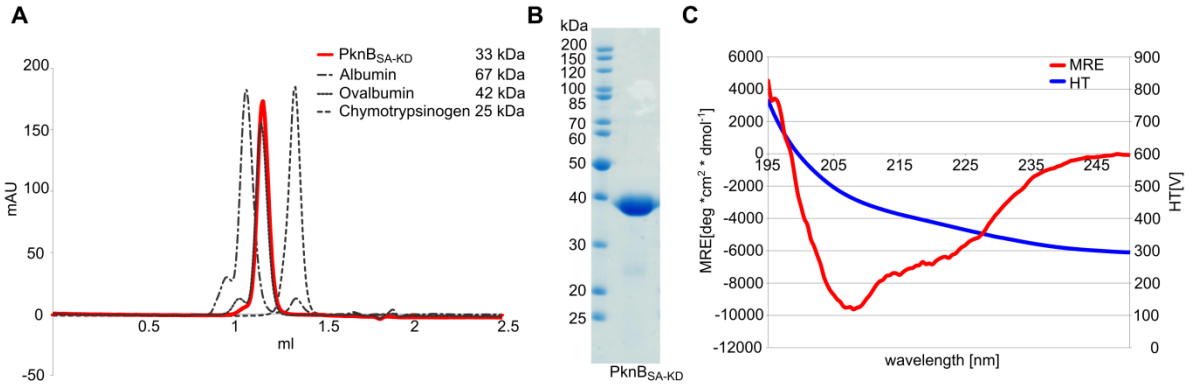

Figure S2 B-factor plot for the six chains of $PknB_{SA\text{-}KD}$ present in the asymmetric unit. Secondary structure elements are aligned below the plot, with α-helices colored in blue and β-strands colored in orange. The red line indicates the overall B-factor average for all six chains.

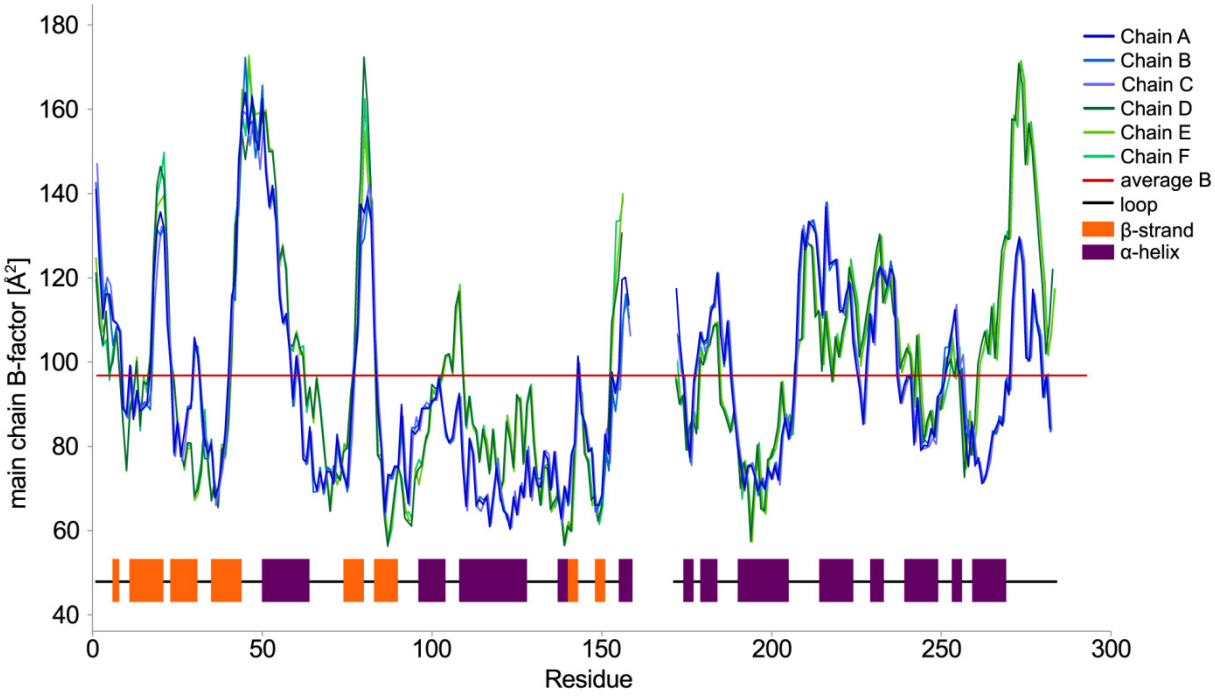

<u>Figure S3</u> Stereo view into the AMP-PNP binding site. The depicted map is an omit map (F_{obs}-F_{calc}) of the ligand, contoured at 3.0 σ and drawn with a radius of 5Å around AMPPNP. Panels A and B show omit maps of the AMP-PNP bound to chains A and D, respectively.

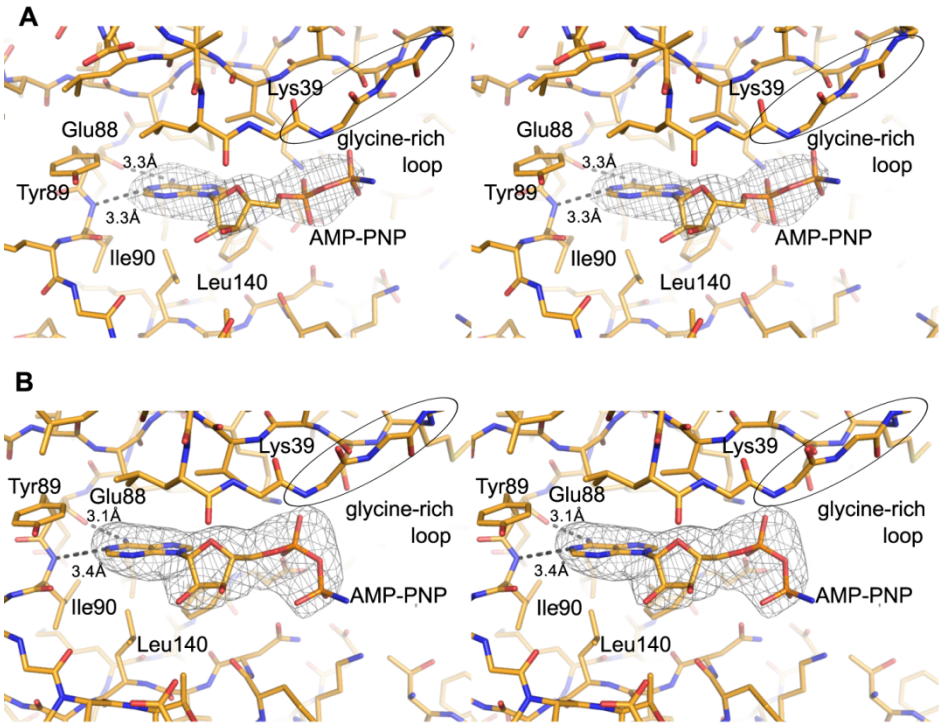

<u>Figure S4</u> Stereo views of representative omit maps of PknB$_{SA-KD}$. All panels show F_{obs}-F_{calc} omit electron density maps contoured at 1.0 σ. In panel A the omit map for the DFG-motif and the inhibition helix is shown. Panel B shows the phosphate binding region. Panels C and D show the omit map for the αF-helix for chain A in panel C and chain D in panel D. Maps were drawn with radii of 3Å (panels A, C and D) and 8Å (panel B) around the depicted coordinates. The larger radius for panel B was chosen to show that no extra density that would account for a magnesium ion exists in the vicinity of the AMP-PNP ligand.

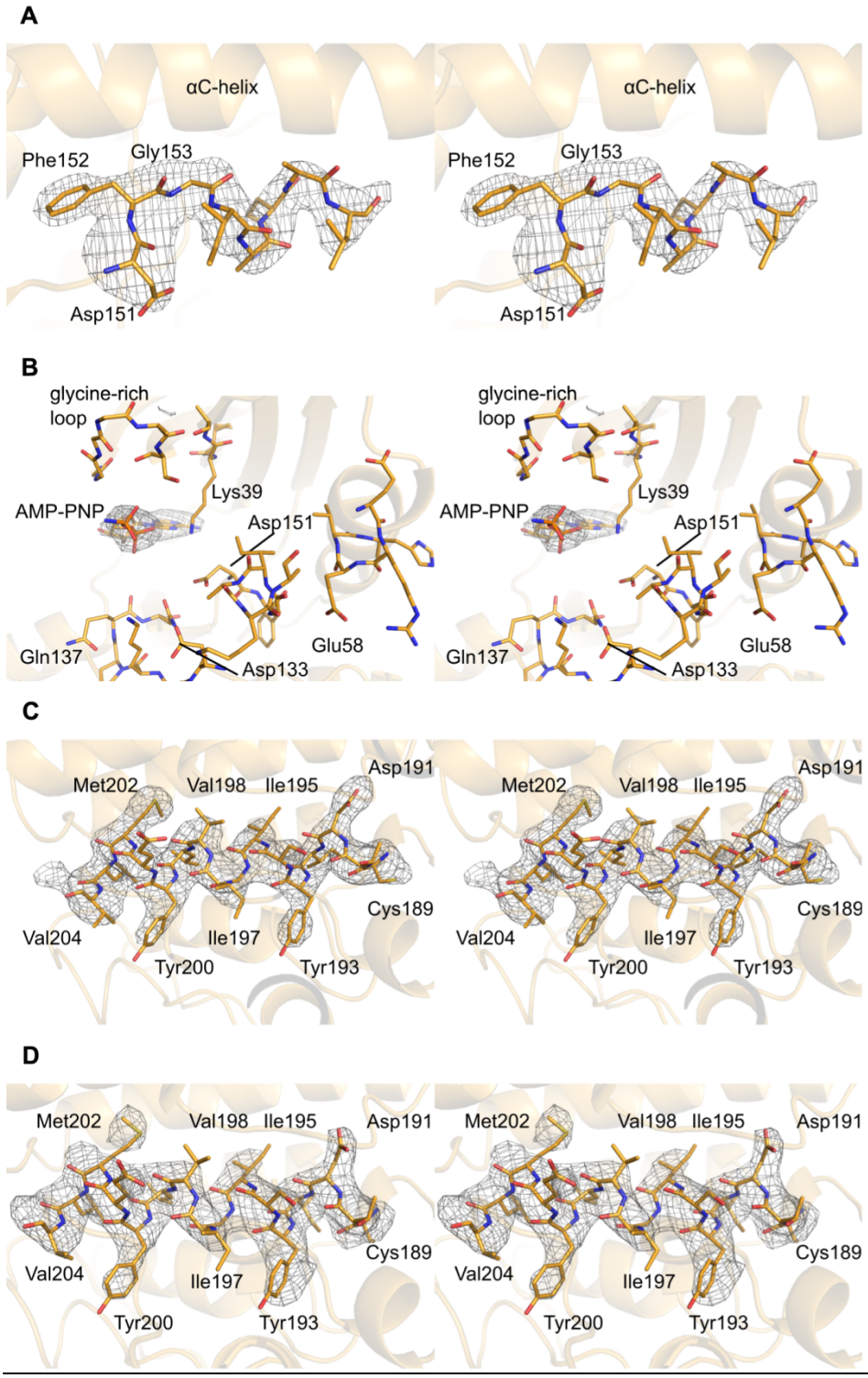

Figure S5 Orientation of the glycine-rich loop. All kinases were aligned with the C-lobe of $PknB_{SA\text{-}KD}$ (residues 100–250). The $PknB_{SA\text{-}KD}$ structure is drawn in orange. The closed PKA structure is shown in green (PDB ID: 1ATP [35]), and the open PKA structure is shown in red (PDB ID: 1CTP [34]). The kinase domain of c-Src (PDB ID: 2SRC [36]) is shown in purple.

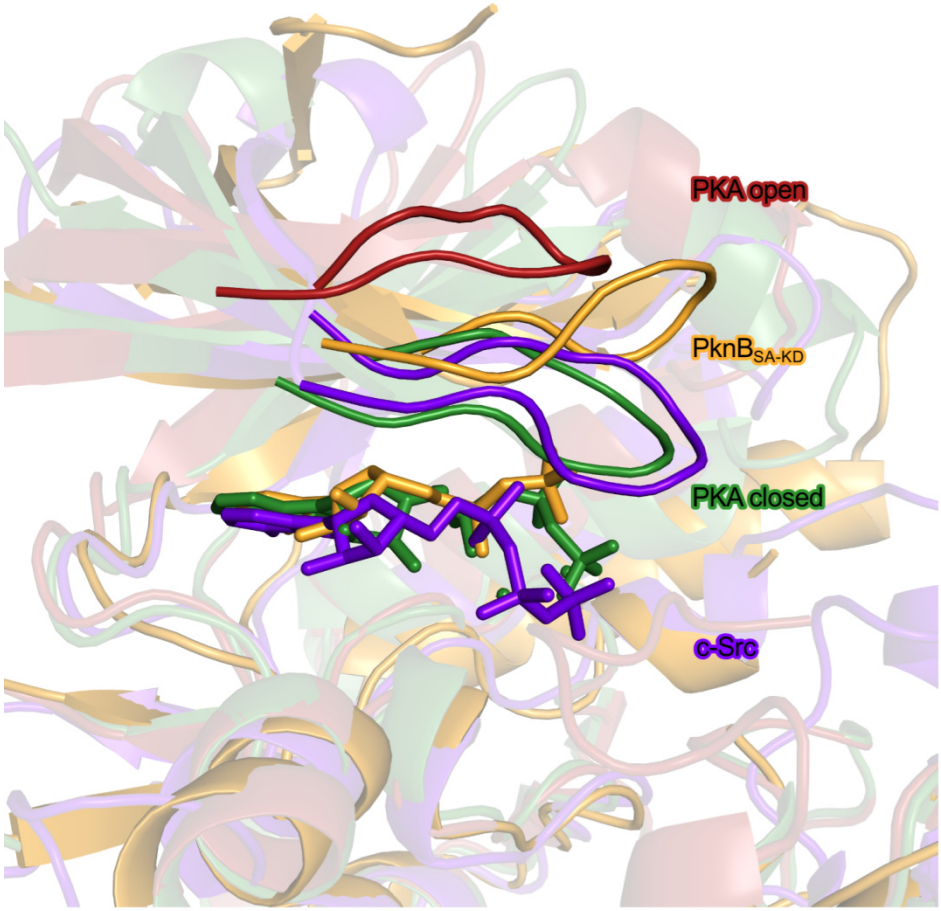

Figure S6 Alignment of selected kinases and analysis of conservation. The kinases were selected according to [10]. Five kinases were omitted due to lack of DFG-, SPE-, HRD-motif or the N-lobe. The color code is identical to that used in Fig 7. Blue indicates highly conserved residues (100–91% conservation in dark blue 88–74% in blue and 69–54% light blue). Residues highly conserved but different in $PknB_{SA\text{-}KD}$ are colored in orange (88– 71% in orange, 69–54% in light orange). The selected kinases are (Uniprot-ID in parentheses): *Staphylococcus aureus*, PknB (Q7A5Z8); *Bacillus subtilis*, PrkC (O34507); *Corynebacterium glutamicum,* PknA (Q8NU97); *Corynebacterium glutamicum*, PknB (Q8NU98); *Corynebacterium glutamicum*, PknG (Q6M299); *Corynebacterium glutamicum*, PknL (Q6M3Q8); *Mycobacterium tuberculosis*, PknA (P65726); *Mycobacterium tuberculosis*, PknB (P0A5S4); *Mycobacterium tuberculosis*, PknD (O05871); *Mycobacterium tuberculosis*, PknE (P72003); *Mycobacterium tuberculosis*, PknF (P72003); *Mycobacterium tuberculosis*, PknG (P65728); *Mycobacterium tuberculosis*, PknH (Q11053); *Mycobacterium tuberculosis*, PknI (P65730); *Mycobacterium tuberculosis*, PknJ (P65732); *Mycobacterium tuberculosis*, PknK (P95078); *Mycobacterium tuberculosis*, PknL (O53510); Myxococcus xanthus, Pkn4 (Q95478); *Myxococcus xanthus*, Pkn8 (Q9XBP6); *Myxococcus xanthus*, Pkn14 (Q93NE3); *Pseudomonas aeruginosa*, PpkA (Q9I758); *Streptococcus pneumonia*, StkP (Q8KY50).

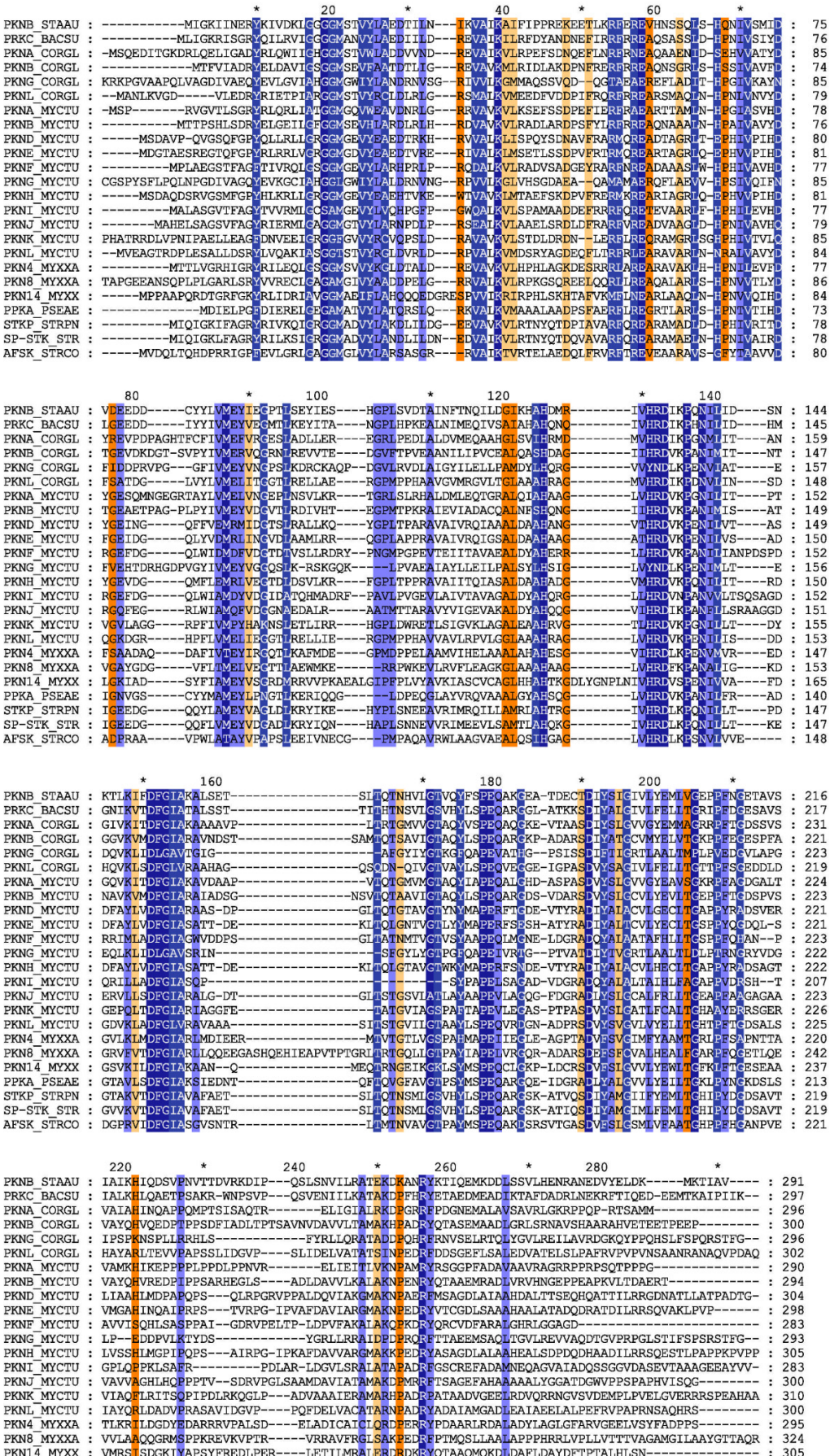

<u>Figure S7</u> Chemical cross-linking of $PknB_{SA-KD}$ and controls with glutaraldehyde. Shown is an SDS-PAGE analysis of the crosslinking experiment. Untreated (ut) protein was loaded on the gel next to each protein as controls. The small bands in $PknB_{SA-KD}$ lanes indicate a weak impurity of $PknB_{SA-KD}$ at 80 kDa.

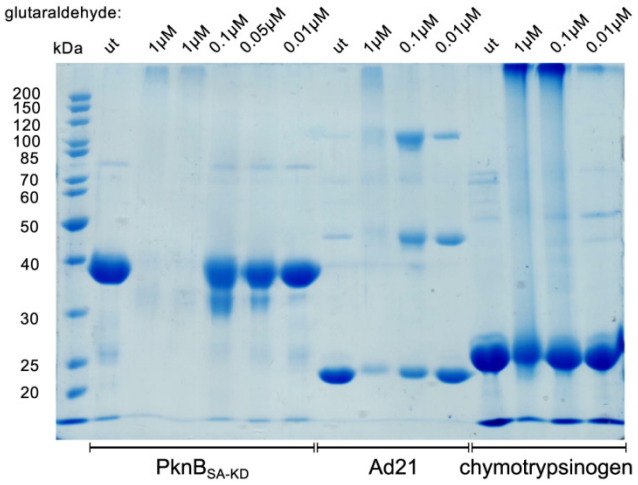

9.3 Transcriptome and functional analysis of the eukaryotic-type serine/threonine kinase PknB in *Staphylococcus aureus*

Transcriptome and functional analysis of the eukaryotic-type serine/threonine kinase PknB in *Staphylococcus aureus*

Donat S, Streker K, Schirmeister T, Rakette S, Stehle T, Liebeke M, Lalk M, Ohlsen K.

J Bacteriol. 2009 Jul;191(13):4056-69. Epub 2009 Apr 17.

JOURNAL OF BACTERIOLOGY, July 2009, p. 4056–4069 Vol. 191, No. 13
0021-9193/09/$08.00+0 doi:10.1128/JB.00117-09

Transcriptome and Functional Analysis of the Eukaryotic-Type Serine/Threonine Kinase PknB in *Staphylococcus aureus*[▽]

Stefanie Donat,[1] Karin Streker,[1] Tanja Schirmeister,[2] Sonja Rakette,[3] Thilo Stehle,[3] Manuel Liebeke,[4] Michael Lalk,[4] and Knut Ohlsen[1]*

Universität Würzburg, Institut für Molekulare Infektionsbiologie, Würzburg, Germany[1]; Universität Würzburg, Institut für Pharmazie und Lebensmittelchemie, Würzburg, Germany[2]; Universität Tübingen, Interfakultäres Institut für Biochemie, Strukturbiologie, Tübingen, Germany[3]; and Ernst-Moritz-Arndt-Universität Greifswald, Institut für Pharmazie, Kompetenzzentrum Functional Genomics, Greifswald, Germany[4]

Received 28 January 2009/Accepted 6 April 2009

The function of the *Staphylococcus aureus* eukaryotic-like serine/threonine protein kinase PknB was investigated by performing transcriptome analysis using DNA microarray technology and biochemical assays. The transcriptional profile revealed a strong regulatory impact of PknB on the expression of genes encoding proteins which are involved in purine and pyrimidine biosynthesis, cell wall metabolism, autolysis, and glutamine synthesis. Functional activity of overexpressed and purified PknB kinase was demonstrated using the myelin basic protein as a surrogate substrate. Phosphorylation occurred in a time-dependent manner with Mn^{2+} as a preferred cofactor. Furthermore, biochemical characterization revealed regulation of adenylosuccinate synthase (PurA) activity by phosphorylation. Phosphorylated PurA showed a 1.8-fold decrease in enzymatic activity compared to unphosphorylated PurA. Loss of PknB led to formation of larger cell clusters, and a *pknB* deletion strain showed 32-fold-higher sensitivity to the cell wall-active antibiotic tunicamycin. The results of this study strongly indicate that PknB has a role in regulation of purine biosynthesis, autolysis, and central metabolic processes in *S. aureus*.

The phosphorylation of proteins is a key regulatory mechanism in the signal transduction pathways of both prokaryotes and eukaryotes. Typically, extracellular signals are translated into cellular responses. The phosphorylation of proteins is carried out by specific protein kinases and is coupled to dephosphorylation reactions catalyzed by protein phosphatases. In prokaryotes sensing of extracellular signals and transduction of information are usually mediated by two-component signal transduction systems consisting of histidine kinase sensors and their associated response regulators (42). In contrast, signal transduction in eukaryotes occurs via phosphorylation of serine, threonine, and tyrosine residues. Serine/threonine and tyrosine kinases and phosphatases control reversible phosphorylation of target proteins in eukaryotes and are essential for cell cycle control and differentiation (17, 19).

It has recently been shown in a number of studies that eukaryotic-type serine/threonine protein kinases (STPKs) and phosphatases are also expressed in many prokaryotes (2). Prokaryotic STPKs regulate various cellular functions, such as stress responses, biofilm formation, sporulation, and metabolic and developmental processes (20, 23, 30, 34, 37, 39, 46). STPKs also play a role in the virulence of many bacterial pathogens, such as streptococci, *Mycobacterium tuberculosis*, *Yersinia pseudotuberculosis*, and *Pseudomonas aeruginosa* (11, 16, 21, 36, 47). Although the functional roles of protein kinases have been described in previous studies, only a small number of target substrates have been identified so far. Moreover, the impact of phosphorylation and dephosphorylation of target protein functions has been investigated in only some cases (33, 38).

A single STPK has been found to be conserved in all sequenced strains of *Staphylococcus aureus*. Originally, this kinase was identified by using a transposon mutagenesis approach used to identify factors that modulate methicillin (meticillin) resistance in methicillin-resistant *S. aureus* (MRSA) (13). Recent work has demonstrated the functional kinase activity of PknB and has identified potential substrates. Most of the identified substrates of PknB are proteins which are involved in the central metabolism of bacteria, such as trigger factor, DnaK, enolase, pyruvate dehydrogenase, and the regulator MgrA (27, 44). These observations suggest a broad regulatory role for PknB in *S. aureus*. Interestingly, some of the MRSA strains in the database encode a second protein with a eukaryote-like tyrosine kinase domain located on the SCCmec element. In contrast to PknB, this putative protein kinase does not contain PASTA (penicillin-binding and Ser/Thr kinase-associated) domains. At present, it is not known if the second eukaryote-like tyrosine kinase is functionally active in *S. aureus*.

In this study, we functionally characterized PknB (SA1063) of *S. aureus* by constructing a *pknB* deletion mutant. To explore the role of PknB in gene expression, we studied expression of genes on a global scale by using comparative DNA microarray hybridization. We report here that *pknB* deletion affects the expression of genes belonging to specific regulons which are involved in central metabolic functions, including purine and pyrimidine biosynthesis, cell wall metabolism, and the citrate cycle. Furthermore, we show that purified PknB kinase phosphorylates myelin basic protein (MBP), which has been used as a surrogate sub-

* Corresponding author. Mailing address: Institut für Molekulare Infektionsbiologie, Röntgenring 11, D-97070 Würzburg, Germany. Phone: 49-931-312155. Fax: 49-931-312578. E-mail: knut.ohlsen@mail.uni-wuerzburg.de.

▽ Published ahead of print on 17 April 2009.

TABLE 1. Bacterial strains, plasmids, and PCR primers used in this study

Strain, plasmid, or primer	Relevant genotype or phenotype or sequence	Source or reference
E. coli strains		
DH5α	F$^-$ *endA1 hsdR17 supE44 thi-1 recA1 gyrA96 relA1*(*A*) Δ(*argF-lac*)*U169* ϕ80d*lacZ*ΔM15	BRL
BL21(DE3)	F$^-$ *ompT hsdS*$_B$ (r_S^- m_S^-) *gal dcm* (DE3)	Novagen
S. aureus strains		
8325	NCTC 8325 (wild type, 11-bp deletion in *rsbU*)	Laboratory stock
RN4220	NCTC 8325-4-r (restriction mutant, 11-bp deletion in *rsbU*)	Laboratory stock
8325Δ*pknB*	*pknB* deletion in strain 8325	This study
8325Δ*pknB*/pRB473*pknB*	8325 containing pRB473*pknB* for Δ*pknB* complementation	This study
COLΔ*pknB*	*pknB* deletion strain COL	This study
Plasmids		
pBT2	Shuttle vector, Ap^r in *E. coli*, Cm^r in *S. aureus*	6
pBT2Δ*pknB*	Deletion vector for *pknB*, *ermB* fragment flanked by fragments upstream and downstream of *pknB* in pBT2, Em^r and Cm^r in *S. aureus*	This study
pGEM-T	Ap^r	Promega
pEC1	Ap^r Em^r *ermB* fragment in pUC18	6
pRB473	Shuttle vector, Ap^r Cm^r	6
pRB473*pknB*	pRB473 containing *pknB* fragment for Δ*pknB* complementation	This study
pKG31	Ap^r Em^r EcoRI-PstI fragment of *ermB* in pGEM-T	This study
pET-28a(+)	His$_6$ expression vector, Kan^r	Novagen
pET-28aPknB	Encodes His$_6$-PknB, cloned in pET28a(+), Kan^r	This study
pET28aPurA	Encodes His$_6$-PurA, cloned in pET28a(+), Kan^r	This study
Primers		
*pknB*EcoRI	5′-CGGAATTCTATCACCTTCAATAGCCGCG-3′	
*pknB*HindIII	5′-CCCAAGCTTGTTTGGTGGTGTGAATGACC-3′	
*pknB*BamHI	5′-CGGGATCCAATAAATTCAGTCTCATAGCC-3′	
*pknB*PstI	5′-AACTGCAGAGTGACGATATTGATGAGGG-3′	
*ermB*EcoRI	5′-CGGAATTCGGTGACATCTCTCTATTGTG-3′	
*ermB*PstI	5′-AACTGCAGGGAAGCTGTCAGTAGTATACC-3′	
SA1063-fw	5′-AGCCATATGATAGGTAAAATAATAAATGAACG-3′	
SA1063-rev	5′-CCGCTCGAGTTATACATCATCATAGCTGACTTC-3′	
SA0016-fw	5′-GCTAGCTCATCAATCGTAGTAGTTGGG-3′	
SA0016-rev	5′-CGCCCTAGGCTACCACAATTCTTTTAATAGG-3′	

strate, in a time-dependent manner and has a preference for Mn^{2+} as a cofactor. In addition, we demonstrated that PknB specifically phosphorylates adenylosuccinate synthase PurA, a key enzyme in purine biosynthesis.

MATERIALS AND METHODS

Strains, media, and growth conditions. The strains and plasmids used in this study are listed in Table 1. *Escherichia coli* and *S. aureus* were grown in Luria-Bertani (LB) medium. Liquid cultures were shaken at 220 rpm. The bacteria were grown at 37°C, unless indicated otherwise. Antibiotics were used at the following concentrations: 100 μg of ampicillin ml^{-1} and 10 μg of chloramphenicol ml^{-1} for *E. coli* and 10 μg of erythromycin ml^{-1} and 10 μg of chloramphenicol ml^{-1} for *S. aureus*.

Antibiotic susceptibility tests. MICs were determined by microdilution according to the recommendations of the Clinical and Laboratory Standards Institute (9). The MICs were determined in 96-well microtiter plates using a final volume of 200 μl without agitation. The initial inoculum was 2×10^5 bacterial cells per well. The plates were incubated for 18 h at 37°C.

Construction of the *S. aureus pknB* deletion strain. A Δ*pknB* mutant of *S. aureus* was constructed by replacing the coding sequence of the *pknB* gene with the coding sequence of the erythromycin resistance cassette (*ermB*) by a double-crossover event, as described by Brückner (6). Fragments upstream and downstream of the target gene were amplified by PCR, and restriction sites were added to the primers to facilitate cloning. All primer sequences are listed in Table 1. For the upstream fragment EcoRI and HindIII restriction sites were used (*pknB*EcoRI and *pknB*HindIII). The length of the fragment was 1,006 bp, and the fragment started 5 nucleotides before the start codon of *pknB*. For the downstream fragment BamHI and PstI restriction sites were used (*pknB*BamHI and *pknB*PstI). The length of the fragment was 1,018 bp, and the fragment contained 363 bp of the 3′ end of the open reading frame (ORF) of *pknB*. The erythromycin resistance cassette (*ermB*) was cloned between the EcoRI and PstI restriction sites. The *ermB* gene was amplified from the pEC1 vector (5), and EcoRI and PstI restriction sites were added to the primers (*ermB*EcoRI and *ermB*PstI). The length of the fragment was 1,364 bp. The fragments were first cloned into the pGEM-T vector (Promega, Mannheim, Germany) and then cut out with the corresponding restriction enzymes and cloned into the temperature-sensitive shuttle vector pBT2. Construction of this deletion vector was carried out using *E. coli* DH5α. The vector construct was introduced into *S. aureus* strain RN4220 by electroporation. Following propagation in RN4220, the vector was introduced into *S. aureus* strain 8325 by transduction with phage ϕ85. In this strain gene inactivation was carried out as described by Brückner (6). To rule out the possibility that the expression of downstream genes is affected by insertion of *ermB* and the possibility that the effects on the transcriptome are indeed caused by *pknB* and not by adjacent genes, we tested expression of downstream genes (SA1064, SA1065, and SA1066) by performing a reverse transcription (RT)-PCR analysis. We did not observe any difference in the expression rates of these genes between the wild type and the mutant. Likewise, in the microarray experiments these genes were not deregulated in the mutant compared to the wild type.

Expression and purification of recombinant proteins for overexpression in pET28a. The gene fragments corresponding to the entire coding sequence of *purA* (SA0016) and *pknB* (SA1063) were synthesized by PCR amplification using genomic DNA of *S. aureus* 8325 as the template and primers listed in Table 1. Each DNA fragment synthesized was restricted with appropriate enzymes and ligated into the pET28a vector (Novagen, Madison, WI). The resulting plasmids were transformed into *E. coli* BL21(DE3) cells for protein expression. The resulting recombinant polyhistidine-tagged proteins were purified under native conditions by affinity chromatography on Protino Ni-TED columns by following the manufacturer's instructions (Macherey-Nagel, Düren, Germany) exactly. To exclude the possibility that His tagging resulted in nonspecific in vitro phosphor-

ylation on serine and threonine residues, thrombin cleavage of the His tag of PknB and PurA was performed according to the manufacturer's instructions (Qiagen, Hilden, Germany). Protein purity was checked by sodium dodecyl sulfate (SDS)-polyacrylamide gel electrophoresis (PAGE), and protein concentrations were determined using the Roti-Nanoquant assay (Roth, Karslruhe, Germany).

RNA techniques. Total RNA was isolated from *S. aureus* cultures in exponential growth phase (optical density at 600 nm [OD_{600}], 1.0). Bacteria were harvested by addition of RNA Protect (Qiagen, Hilden, Germany) according to the manufacturer's instructions. The cells were centrifuged for 10 min at 5,000 × *g*, and the bacterial pellet was resuspended in 1 ml RLT buffer and mechanically disrupted with glass beads in a Fast Prep shaker (Qbiogene, Heidelberg, Germany) two times for 45 s at a speed of 6.5. The cell lysate was centrifuged for 30 s at 13,000 × *g*, and the supernatant was used for RNA isolation. RNA was isolated using an RNeasy mini kit (Qiagen) according to the standard Qiagen RNeasy protocol. The isolated RNA was treated with RNase-free DNase I (Roche, Penzberg, Germany) to remove the DNA template. The integrity of RNA was monitored by analysis with a bioanalyzer (Agilent Technologies). Only probes with an RNA integrity number of >9 were used in subsequent experiments.

Real-time PCR. Real-time PCR was performed by using the MyiQ device (Bio-Rad, Munich, Germany). RT was carried out using 2 μg RNA, 200 ng of a random hexamer primer mixture (Amersham, Freiburg, Germany), and Superscript III reverse transcriptase (Invitrogen, Karlsruhe, Germany) at 50°C for 1 h. The reaction was stopped by incubating the mixture at 70°C for 15 min. The cDNA was amplified in different PCRs (including negative controls) with primers specific for the corresponding genes. The iQ SYBR green supermixture (Bio-Rad) was used for the amplification reaction. Relative quantification was performed as described by Pfaffl (35).

DNA microarray analysis. *S. aureus* N315 full-genome microarrays containing PCR products of 2,666 genes were used for microarray analysis (Scienion, Berlin, Germany). Each slide contained 6,912 features corresponding to duplicate copies of each ORF and several controls (32). The RNA was isolated from cultures in the exponential growth phase at an OD_{600} of 1.0 at 37°C. Ten micrograms of total RNA from *S. aureus* 8325 was used for RT with random primers and Superscript III reverse transcriptase (Invitrogen). The integrity of RNA was analyzed with a bioanalyzer (Agilent Technologies). Fluorescent labeling was performed during the RT reaction by incorporating the dyes Cy3 and Cy5 according to the manufacturer's instructions (Scienion, Berlin, Germany). Four different biological experiments were performed, and a reverse labeling (dye switch) experiment was performed to minimize bias due to differential dye bleaching or incorporation of Cy3 and Cy5 dyes during the RT reaction. Microarray hybridization and washing of slides were carried out as recommended by the manufacturer (Scienion, Berlin, Germany). The intensity of the fluorescence of the microarray was determined with a GenePix 4000B laser scanner (Axon Instruments Inc., Union City, CA), and individual signal intensities were analyzed using Acuity 4.0 software (Axon Instruments Inc.) according to the manufacturer's instructions. Normalization was performed by applying the LOWESS algorithm. Finally, significant changes in gene expression were identified with the SAM (significance analysis of microarrays) software using the one-class response type and a false discovery rate of <1.5% (45). The data were filtered for genes having at least a 1.5-fold change in expression.

In vitro phosphorylation assay. In vitro phosphorylation of about 1 to 2 μg of purified PurA and PknB was performed for 20 min at 37°C in 20 μl of a reaction buffer containing 50 mM HEPES (pH 7.5), 1 mM dithiothreitol, 0.01% Brij 35, 3 mM $MnCl_2$, 3 mM $MgCl_2$, and 200 μCi [γ-^{32}P]ATP/ml. MBP (Sigma, Deisenhofen, Germany) was used as a surrogate substrate to test the divalent cation dependence of the phosphorylation reaction. In this experiment, 50 μg/ml MBP and 25 μg/ml PknB were used along with the cations Mn^{2+}, Mg^{2+}, and Ca^{2+} at appropriate concentrations. In each case, the reaction was stopped by adding 4× SDS-protein buffer. One-dimensional gel electrophoresis was performed as previously described (25). Finally, radioactive proteins were visualized by autoradiography using direct-exposure film.

Adenylosuccinate synthase (PurA) activity assay. The activity of PurA was assayed as described previously (22). The assay used measures the increase in absorbance at 280 nm that accompanies the conversion of IMP to adenylosuccinate in the presence of aspartate. As a control, reference reactions without aspartate were run simultaneously. Specific activity was calculated using a molar extinction coefficient of 11,700 M^{-1} cm^{-1} as described previously and was expressed in U/mg protein (22).

Triton X-100-induced autolysis assay. The autolysis assay was performed as described by Mani et al. (31). Bacteria were grown in LB medium containing 1 M NaCl to an OD_{600} of ~1.0 at 37°C with shaking at 220 rpm. The bacteria were washed once with phosphate-buffered saline, and the cells were resuspended in the same volume of 0.05 M Tris-HCl buffer (pH 7.5) containing 0.1% Triton X-100. The bacteria were incubated at 37°C with shaking, and the OD_{600} was measured at 30-min intervals.

Scanning electron microscopy. The bacteria were grown overnight in tryptic soy broth on polystyrene chamber slides at 37°C. The slides were washed with 1× phosphate-buffered saline, mounted on aluminum stubs, and shadowed with gold. For visualization, a scanning electron microscope (Zeiss DSM962) was used at 15 kV.

Metabolome analysis. *S. aureus* wild-type strain 8325 and the isogenic Δ*pknB* mutant were grown to an OD_{600} of 1 in 100 ml of LB medium. Samples used for intracellular metabolite analysis were obtained by fast filtration over a 0.22-μm sterility filter with a vacuum. Cells were washed immediately with a cooled isotonic NaCl solution and quenched with liquid nitrogen. Metabolite extraction was performed by cell disruption with glass beads and an ethanol-water solution. Samples were dried and prepared as described by Liebeke et al. (26). Detection of metabolites was performed by using ion pair liquid chromatography-mass spectrometry. The system consisted of an Agilent System 1100 liquid chromatograph (Agilent Technologies, Santa Clara, CA) coupled with a micrOTOF (Bruker, Rheinstetten, Germany) operating in electrospray negative-ionization mode. Samples were resolved with distilled water prior to injection, and chromatographic separation was performed at room temperature using an RP18 Waters SymmetryShield column (150 mm by 4.6 mm; 3.5 μm) connected to a Waters C_{18} precolumn. The mobile phase consisted of the following components: 5% methanol and 95% water containing 10 mM tributylamine as an ion-pairing reagent and acetic acid for adjustment of the pH to pH 4.8 (component A) and 100% methanol (component B). The elution gradient started with 100% component A for 2 min, which was followed by increases from 0 to 20% component B in 2 min, from 20 to 31% component B in 11 min, from 31 to 60% component B in 19 min, and from 60 to 100% component B in 5 min, 100% component B for 15 min, a decrease from 100 to 0% component B in 6 min, and then 3 min with 0% component B. The gradient flow rate was 0.3 ml/min. For quantitative analysis, standard solutions of metabolites were prepared and analyzed as described above. Accurate masses were extracted, and integration of designated peaks was performed by using QuantAnalysis (Bruker, Rheinstetten, Germany). Normalization of acquired data was performed by comparing the area of the added internal standard Br-ATP for each sample. The *P* values reported below are the results of a one-sided unpaired *t* test. Differences were considered significant if the *P* value was ≤0.05.

Microarray data accession number. Additional information for the microarray platform, as well as the processed and raw microarray data from this study, have been deposited in the NCBI Gene Expression Omnibus (GEO) database (http://www.ncbi.nlm.nih.gov/geo/) under GEO series accession number GSE15346.

RESULTS AND DISCUSSION

In silico identification of an STPK-encoding gene in *S. aureus*. To identify *S. aureus* genes encoding an Ser/Thr kinase domain (S_TKc domain; SMART accession no. SM0020), domain library browse and search tools available at the SMART (http://smart.embl-heidelberg.de) and TIGR (www.tigr.org) databases were used. This search yielded a single gene (TIGR locus SA1063 in the *S. aureus* N315 genome), which we designated *pknB* due to a high level of sequence identity with *pknB* of *M. tuberculosis* (37% identity at the protein level) encoding a complete eukaryotic-type Ser/Thr kinase. Figure 1 shows the bipartite domain architecture of PknB, with the presumably cytoplasmic kinase domain separated by a putative transmembrane domain and three extracellular repeats of the PASTA domain (E values for PASTA domains, 6.37e-16, 2.38e-15, and 1.73e-17). The kinase domain of *S. aureus* PknB is predicted to belong to the STPK family with a high degree of statistical significance (E value, 7.12e-70) and contains all highly conserved residues characteristic of this family, including those required for catalytic activity. Thus, PknB of *S. aureus* possesses the typical domain architecture of the bacterial STPKs. Interestingly, a second protein with a eukaryote-like Ser/Tyr/Thr kinase domain has been found in the database for the

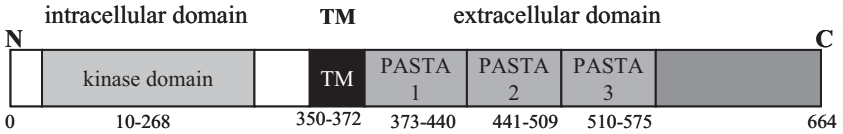

FIG. 1. Domain architecture for *S. aureus* PknB. TM, transmembrane domain. The domain library is available at SMART.

prototype MRSA strain N315 (SA0077) and some other MRSA strains (JH1, JH9, MRSA252, and Mu50). The putative 502-amino-acid protein is encoded in the SCCmec element and contains a protein kinase domain (STYKc; E value, 5.55e-12) but no PASTA domains. However, the specificity of this class of kinases cannot be predicted, and they may possibly act as dual-specificity Ser/Thr/Tyr kinases. At present, it is not known if the kinase is functionally active.

PknB is a manganese-dependent kinase. PknB contains all essential residues present in the kinase domain of STPKs (17). To study its phosphorylation activity, N-terminal His-tagged PknB was expressed under control of the T7 promoter in *E. coli* and purified as described in Materials and Methods. First, purified PknB was examined to determine its functional activity by performing phosphorylation assays using the surrogate substrate MBP, which is known to be phosphorylated by various STPKs, such as PknB from *M. tuberculosis* (1). As shown in Fig. 2A, purified PknB is able to phosphorylate MBP in a time-dependent manner. Next, we studied the phosphorylation reaction by varying the concentrations of bivalent cations. Maximal kinase activity was detected in the presence of up to 5 mM Mn^{2+}, while concentrations between 5 mM and 10 mM were required for Mg^{2+}; 10 mM Mn^{2+} inhibited phosphorylation of MBP as well as the absence of Mn^{2+} or Mg^{2+} (Fig. 2B). These experiments show that in vitro Mn^{2+} was more effective as a cofactor than Mg^{2+}. However, the possibility that in vivo Mg^{2+} is the cofactor in phosphorylation reactions preferred by PknB cannot be ruled out as high concentrations of manganese may be toxic to bacterial cells. The presence of Ca^{2+} has no effect on the phosphorylation activity of PknB (data not shown).

Global transcription profile of Δ*pknB* mutant. To investigate the functional role of PknB in *S. aureus*, DNA microarray experiments were performed. We compared exponentially growing (OD_{600}, 1.0) mutant strain Δ*pknB* and parental strain 8325 using an *S. aureus* full-genome chip. The expression of 72 ORFs of the 2,666 genes evaluated was repressed in the Δ*pknB* strain, whereas the expression of 185 ORFs was increased in this mutant strain (Table 2 and 3). As an internal control, *pknB* transcripts were not detected for the Δ*pknB* mutant compared to the wild-type strain (Table 2). Importantly, the expression of genes involved in nucleotide biosynthesis, cell wall metabolism, and central metabolic pathways was affected by deletion of *pknB* (Table 2, 3).

Most strikingly, genes encoding proteins involved in de novo purine and pyrimidine biosynthesis were downregulated 2.0- to 6.8-fold in the Δ*pknB* mutant (Table 2). In particular, *purK*, *purQ*, *purL*, *purF*, *purM*, *purN*, *purH*, and *purD* of the purine biosynthesis pathway and *pyrP*, *pyrR*, *pyrB*, *pyrC*, *pyrAA*, *pyrAB*, *pyrF*, and *pyrE* involved in pyrimidine metabolism were significantly downregulated in the *pknB*-deficient strain compared to the wild-type strain. To confirm the decreased expression of genes involved in purine biosynthesis in the Δ*pknB* strain, we performed RT-PCR with selected target genes by using the same RNA samples that were used for microarray assays. As shown in Table 4, the *purF* and *purH* transcript levels were two- to threefold lower in the Δ*pknB* strain, confirming the results of the microarray analysis.

Effect of phosphorylation on PurA enzyme activity. To further assess the role of PknB in purine biosynthesis, we investigated the effect of phosphorylation on the activity of PurA (adenylosuccinate synthase), an enzyme involved in synthesis

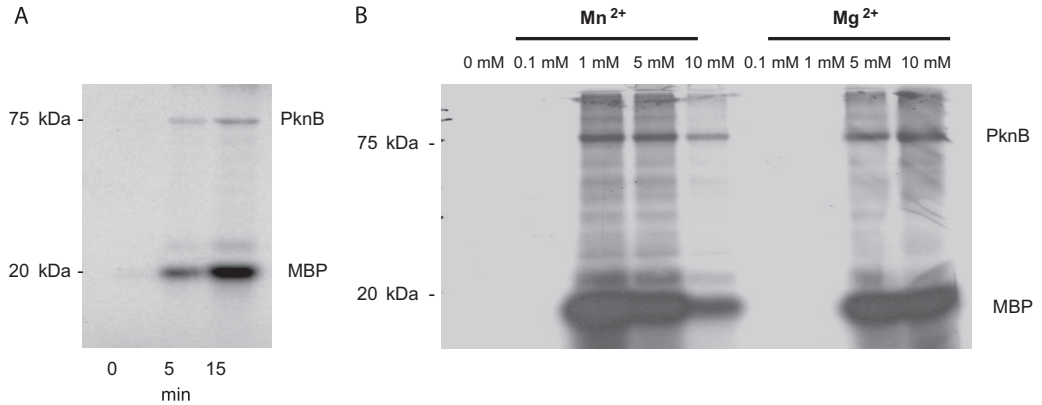

FIG. 2. Phosphorylation of MBP by PknB. Purified PknB was incubated with the surrogate kinase substrate MBP and [γ-^{32}P]ATP in the presence or absence of Mn^{2+} or Mg^{2+}. The reaction products were resolved on a 12% SDS-PAGE gel that was stained with Coomassie blue (not shown) and visualized by autoradiography. (A) Time-dependent phosphorylation of MBP. (B) Concentration-dependent phosphorylation with different Mn^{2+} or Mg^{2+} concentrations. The positions and masses (in kDa) of protein standards are indicated on the left. Besides phosphorylation of MBP autophosphorylation of PknB is visible.

TABLE 2. Downregulated genes in the Δ*pknB* mutant strain

N315 ORF	Gene	Description or predicted function	Change (fold)[a]
Purine and pyrimidine metabolism			
SA0373	*xprT*	Xanthine phosphoribosyltransferase	3.7
SA0917	*purK*	Phosphoribosylaminoimidazole carboxylase carbon dioxide fixation chain PurK homolog	1.4
SA0920	*purQ*	Phosphoribosylformylglycinamidine synthase I	2.0
SA0921	*purL*	Phosphoribosylformylglycinamidine synthetase	2.2
SA0922	*purF*	Phosphoribosylpyrophosphate amidotransferase	3.0[b]
SA0923	*purM*	Phosphoribosylformylglycinamidine cycloligase	2.5[b]
SA0924	*purN*	Phosphoribosylglycinamide formyltransferase	2.2
SA0925	*purH*	Phosphoribosylaminoimidazole carboxamide formyltransferase	1.8
SA0926	*purD*	Phosphoribosylamine glycine ligase	6.2[b]
SA1041	*pyrR*	Pyrimidine operon repressor chain A	3.1
SA1043	*pyrB*	Aspartate transcarbamoylase chain A	4.1
SA1044	*pyrC*	Dihydroorotase	4.7
SA1045	*pyrAA*	Carbamoyl-phosphate synthase small chain	5.6
SA1046	*pyrAB*	Carbamoyl-phosphate synthase large chain	6.4
SA1047	*pyrF*	Orotidine-5-phosphate decarboxylase	6.8
SA1048	*pyrE*	Orotate phosphoribosyltransferase	5.6
ABC transporter/transporter proteins			
SA0255		Hypothetical protein, similar to phosphotransferase system beta-glucoside-specific enzyme II	2.2
SA0616	*vraF*	ABC transporter ATP-binding protein	1.8
SA0617	*vraG*	ABC transporter permease	1.7
SA0845	*oppB*	Oligopeptide transport system permease protein	1.8
SA0847	*oppD*	Oligopeptide transport system ATP-binding protein OppD homolog	2.5
SA0848	*oppF*	Oligopeptide transport system ATP-binding protein OppF homolog	2.0
SA0849	*oppA*	Hypothetical protein, similar to peptide-binding protein	2.0
SA1960	*mtlF*	Phosphotransferase system, mannitol-specific IIBC component	4.1
SA2079	*fhuD2*	Hypothetical protein, similar to ferrichrome ABC transporter FhuD2	1.8
SA2132		Hypothetical protein, similar to ABC transporter	2.2
SA2143		Hypothetical protein, similar to ABC transporter	2.6
SA2200		Hypothetical protein, similar to ABC transporter, ATP-binding subunit	1.6
SA2202		Hypothetical protein, similar to ABC transporter periplasmic amino acid-binding protein	1.9
SA2253		Oligopeptide transporter putative membrane permease domain	1.5
SA2302		Hypothetical protein, similar to ABC transporter	1.8
SA2434		Fructose phosphotransferase system enzyme, FruA homolog	2.5
Information pathways—DNA replication/RNA synthesis/protein synthesis			
SA0442		Probable DNA polymerase III, delta prime subunit	1.7
SA1120		Hypothetical protein, similar to transcription regulator GntR family	1.9
SA1704	*map*	Methionyl aminopeptidase	1.6
SA1717		Glutamyl-tRNA^{Gln} amidotransferase subunit C	1.7
SA1961		Hypothetical protein, similar to transcription antiterminator BglG	1.9
Metabolism of amino acids and related molecules			
SA1121		Hypothetical protein, similar to processing proteinase homolog	1.8
SA1150	*glnA*	Glutamine-ammonia ligase	1.6
Metabolism of carbohydrates and related molecules			
SA1945		Hypothetical protein, similar to mannnose-6 phospate isomerase Pmi	2.5
Metabolism of nucleotides and nucleic acids			
SA0468		Hypoxanthine-guanine phosphoribosyltransferase homolog	1.8
SA0687	*nrdF*	Ribonucleoside-diphosphate reductase minor subunit	1.7
SA1921	*tdk*	Thymidine kinase	1.6
SA2375		Hypothetical protein, similar to dihydroorotate dehydrogenase	2.1
SA2410		Anaerobic ribonucleoside triphosphate reductase	1.6
Metabolism of coenzymes and prosthetic groups			
SA1442		Hypothetical protein, similar to caffeoyl-CoA *O*-methyltransferase	1.8
SA1734		Pyrazinamidase/nicotinamidase homolog	1.7
Miscellaneous			
SA0231		Hypothetical protein, similar to flavohemoprotein	2.0

Continued on following page

TABLE 2—*Continued*

N315 ORF	Gene	Description or predicted function	Change (fold)[a]
Cell envelope and cellular processes			
SA0265	*lytM*	Peptidoglycan hydrolase	1.7
SA0423		Hypothetical protein, similar to autolysin	2.1
SA0531	*proP*	Proline/betaine transporter homolog ProP	2.1
SA0905	*atl*	Autolysin (*N*-acetylmuramyl-L-alanine amidase and endo-β-*N*-acetylglucosaminidase)	1.6
SA1042	*pyrP*	Uracil permease	4.1
SA1063	*pknB*	STPK	8.4
SA1302	*gerCC*	Heptaprenyl diphosphate syntase component II	2.1
SA2142		Hypothetical protein, similar to multidrug resistance protein	1.8
SA2203		Hypothetical protein, similar to multidrug resistance protein	1.7
Membrane bioenergetics (electron transport chain and ATP synthase)			
SA0937		Cytochrome *d* ubiquinol oxidase subunit 1 homolog	1.6
Pathogenic factors			
SA2097	*ssaA*	Hypothetical protein, similar to secretory antigen precursor SsaA	2.4
SA2356	*isaA*	Immunodominant antigen A	1.6
Detoxification			
SA0781		Hypothetical protein, similar to 2-nitropropane dioxygenase	1.6
Unknown functions and hypothetical proteins			
SA0269		Hypothetical protein	3.2
SA0289		Conserved hypothetical protein	1.5
SA0290		Conserved hypothetical protein	1.7
SA0291		Hypothetical protein	1.6
SA0467		Hypothetical protein	2.1
SA0725		Conserved hypothetical protein	1.8
SA0814		Hypothetical protein	2.5
SA0885		Hypothetical protein	2.6
SA1049		Hypothetical protein	5.6
SA1056		Hypothetical protein	1.6
SA1130		Conserved hypothetical protein	1.7
SA1890		Conserved hypothetical protein	1.8
SA2059		Hypothetical protein	1.5
SA2332		Hypothetical protein	2.6
SAS007		Hypothetical protein	1.6

[a] Data for genes with changes of ≥1.5-fold are shown. All genes had a q value that was <0.015, unless indicated otherwise.
[b] Gene with a q value of <0.03.

of AMP. Recently, regulation of purine biosynthesis by phosphorylation and dephosphorylation of PurA has been described for *Streptococcus agalactiae*, in which the serine/threonine kinase Stk1 negatively affects PurA activity by phosphorylation (38). In our study, in vitro phosphorylation of PurA was performed in the presence of PknB and ATP. To exclude the possibility that His tagging results in nonspecific in vitro phosphorylation on serine and threonine residues as described by Boitel et al. (5), fusion proteins PknB-His_6 and PurA-His_6 were cleaved with thrombin to obtain recombinant PknB and PurA without a tag (Fig. 3). PurA assays were conducted as described in Materials and Methods. The results are summarized in Table 5. As controls we used reactions with unphosphorylated PurA lacking either PknB or ATP. Interestingly, we observed a 1.8-fold decrease in the activity of phosphorylated PurA (reactions performed after phosphorylation of PurA by PknB) compared to the activity of unphosphorylated PurA (control reactions without PknB or ATP). This indicates that phosphorylation of PurA by PknB decreases PurA enzyme activity. The results of these experiments support the idea that PknB phosphorylates and thereby inhibits PurA when intracellular A nucleotide pools (including the ATP concentration) increase. This would lead to suppression of further AMP and ATP synthesis. To prove this hypothesis, the intracellular concentrations of AMP, ADP, and ATP were measured by liquid chromatography-mass spectrometry. The AMP, ADP, and ATP concentrations were 1.2-fold to 1.4-fold higher in the *pknB* mutant than in the wild type (for AMP, 0.14 ± 0.02 $\mu M/OD_{600}$ unit versus 0.11 ± 0.01 $\mu M/OD_{600}$ unit; for ADP, 0.75 ± 0.02 $\mu M/OD_{600}$ unit versus 0.54 ± 0.09 $\mu M/OD_{600}$ unit; for ATP, 3.17 ± 0.29 $\mu M/OD_{600}$ unit versus 2.53 ± 0.24 $\mu M/OD_{600}$ unit). These results may have been due to the observed higher enzyme activity of PurA in its unphosphorylated form in cells lacking PknB, generating more AMP, ADP, and ATP.

This observation seems to be in contrast to the microarray expression data, where the *pur* operon was downregulated in the *pknB* mutant. However, in rich medium AMP, ADP, and ATP are preferentially generated via the salvage pathway that feeds the PurA reaction starting from IMP. Consequently, there is no need for de novo biosynthesis of either purines or pyrimidines in rich medium. The strong downregulation of purine biosynthesis genes observed in the microarray experiments may have resulted from a regulatory feedback loop in which elevated concentrations of the end products AMP and

TABLE 3. Upregulated genes in the Δ*pknB* mutant strain

N315 ORF	Gene	Description or predicted function	Change (fold)[a]
Citrate cycle			
SA1244	*odhB*	Dihydrolipoamide succinyltransferase	2.4
SA1245	*odhA*	Oxoglutarate dehydrogenase E1	2.2
Two-component system			
SA0252	*lrgA*	Holin-like protein LrgA	2.8
SA0253	*lrgB*	Holin-like protein LrgB	2.3
SA1700	*vraR*	Vancomycin resistance-associated two-component response regulator	2.7
SA1701	*vraS*	Vancomycin resistance-associated two-component sensor histidine kinase	2.5
SA1843	*agrC*	Accessory gene regulator C	2.1
SA1844	*agrA*	Accessory gene regulator A	2.3
SA1882	*kdpD*	Sensor protein	2.8
ABC transporter or transporter proteins			
SA0209		Maltose/maltodextrin transport permease homolog	2.5
SA0599		ATP-binding cassette transporter A	2.5
SA1243		ABC transporter homolog	1.6
SA1744		ABC-2-type transport system/permease protein	3.9
SA1745		Hypothetical protein, similar to ABC transporter, ATP-binding protein	3.4
SA2227		Truncated hypothetical protein, similar to D-serine/D-alanine/glycine transporter	1.9
Phosphotransferase system			
SA0186		Phosphotransferase system, sucrose-specific IIBC component, putative	3.1
SA0318		Phosphotransferase system, unknown pentitol phosphotransferase enzyme IIC component	2.9
SA0320		Putative phosphotransferase system enzyme IIA component	2.8
SA1255		Phosphotransferase system, glucose-specific enzyme II, A component	2.0
SA2114	*glvC*	Phosphotransferase system, arbutin-like IIBC component	1.7
Membrane bioenergetics (electron transport chain and ATP synthase)			
SA0210		Hypothetical protein, similar to NADH-dependent dehydrogenase	2.0
SA0411	*ndhF*	NADH dehydrogenase subunit 5	2.5
SA0799		Hypothetical protein, similar to NADH dehydrogenase	1.5
SA1904	*atpC*	F_oF_1-ATP synthase epsilon subunit	1.8
SA1905	*atpD*	ATP synthase beta chain	1.6
Cell envelope and cellular processes and cell wall			
SA0115	*sbnD*	Hypothetical protein, similar to multidrug resistance efflux pump	2.3
SA0172	*lmrP*	Hypothetical protein, similar to integral membrane protein	1.7
SA0207		Hypothetical protein, similar to maltose/maltodextrin-binding protein	1.6
SA0248		Hypothetical protein similar to beta-glycosyltransferase	1.5
SA0259	*rbsD*	Ribose permease	1.9
SA0260	*rbsU*	Hypothetical protein, similar to ribose transporter	1.7
SA0303		Hypothetical protein, similar to sodium-coupled permease	2.2
SA0719	*trxB*	Thioredoxin reductase	1.5
SA0758		Hypothetical protein, similar to thioredoxin	1.6
SA1283	*pbp2*	Penicillin-binding protein 2	1.5
SA1691	*sgtB*	Hypothetical protein, similar to penicillin-binding protein 1A/1B	2.5
SA1718	*putP*	High-affinity proline permease	2.1
SA1926	*murZ*	UDP-*N*-acetylglucosamine 1-carboxylvinyl transferase 2	1.5
SA2437		Hypothetical protein, similar to autolysin precursor	1.9
SA2480	*drp35*	Drp35	4.1
SAS023		Hypothetical protein, similar to thioredoxin	1.5
Information pathways: RNA synthesis, protein folding, and DNA modification and repair			
SA0006	*gyrA*	DNA gyrase subunit A	1.5
SA0009	*serS*	Seryl-tRNA synthetase	1.5
SA0187		Hypothetical protein, similar to transcription regulator	3.9
SA0189	*hsdR*	Probable type I restriction enzyme restriction chain	1.9
SA0321		Hypothetical protein, similar to transcription antiterminator BglG family	2.2
SA0480	*ctsR*	Transcription repressor of class III stress gene homolog	1.9
SA0498	*rplL*	50S ribosomal protein L7/L12	1.5
SA0652		Hypothetical protein, similar to transcription regulation protein	1.6
SA0653		Hypothetical protein, similar to transcription repressor of fructose operon	1.5
SA1257		Peptide methionine sulfoxide reductase	1.7

Continued on following page

TABLE 3—*Continued*

N315 ORF	Gene	Description or predicted function	Change (fold)[a]
SA1287	*asnS*	Asparaginyl-tRNA synthetase	1.6
SA1305	*hu*	DNA-binding protein II (HB)	1.6
SA1360		Xaa-Pro dipeptidase	1.5
SA1586	*rot*	Repressor of toxins	1.8
SA1659	*prsA*	Peptidyl-prolyl *cis*/*trans*-isomerase homolog	2.9
SA1748		Hypothetical protein, similar to transcription regulator, GntR family	2.8
SA1836	*groEL*	GroEL protein	1.8
SA2089	*sarR*	Staphylococcal accessory regulator A homolog	2.3
SA2103	*lytR*	Hypothetical protein, similar to Lyt divergon expression attenuator	2.3
SA2108		Hypothetical protein, similar to transcription regulator, RpiR family	2.2
SA2296		Hypothetical protein, similar to transcriptional regulator, MerR family	2.0
Metabolism of amino acids and related molecules			
SA0008	*hutH*	Histidine ammonia lyase	1.9
SA0818	*rocD*	Ornithine aminotransferase	2.5
SA0819	*gudB*	NAD-specific glutamate dehydrogenase	2.0
SA1348	*bfmBAA*	Branched-chain alpha-keto acid dehydrogenase E1	1.5
SA1365		Glycine dehydrogenase (decarboxylating) subunit 2 homolog	2.4
SA1366		Glycine dehydrogenase (decarboxylating) subunit 1	2.2
SA1367		Aminomethyltransferase	1.5
SA1531	*ald*	Alanine dehydrogenase	2.3
SA1585		Proline dehydrogenase homolog	3.3
SA1931	*blt*	Hypothetical protein, similar to spermine/spermidine acetyltransferase	1.5
SA1968	*arg*	Arginase	2.4
SA2084	*ureC*	Urease alpha subunit	1.7
SA2085	*ureE*	Urease accessory protein	1.7
SA2122	*hutU*	Urocanate hydratase	2.6
SA2125		Hypothetical protein, similar to formiminoglutamase	1.9
SA2220		Glycerate kinase	2.1
SA2318		Putative L-serine dehydratase	2.4
SA2319		Putative beta subunit of L-serine dehydratase	2.0
SA2341	*rocA*	1-Pyrroline-5-carboxylate dehydrogenase	3.5
Metabolism of coenzymes and prosthetic groups			
SA0181		Hypothetical protein, similar to isochorismatase	2.0
SA0915	*folD*	FolD bifunctional protein	1.7
SA1587	*ribA*	Riboflavin biosynthesis protein	1.8
SA1588	*ribB*	Riboflavin synthase alpha chain	1.6
Metabolism of nucleotides and nucleic acids			
SA0133	*dra*	Deoxyribose phosphate aldolase	1.7
SA0511		Hypothetical protein, similar to UDP-glucose 4-epimerase-related protein	1.7
SA0545	*pta*	Phosphotransacetylase	1.8
SA1308		30S ribosomal protein S1	1.8
SA1938	*pdp*	Pyrimidine nucleoside phosphorylase	1.7
SA1939		Deoxyribose phosphate aldolase	1.8
Metabolism of lipids			
SA0224		Hypothetical protein, similar to 3-hydroxyacyl-CoA dehydrogenase	2.6
SA0225		Hypothetical protein, similar to glutaryl-CoA dehydrogenase	3.1
SA1075	*hmrB*	HmrB protein	1.5
SA2240		Hypothetical protein, similar to *para*-nitrobenzyl esterase chain A	1.5
SA2334	*mvaS*	Hydroxymethylglutaryl-CoA synthase	2.0
Metabolism of carbohydrates and related molecules			
SA0162	*aldA*	Aldehyde dehydrogenase	2.7
SA0182		Hypothetical protein, similar to indole-3-pyruvate decarboxylase	1.8
SA0239		Sorbitol dehydrogenase	1.8
SA0258	*rbsK*	Ribokinase	2.1
SA0304	*nanA*	*N*-Acetylneuraminate lyase subunit	2.0
SA0342		Acetyl-CoA C-acetyltransferase homolog	1.9
SA0823	*pgi*	Glucose-6-phosphate isomerase A	1.5
SA0945	*pdhC*	Dihydrolipoamide *S*-acetyltransferase component of pyruvate dehydrogenase complex E2	1.5
SA0946	*pdhD*	Dihydrolipoamide dehydrogenase component of pyruvate dehydrogenase E3	1.5
SA0958		*myo*-Inositol-1 (or -4) monophosphatase homolog	1.7

Continued on following page

TABLE 3—*Continued*

N315 ORF	Gene	Description or predicted function	Change (fold)[a]
SA0995	*sdhA*	Succinate dehydrogenase flavoprotein subunit	1.7
SA0996	*sdhB*	Succinate dehydrogenase iron-sulfur protein subunit	1.9
SA1088	*sucC*	Succinyl-CoA synthetase beta subunit	1.9
SA1089	*sucD*	Succinyl-CoA synthetase alpha chain	2.2
SA1141	*glpK*	Glycerol kinase	1.8
SA1142	*glpD*	Aerobic glycerol-3-phosphate dehydrogenase	1.8
SA1184	*citB*	Aconitate hydratase	1.7
SA1517	*citC*	Isocitrate dehyrogenase	1.6
SA1553	*fhs*	Formyltetrahydrofolate synthetase	2.1
SA1554	*acsA*	Acetyl-CoA synthetase	1.9
SA1609	*pckA*	Phosphoenolpyruvate carboxykinase	2.6
SA1669	*citG*	Fumarate hydratase, class II	1.7
SA1679		Hypothetical protein, similar to D-3-phosphoglycerate dehydrogenase	1.5
SA1927	*fbaA*	Fructose bisphosphate aldolase	1.5
SA2155		Hypothetical protein, similar to malate:quinone oxidoreductase	1.5
SA2304	*fbp*	Fructose bisphosphatase	1.7
SAS020		Hypothetical protein, similar to phosphoglycerate mutase	1.6
Miscellaneous			
SA0114	*sbnC*	Siderophore biosynthesis protein	1.8
SA0117	*sbnF*	Siderophore biosynthesis protein	1.6
SA0173		Hypothetical protein, similar to surfactin synthetase	1.8
SA0914		Hypothetical protein, similar to chitinase B	2.3
SA1238		Hypothetical protein, similar to tellurite resistance protein	1.6
SA1549	*htrA*	Hypothetical protein, similar to serine proteinase Do, heat shock protein	1.6
SA1606		Plant metabolite dehydrogenase homolog	2.1
SA1617		Hypothetical protein, similar to latent nuclear antigen	1.7
SA1656	*hit*	Hit-like protein involved in cell cycle regulation	1.5
Pathogenic factors			
SA0091	*plc*	1-Phosphatidylinositol phosphodiesterase precurosr	1.5
SA0483	*clpC*	Endopeptidase	2.3
SA0909	*fmtA*	FmtA, autolysis and methicillin resistance-related protein	2.3
SA1007		Alpha-hemolysin precursor	3.1
SA1752	*hlb*	Truncated beta-hemolysin	23.1
SA1811	*hlb*	Truncated beta-hemolysin	13.9
SA2209	*hlgB*	Gamma-hemolysin component B	2.0
SA2463	*lip*	Triacylglycerol lipase precursor	4.8
Unknown functions and hypothetical proteins			
SA0079		Conserved hypothetical protein	2.3
SA0129		Hypothetical protein	1.7
SA0174		Conserved hypothetical protein	2.4
SA0184		Conserved hypothetical protein	3.6
SA0185		Conserved hypothetical protein	4.5
SA0307		Conserved hypothetical protein	1.8
SA0372		Hypothetical protein	1.8
SA0403		Hypothetical protein (pathogenicity island SaPIn2) lpl7	2.9
SA0412		Conserved hypothetical protein	2.7
SA0413		Conserved hypothetical protein	1.7
SA0546		Conserved hypothetical protein	1.9
SA0570		Hypothetical protein	1.8
SA0606		Conserved hypothetical protein	2.6
SA0607		Conserved hypothetical protein	2.7
SA0707		Conserved hypothetical protein	1.9
SA0752		Hypothetical protein	2.0
SA0861		Conserved hypothetical protein	1.6
SA0873		Conserved hypothetical protein	1.8
SA1001		Hypothetical protein	3.0
SA1019		Conserved hypothetical protein	2.0
SA1256		Conserved hypothetical protein	1.8
SA1281		Conserved hypothetical protein	1.9
SA1331		Conserved hypothetical protein	1.7
SA1432		Conserved hypothetical protein	1.6
SA1476		Hypothetical protein	2.8

Continued on following page

TABLE 3—*Continued*

N315 ORF	Gene	Description or predicted function	Change (fold)[a]
SA1528		Conserved hypothetical protein	1.6
SA1529		Conserved hypothetical protein	1.7
SA1532		Conserved hypothetical protein	2.0
SA1578		Conserved hypothetical protein	1.6
SA1583		Conserved hypothetical protein	1.7
SA1618		Conserved hypothetical protein	1.7
SA1682		Conserved hypothetical protein	1.6
SA1702		Conserved hypothetical protein	2.4
SA1703		Hypothetical protein	2.0
SA1712		Conserved hypothetical protein	2.2
SA1726		Hypothetical protein	2.2
SA1746		Hypothetical protein	3.9
SA1867		Conserved hypothetical protein	1.5
SA1925		Conserved hypothetical protein	1.5
SA1937		Conserved hypothetical protein	1.7
SA1942		Conserved hypothetical protein	2.1
SA1976		Conserved hypothetical protein	2.3
SA2221		Hypothetical protein	2.4
SA2323		Conserved hypothetical protein	1.5
SA2331		Hypothetical protein	1.7
SA2366		Conserved hypothetical protein	1.5
SAS089		Hypothetical protein	1.6

[a] Data for genes with changes of ≥1.5-fold are shown. All genes had a q value that was <0.015.

ATP inhibited transcription of the *pur* operon. Indeed, IMP concentrations were also increased in the Δ*pknB* strain (0.09 ± 0.02 μM/OD_{600} unit versus 0.05 ± 0.01 μM/OD_{600} unit). Some features of regulation of purine biosynthesis by PknB in *S. aureus* resemble the situation in *S. agalactiae*. In this pathogen, PurA activity is modulated by phosphorylation and dephosphorylation performed by the enzyme Stk1 homologous to PknB (38). In an *stk1* mutant strain, AMP concentrations were also slightly increased, as shown for the *pknB* mutant of *S. aureus* in our study. In contrast to the findings for *S. agalactiae*, the guanine nucleotide concentrations were not altered in the PknB-deficient *S. aureus* strain, suggesting that there are differences in the regulation of A and G nucleotide metabolism in *S. agalactiae* and *S. aureus* (data not shown).

In gram-positive bacteria the organization of genes involved in purine metabolism and the regulation of these genes have been studied best in *Bacillus subtilis*. In contrast to *E. coli*, in which the purine biosynthesis genes are scattered throughout the genome, in *B. subtilis* and many other gram-positive organisms, such as *S. aureus*, almost all de novo purine biosynthesis genes are organized in an operon as a single transcriptional unit. The transcription of the operon is controlled by a repressor which is encoded by the *purR* gene and which at low 5-phosphoribosyl-1-pyrophosphate concentrations binds specifically to a DNA sequence in the promoter region (48). Thus, 5-phosphoribosyl-1-pyrophosphate acts as an indicator of purine availability. In general, regulation of purine biosynthesis is poorly characterized in *S. aureus*. Recently, it has been reported that the repressor of the *pur* operon PurR is functionally active in *S. aureus*, although binding of PurR to a consensus Pur box has not been shown (15). Fox et al. (15) observed variable PurM and PurH expression levels independent of PurR concentrations, and they concluded that in addition to PurR other regulators of

TABLE 4. RT-PCR confirmation of microarray data

Gene product	Gene	N315 ORF	DNA microarray expression[a]	RT-PCR expression[b]
Phosphoribosylpyrophosphate amidotransferase	*purF*	SA0922	−3.0	−3.0
Phosphoribosylaminoimidazole carboxamide formyltransferase	*purH*	SA0925	−1.8	−2.0
Autolysis and methicillin resistance-related protein	*fmtA*	SA0909	2.3	3.5
Hypothetical protein, similar to penicillin-binding protein 1A/1B	*sgtB*	SA1691	2.5	4.0
Holin-like protein	*lrgA*	SA0252	2.8	3.0
Peptidyl-prolyl *cis*/*trans*-isomerase homolog	*prsA*	SA1659	2.9	3.4
1-Pyrroline-5-carboxylate dehydrogenase	*rocA*	SA2341	3.5	9.0
Ornithine aminotransferase	*rocD*	SA0818	2.5	3.0
Vancomycin resistance-associated two-component sensor histidine kinase	*vraS*	SA1701	2.5	10.0

[a] Expression of genes was filtered by using a change of >1.5-fold and a false discovery rate of <1.5%. Negative values indicate downregulation in the Δ*pknB* mutant strain compared to isogenic wild-type strain *S. aureus* 8325. Positive values indicate upregulation in the Δ*pknB* mutant.

[b] Expression levels were analyzed by RT-PCR. Negative values indicate downregulation in the Δ*pknB* mutant strain compared to isogenic wild-type strain *S. aureus* 8325. Positive values indicate upregulation in the Δ*pknB* mutant.

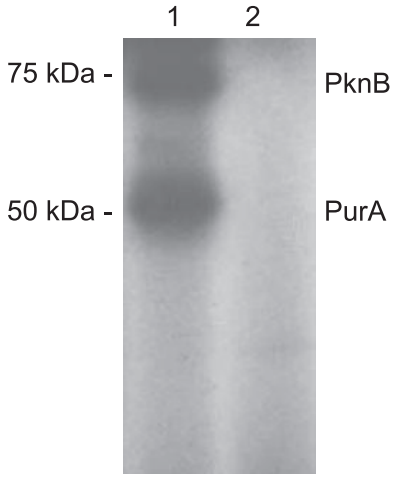

FIG. 3. Phosphorylation of PurA by PknB. The phosphorylation reaction was performed in the presence or absence of PknB as described in Materials and Methods. The His tag of both PknB and PurA was cleaved to exclude the possibility of a nonspecific in vitro phosphorylation effect. All reaction products were analyzed on a 12% SDS-PAGE gel, stained with Coomassie blue, and subjected to autoradiography. Lane 1 shows phosphorylation of PurA in the presence of PknB. Lane 2 contained the control without PknB. The positions and masses (in kDa) deduced from comparison with protein standards are indicated on the left.

purine biosynthesis in *S. aureus* are likely active in modulation of the expression levels of purine biosynthesis genes. We show here that PknB acts as an additional regulator of purine biosynthesis by regulating PurA activity via phosphorylation, thereby regulating A nucleotide synthesis. In our study, *purR* expression was not significantly changed in the microarray experiments.

Autolysis. The microarray analysis showed that expression of two regulators of autolysis, *fmtA* and *lytR*, was induced ~2.3-fold in the Δ*pknB* strain. Furthermore, expression of regulators of the murein hydrolase genes *lrgA* and *lrgB* was induced 2.3- to 2.8-fold in the Δ*pknB* strain (Table 3). In contrast, the expression of the autolysin gene *atl* was decreased 2.2-fold (Table 2). To determine the effect of *pknB* deletion on autolysis, an assay was performed by treating cells with Triton X-100. The Δ*pknB* strain showed decreased autolysis starting after 30 min of growth compared to the wild type, confirming the microarray data (Fig. 4). After 3.5 h of incubation ~86% of the wild-type cells were lysed, whereas only ~58% of the mutant cells were lysed at this time point.

TABLE 5. Effect of phosphorylation on PurA activity

Conditions	Sp act (U min^{-1} mg^{-1})[a]
PurA+ PknB + ATP	1.42 ± 0.06
PurA + PknB	2.78 ± 0.27
PurA+ ATP	2.98 ± 0.09
PurA	2.68 ± 0.46

[a] In vitro phosphorylation of PurA was performed in the presence of PknB and ATP as described in Materials and Methods. The controls included unphosphorylated PurA and reaction mixtures that did not contain either ATP or PknB. PurA enzyme assays were conducted in the presence or absence of aspartate. The average specific activities and standard deviations obtained in three independent experiments are shown. One unit was defined as the amount of enzyme required for the formation of 1 μmol of AMP per min.

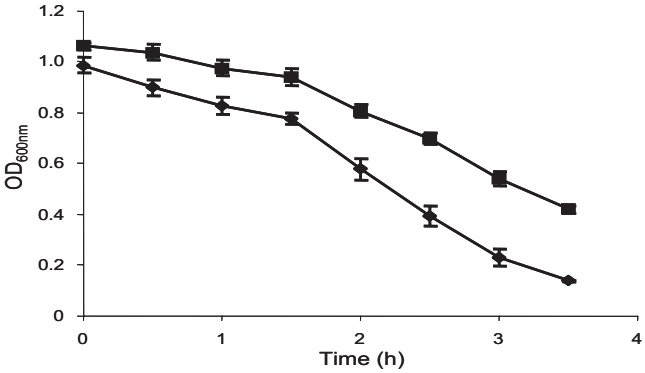

FIG. 4. Autolysis of whole cells of *S. aureus* wild-type strain 8325 (◆) and the 8325 Δ*pknB* mutant (■) during growth with Triton X-100. The results are expressed as decreases in the OD_{600} over time, which represented increases in autolysis (for details see Materials and Methods). The data are the means ± standard deviations of three independent experiments.

The LytR regulator of autolysis is a potential response regulator of a two-component system, which positively regulates *lrgA* and *lrgB*. Both the LrgA and LrgB proteins are involved in the regulation of peptidoglycan hydrolase activity (7, 8). LrgA and LrgB show similarities to a family of bacteriophage proteins known as holins (3). Holins are membrane-spanning proteins that allow phage cell wall hydrolases to access the cell wall murein by forming transmembrane holes. Deletion of the regulator *lytR* gene resulted in increased autolysis (8). The main autolysin Atl has been suggested to be involved in the separation of the daughter cells during development (4, 43). It is the predominant peptidoglycan hydrolase in staphylococci. An *atlA* mutant forms larger cell clusters and is defective in cell separation (4). Because our microarray data showed decreased *atl* expression together with increased transcription of *fmtA* and *lytR*, it is suggested that altered transcription of these factors contributes to the decreased autolysis detected in the mutant strain.

Role of *pknB* in cell wall metabolism. Interestingly, the microarray data also showed that there was altered transcription of genes known to modulate the regulation of cell wall biosynthesis. We detected 2.4- to 2.7-fold upregulation of genes coding for the VraSR two-component system, which was confirmed by RT-PCR analysis (Table 4). VraSR is thought to be a positive regulator of cell wall peptidoglycan synthesis and is involved in the expression of β-lactam and glycopeptide resistance in *S. aureus* (24). Kuroda et al. (24) reported induction of VraSR by several cell wall synthesis inhibitors, suggesting that the sensor kinase VraS responds to damage to cell wall structure or inhibition of cell wall biosynthesis. Interestingly, 9 of 13 genes of the VraSR regulon (*proP*, SA2220, *sgtB*, *murZ*, *prsA*, SA1476, SA1702, SA1703, and SA2221) that were described by Kuroda et al. under non-antibiotic-induced conditions are upregulated in the *pknB* mutant.

In addition, several cell wall-active antibiotics have been tested, and the MICs of tunicamycin, methicillin, fosfomycin, D-cycloserine, vancomycin, bacitracin, cefepime, and ceftriaxone for the Δ*pknB* strain and the isogenic wild-type strain have

TABLE 6. MICs of antibiotics for *S. aureus* wild-type strain 8325 and the isogenic Δ*pknB* mutant

Antibiotic	MIC(μg/ml)	
	S. aureus wild-type strain 8325	*S. aureus* 8325Δ*pknB*
Fosfomycin	16	8
Tunicamycin	64	2
Methicillin	0.25	0.125
D-Cycloserine	32	32
Vancomycin	1	1
Bacitracin	32	32
Cefepime	2	2
Ceftriaxone	2	2
Kanamycin	1	1

been determined. Interestingly, tunicamycin, an inhibitor of MraY transferase, which catalyzes the formation of the first lipid intermediate of peptidoglycan synthesis, was 32-fold more active against the *pknB* mutant than against the wild type (Table 6). Other cell wall-active antibiotics only slightly affected MICs; e.g., the MICs of fosfomycin and methicillin observed for the wild type were twofold-higher than those for the Δ*pknB* strain. Interestingly, deletion of *pknB* in the methicillin-resistant strain COL led to a phenotype with reduced methicillin resistance (MIC for COL, 256 μg/ml; MIC for COLΔ*pknB*, 16 μg/ml). This result supports the hypothesis that PknB has a role in cell wall metabolic pathways. In contrast, no differences in MICs between the wild type and the Δ*pknB* strain were detectable for D-cycloserine, bacitracin, vancomycin, cefepime, and ceftriaxone. In another study, Dèbarbouillè et al. found that the Δ*stk1* mutant expressed greater resistance to fosfomycin (2 logs) than wild-type strain 8325-4 expressed (12). This is in contrast to our results, and the difference may be due to the different strain backgrounds in the two studies.

Most proteins that contain PASTA domains are directly involved in peptidoglycan metabolism (e.g., penicillin-binding proteins) by interacting with un-cross-linked peptidoglycan (49). Therefore, it has been postulated that STPKs such as PrkC of *Enterococcus faecalis* may monitor the integrity of the cell wall by detecting the accumulation of peptidoglycan precursors or un-cross-linked peptidoglycan polymers (23). In addition, it was shown recently by Shah and colleagues (40) that the STPK PrkC of *B. subtilis* is indeed capable of binding peptidoglycan. These workers tested various His-tagged domains of PrkC in a peptidoglycan binding assay and identified the extracellular PASTA domains as binding partners. A similar function may be played by PknB; however, there are no experimental data demonstrating that PASTA domains of PknB of *S. aureus* are involved in sensing cell wall precursors and thereby regulating parts of the cell wall synthesis machinery.

Furthermore, the morphology of Δ*pknB* and wild-type cells was investigated by scanning electron microscopy. As shown in Fig. 5A, mutant cells formed larger cell clusters than the wild-type cells formed (Fig. 5B). This phenotype of the mutant cells could be restored by complementation (not shown) and might be directly linked to decreased expression of *atl*, which results in the formation of larger cell clusters due to incomplete separation of cells during growth.

Collectively, the data from the microarray analysis, the formation of larger clusters by the mutant, and the increased sensitivity of the Δ*pknB* mutant to cell wall-active antibiotics indicate that PknB has a role in cell wall synthesis and metabolism. Our results support the hypothesis that the VraSR regulon is activated in part as a response to altered cell wall biosynthesis in the *pknB* mutant.

Transcription of genes involved in amino acid metabolism. In addition to the altered expression of genes involved in nucleotide biosynthesis and cell wall metabolism, the microarray data revealed higher levels of expression of genes involved in amino acid metabolism. The *rocA* and *rocD* genes, encoding a 1-pyrroline-5-carboxylate dehydrogenase and an ornithine aminotransferase, are induced 3.5- and

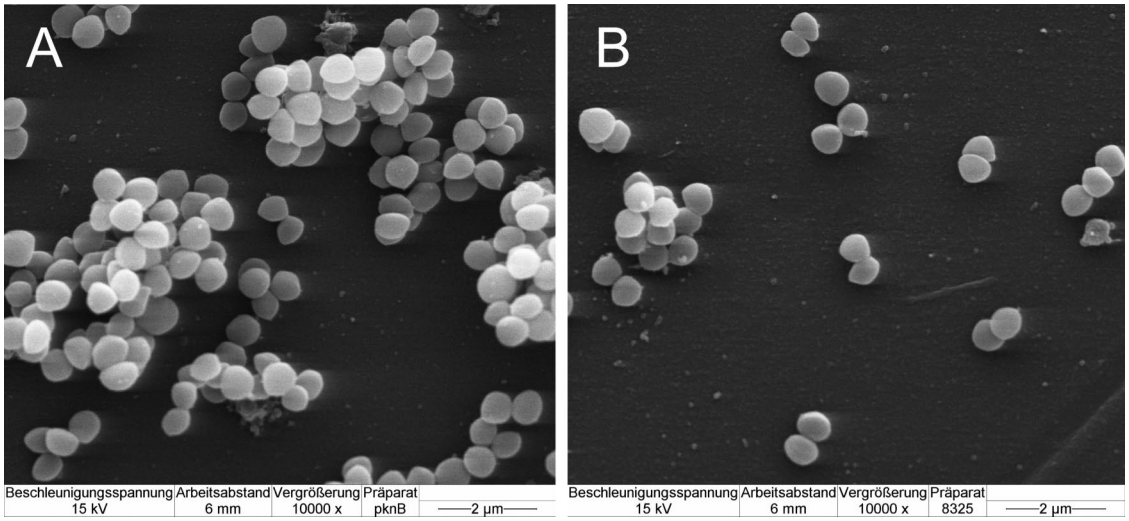

FIG. 5. Scanning electron microscopy of the 8325 Δ*pknB* mutant (A) and wild-type strain 8325 (B) grown on polystyrene surfaces. Cells of the Δ*pknB* strain formed larger cell clusters than cells of the wild-type strain formed.

2.5-fold, respectively, in the Δ*pknB* mutant. Both *rocA* and *rocD* encode proteins that are responsible for the degradation of L-ornithine to L-glutamate. Enhanced expression of these genes was also detected by RT-PCR (Table 4). Furthermore, the expression of *gudB* was increased ~2-fold in the *S. aureus* Δ*pknB* strain. *gudB* encodes an NAD-specific glutamate dehydrogenase which catalyzes the conversion of L-glutamate to 2-oxoglutamate. To a large extent, genes involved in pyruvate metabolism are expressed at higher levels in the *pknB* mutant. For example, *aldA* (aldehyde dehydrogenase), *pta* (phosphotransacetylase), *acsA* (acetyl-coenzyme A [acetyl-CoA] synthetase), and *pckA* (phosphoenolpyruvate carboxykinase), as well as genes encoding proteins of the citrate cycle, such as *odhB* (dihydrolipoamide succinyltransferase) and *odhA* (oxoglutarate dehydrogenase E1), were induced in the Δ*pknB* mutant. These results suggest that in the Δ*pknB* mutant there is altered synthesis of central metabolic precursors compared to the wild type. Interestingly, phosphorylation of proteins involved in glycolysis, such as pyruvate dehydrogenase, enolase, phosphate acetyltransferase, and fructose biphosphate aldolase, has been demonstrated recently (27). Lomas-Lopez et al. (27) used purified PknB to study phosphorylation of these putative substrates. The results of our microarray analysis are consistent with the observation of Lomas-Lopez (27) that PknB is involved in regulation of central metabolic functions. PknB probably links substrate requirements of growing cells by sensing the pool of unlinked peptidoglycan precursors with synthesis of purines and pyrimidines and amino acids such as glutamine and lysine. Both glutamine and lysine are essential constituents of murein monomer precursors. To maintain the glutamine pool in the Δ*pknB* strain, activation of enzymes of the citrate cycle resulting in the production of 2-oxoglutarate from oxaloacetate might be important for the cells. Likewise, Cowley et al. described accumulation of glutamate and glutamine in an STPK deletion (Δ*pknG*) mutant of *M. tuberculosis* (10).

Conclusion. Protein phosphorylation on serine and threonine residues seems to be a common theme in regulation of cellular functions in prokaryotes and eukaryotes. PknB probably is the only eukaryote-like STPK of *S. aureus* that is involved in the regulation of several central metabolic functions, such as purine and pyrimidine synthesis, cell wall synthesis, and glycolysis and the citrate cycle. Recently, the serine/threonine/tyrosine phosphoproteomes of the gram-positive model organism *B. subtilis*, the lactic acid bacterium *Lactococcus lactis*, and the gram-negative model bacterium *E. coli* have been determined (14, 28, 29, 30, 41). Comparison of phosphorylation sites in these three species revealed that the majority of phosphorylated proteins were species specific. Therefore, it has been concluded that phosphorylation by eukaryote-like STPKs probably coevolved with adaptation of the bacteria to specific ecological niches. Most strikingly, serine/threonine/tyrosine phosphorylation has been found in housekeeping pathways and in central carbon metabolism processes, such as glycolysis, in all three species. The results of these phosphoproteome studies are in agreement with our microarray data with respect to modulation of functions of central metabolism, such as glycolysis. Genes that are involved in central metabolic functions were clearly overrepresented in the deregulated genes in the *pknB* mutant compared to the wild-type strain. PurA and other enzymes involved in purine biosynthesis have not been found in recent phosphoproteome studies of *B. subtilis* and *L. lactis*, but this pathway has been shown to be regulated by an enzyme homologous to PknB in *S. agalactiae*. Obviously, phosphorylation on the functional level by eukaryote-like STPKs may be conserved among different bacterial species, and at least glycolysis seems to be a common theme of regulation by serine/threonine/tyrosine phosphorylation and dephosphorylation in many bacteria. However, specific Ser/Thr/Tyr phosphorylation has evolved more recently under the particular requirements of the niches in which these bacteria compete (e.g., *B. subtilis* in soil, *L. lactis* in dairy products, and *S. aureus* and *S. agalactiae* on mucosal surfaces).

The exact role of PknB in *S. aureus* remains to be determined; however, all the data available, such as the data for the regulation of PurA activity described in this report, suggest that there is fine regulation of enzymatic activity by PknB rather than an "on-off" mechanism due to phosphorylation and dephosphorylation of serine and threonine residues of target enzymes. Importantly, a lack of PknB resulted in decreased virulence in a murine model of kidney infection. The mutant strain showed significantly less ability to colonize kidneys after intravenous challenge (12). Based on our microarray data, it is more likely that the reduced virulence of the *pknB* mutant strain results from an impaired ability to survive in the host due to metabolic limitation rather than from reduced expression of virulence determinants.

ACKNOWLEDGMENTS

This study was supported by grants from the Deutsche Forschungsgemeinschaft (TRR34, SFB630) and the EU (LSHM-CT-2006-019064-StaphDynamics).

We thank Ursula Wallner and Martin Eckart for technical assistance.

REFERENCES

1. **Av-Gay, Y., S. Jamil, and S. J. Drews.** 1999. Expression and characterization of the *Mycobacterium tuberculosis* serine/threonine protein kinase PknB. Infect. Immun. **67:**5676–5682.
2. **Bakal, C. J., and J. E. Davies.** 2000. No longer an exclusive club: eukaryotic signalling domains in bacteria. Trends Cell Biol. **10:**32–38.
3. **Bayles, K. W.** 2000. The bactericidal action of penicillin: new clues to an unsolved mystery. Trends Microbiol. **8:**274–278.
4. **Biswas, R., L. Voggu, U. K. Simon, P. Hentschel, G. Thumm, and F. Götz.** 2006. Activity of the major staphylococcal autolysin Atl. FEMS Microbiol. Lett. **259:**260–268.
5. **Boitel, B., M. Ortiz-Lombardia, R. Duran, F. Pompeo, S. T. Cole, C. Cervenansky, and P. M. Alzari.** 2003. PknB kinase activity is regulated by phosphorylation in two Thr residues and dephosphorylation by PstP, the cognate phospho-Ser/Thr phosphatase, in *Mycobacterium tuberculosis*. Mol. Microbiol. **49:**1493–1508.
6. **Brückner, R.** 1997. Gene replacement in *Staphylococcus carnosus* and *Staphylococcus xylosus*. FEMS Microbiol. Lett. **151:**1–8.
7. **Brunskill, E. W., and K. W. Bayles.** 1996. Identification and molecular characterization of a putative regulatory locus that affects autolysis in *Staphylococcus aureus*. J. Bacteriol. **178:**611–618.
8. **Brunskill, E. W., and K. W. Bayles.** 1996. Identification of LytSR-regulated genes from *Staphylococcus aureus*. J. Bacteriol. **178:**5810–5812.
9. **Clinical and Laboratory Standards Institute.** 2006. Methods for dilution antimicrobial susceptibility tests for bacteria that grow aerobically. Document M7-A7. CLSI, Wayne, PA.
10. **Cowley, S., M. Ko, N. Pick, R. Chow, K. J. Downing, B. G. Gordhan, J. C. Betts, V. Mizrahi, D. A. Smith, R. W. Stokes, and Y. Av-Gay.** 2004. The *Mycobacterium tuberculosis* protein serine/threonine kinase PknG is linked to cellular glutamate/glutamine levels and is important for growth in vivo. Mol. Microbiol. **52:**1691–1702.
11. **Curry, J. M., R. Whalan, D. M. Hunt, K. Gohil, M. Strom, L. Rickman, M. J. Colston, S. J. Smerdon, and R. S. Buxton.** 2005. An ABC transporter containing a forkhead-associated domain interacts with a serine-threonine protein kinase and is required for growth of *Mycobacterium tuberculosis* in mice. Infect. Immun. **73:**4471–4477.

12. **Dèbarbouillè, M., S. Dramsi, O. Dussurget, M.-A. Nahori, E. Vaganay, G. Jouvion, A. Cozzone, T. Msadek, and B. Duclos.** 24 April 2009. Characterization of a serine/threonine kinase involved in virulence of *Staphylococcus aureus*. J. Bacteriol. **191:**4070–4081.
13. **De Lencastre, H., S. W. Wu, M. G. Pinho, A. M. Ludovice, S. Filipe, S. Gardete, R. Sobral, S. Gill, M. Chung, and A. Tomasz.** 1999. Antibiotic resistance as a stress response: complete sequencing of a large number of chromosomal loci in *Staphylococcus aureus* strain COL that impact on the expression of resistance to methicillin. Microb. Drug Resist. **5:**163–175.
14. **Eymann, C., D. Becher, J. Bernhardt, K. Gronau, A. Klutzny, and M. Hecker.** 2007. Dynamics of protein phosphorylation on Ser/Thr/Tyr in *Bacillus subtilis*. Proteomics **7:**3509–3526.
15. **Fox, P. M., M. W. Climo, and G. L. Archer.** 2007. Lack of relationship between purine biosynthesis and vancomycin resistance in *Staphylococcus aureus*: a cautionary tale for microarray interpretation. Antimicrob. Agents Chemother. **51:**1274–1280.
16. **Galyov, E. E., S. Hakansson, A. Forsberg, and H. Wolf-Watz.** 1993. A secreted protein kinase of *Yersinia pseudotuberculosis* is an indispensable virulence determinant. Nature **361:**730–732.
17. **Hanks, S. K., A. M. Quinn, and T. Hunter.** 1988. The protein kinase family: conserved features and deduced phylogeny of the catalytic domains. Science **241:**42–52.
18. Reference deleted.
19. **Hunter, T.** 1995. Protein kinases and phosphatases: the yin and yang of protein phosphorylation and signaling. Cell **80:**225–236.
20. **Hussain, H., P. Branny, and E. Allan.** 2006. A eukaryotic-type serine/threonine protein kinase is required for biofilm formation, genetic competence, and acid resistance in *Streptococcus mutans*. J. Bacteriol. **188:**1628–1632.
21. **Jin, H., and V. Pancholi.** 2006. Identification and biochemical characterization of a eukaryotic-type serine/threonine kinase and its cognate phosphatase in *Streptococcus pyogenes*: their biological functions and substrate identification. J. Mol. Biol. **357:**1351–1372.
22. **Juang, R. H., K. F. McCue, and D. W. Ow.** 1993. Two purine biosynthetic enzymes that are required for cadmium tolerance in *Schizosaccharomyces pombe* utilize cysteine sulfinate in vitro. Arch. Biochem. Biophys. **304:**392–401.
23. **Kristich, C. J., C. L. Wells, and G. M. Dunny.** 2007. A eukaryotic-type Ser/Thr kinase in *Enterococcus faecalis* mediates antimicrobial resistance and intestinal persistence. Proc. Natl. Acad. Sci. USA **104:**3508–3513.
24. **Kuroda, M., H. Kuroda, T. Oshima, F. Takeuchi, H. Mori, and K. Hiramatsu.** 2003. Two-component system VraSR positively modulates the regulation of cell wall biosynthesis pathway in *Staphylococcus aureus*. Mol. Microbiol. **49:**807–821.
25. **Laemmli, U. K.** 1970. Cleavage of structural proteins during the assembly of the head of bacteriophage T4. Nature **227:**680–685.
26. **Liebeke, M., D. C. Pother, N. van Duy, D. Albrecht, D. Becher, F. Hochgrafe, M. Lalk, M. Hecker, and H. Antelmann.** 2008. Depletion of thiol-containing proteins in response to quinones in *Bacillus subtilis*. Mol. Microbiol. **69:**1513–1529.
27. **Lomas-Lopez, R., P. Paracuellos, M. Riberty, A. J. Cozzone, and B. Duclos.** 2007. Several enzymes of the central metabolism are phosphorylated in *Staphylococcus aureus*. FEMS Microbiol. Lett. **272:**35–42.
28. **Macek, B., F. Gnad, B. Soufi, C. Kumar, J. V. Olsen, I. Mijakovic, and M. Mann.** 2008. Phosphoproteome analysis of E. coli reveals evolutionary conservation of bacterial Ser/Thr/Tyr phosphorylation. Mol. Cell. Proteomics **7:**299–307.
29. **Macek, B., I. Mijakovic, J. V. Olsen, F. Gnad, C. Kumar, P. R. Jensen, and M. Mann.** 2007. The serine/threonine/tyrosine phosphoproteome of the model bacterium *Bacillus subtilis*. Mol. Cell. Proteomics **6:**697–707.
30. **Madec, E., A. Laszkiewicz, A. Iwanicki, M. Obuchowski, and S. Seror.** 2002. Characterization of a membrane-linked Ser/Thr protein kinase in *Bacillus subtilis*, implicated in developmental processes. Mol. Microbiol. **46:**571–586.
31. **Mani, N., P. Tobin, and R. K. Jayaswal.** 1993. Isolation and characterization of autolysis-defective mutants of *Staphylococcus aureus* created by Tn*917-lacZ* mutagenesis. J. Bacteriol. **175:**1493–1499.
32. **Michel, A., F. Agerer, C. R. Hauck, M. Herrmann, J. Ullrich, J. Hacker, and K. Ohlsen.** 2006. Global regulatory impact of ClpP protease of *Staphylococcus aureus* on regulons involved in virulence, oxidative stress response, autolysis, and DNA repair. J. Bacteriol. **188:**5783–5796.
33. **Nariya, H., and S. Inouye.** 2002. Activation of 6-phosphofructokinase via phosphorylation by Pkn4, a protein Ser/Thr kinase of *Myxococcus xanthus*. Mol. Microbiol. **46:**1353–1366.
34. **Neu, J. M., S. V. MacMillan, J. R. Nodwell, and G. D. Wright.** 2002. StoPK-1, a serine/threonine protein kinase from the glycopeptide antibiotic producer *Streptomyces toyocaensis* NRRL 15009, affects oxidative stress response. Mol. Microbiol. **44:**417–430.
35. **Pfaffl, M. W.** 2001. A new mathematical model for relative quantification in real-time RT-PCR. Nucleic Acids Res. **29:**e45.
36. **Rajagopal, L., A. Clancy, and C. E. Rubens.** 2003. A eukaryotic type serine/threonine kinase and phosphatase in *Streptococcus agalactiae* reversibly phosphorylate an inorganic pyrophosphatase and affect growth, cell segregation, and virulence. J. Biol. Chem. **278:**14429–14441.
37. **Rajagopal, L., A. Vo, A. Silvestroni, and C. E. Rubens.** 2006. Regulation of cytotoxin expression by converging eukaryotic-type and two-component signalling mechanisms in *Streptococcus agalactiae*. Mol. Microbiol. **62:**941–957.
38. **Rajagopal, L., A. Vo, A. Silvestroni, and C. E. Rubens.** 2005. Regulation of purine biosynthesis by a eukaryotic-type kinase in *Streptococcus agalactiae*. Mol. Microbiol. **56:**1329–1346.
39. **Saskova, L., L. Novakova, M. Basler, and P. Branny.** 2007. Eukaryotic-type serine/threonine protein kinase StkP is a global regulator of gene expression in *Streptococcus pneumoniae*. J. Bacteriol. **189:**4168–4179.
40. **Shah, I. M., M. H. Laaberki, D. L. Popham, and J. Dworkin.** 2008. A eukaryotic-like Ser/Thr kinase signals bacteria to exit dormancy in response to peptidoglycan fragments. Cell **135:**486–496.
41. **Soufi, B., F. Gnad, P. R. Jensen, D. Petranovic, M. Mann, I. Mijakovic, and B. Macek.** 2008. The Ser/Thr/Tyr phosphoproteome of *Lactococcus lactis* IL1403 reveals multiply phosphorylated proteins. Proteomics **8:**3486–3493.
42. **Stock, A. M., V. L. Robinson, and P. N. Goudreau.** 2000. Two-component signal transduction. Annu. Rev. Biochem. **69:**183–215.
43. **Takahashi, J., H. Komatsuzawa, S. Yamada, T. Nishida, H. Labischinski, T. Fujiwara, M. Ohara, J. Yamagishi, and M. Sugai.** 2002. Molecular characterization of an *atl* null mutant of *Staphylococcus aureus*. Microbiol. Immunol. **46:**601–612.
44. **Truong-Bolduc, Q. C., Y. Ding, and D. C. Hooper.** 2008. Posttranslational modification influences the effects of MgrA on *norA* expression in *Staphylococcus aureus*. J. Bacteriol. **190:**7375–7381.
45. **Tusher, V. G., R. Tibshirani, and G. Chu.** 2001. Significance analysis of microarrays applied to the ionizing radiation response. Proc. Natl. Acad. Sci. USA **98:**5116–5121.
46. **Umeyama, T., P. C. Lee, and S. Horinouchi.** 2002. Protein serine/threonine kinases in signal transduction for secondary metabolism and morphogenesis in *Streptomyces*. Appl. Microbiol. Biotechnol. **59:**419–425.
47. **Wang, J., C. Li, H. Yang, A. Mushegian, and S. Jin.** 1998. A novel serine/threonine protein kinase homologue of *Pseudomonas aeruginosa* is specifically inducible within the host infection site and is required for full virulence in neutropenic mice. J. Bacteriol. **180:**6764–6768.
48. **Weng, M., P. L. Nagy, and H. Zalkin.** 1995. Identification of the *Bacillus subtilis pur* operon repressor. Proc. Natl. Acad. Sci. USA **92:**7455–7459.
49. **Yeats, C., R. D. Finn, and A. Bateman.** 2002. The PASTA domain: a beta-lactam-binding domain. Trends Biochem. Sci. **27:**438.

9.4 Staphylococcal PknB as the first prokaryotic representative of the proline-directed kinases

Staphylococcal PknB as the first prokaryotic representative of the proline-directed kinases.

Miller M, Donat S, Rakette S, Stehle T, Kouwen TR, Diks SH, Dreisbach A, Reilman E, Gronau K, Becher D, Peppelenbosch MP, van Dijl JM, Ohlsen K.

PLoS One. 2010 Feb 4;5(2):e9057

OPEN ACCESS Freely available online

PLoS one

Staphylococcal PknB as the First Prokaryotic Representative of the Proline-Directed Kinases

Malgorzata Miller[1], Stefanie Donat[2], Sonja Rakette[4], Thilo Stehle[4,6], Thijs R. H. M. Kouwen[1], Sander H. Diks[3], Annette Dreisbach[1], Ewoud Reilman[1], Katrin Gronau[5], Dörte Becher[5], Maikel P. Peppelenbosch[3], Jan Maarten van Dijl[1]*, Knut Ohlsen[2]

1 Department of Medical Microbiology, University Medical Center Groningen and University of Groningen, Groningen, The Netherlands, **2** Institut für Molekulare Infektionsbiologie, Universität Würzburg, Würzburg, Germany, **3** Department of Cell Biology, University Medical Center Groningen and University of Groningen, Groningen, The Netherlands, **4** Interfakultäres Institut für Biochemie, Universität Tübingen, Tübingen, Germany, **5** Institut für Mikrobiologie, Ernst-Moritz-Arndt Universität Greifswald, Greifswald, Germany, **6** Department of Pediatrics, Vanderbilt University School of Medicine, Nashville, Tennessee, United States of America

Abstract

In eukaryotic cell types, virtually all cellular processes are under control of proline-directed kinases and especially MAP kinases. Serine/threonine kinases in general were originally considered as a eukaryote-specific enzyme family. However, recent studies have revealed that orthologues of eukaryotic serine/threonine kinases exist in bacteria. Moreover, various pathogenic species, such as *Yersinia* and *Mycobacterium*, require serine/threonine kinases for successful invasion of human host cells. The substrates targeted by bacterial serine/threonine kinases have remained largely unknown. Here we report that the serine/threonine kinase PknB from the important pathogen *Staphylococcus aureus* is released into the external milieu, which opens up the possibility that PknB does not only phosphorylate bacterial proteins but also proteins of the human host. To identify possible human targets of purified PknB, we studied *in vitro* phosphorylation of peptide microarrays and detected 68 possible human targets for phosphorylation. These results show that PknB is a proline-directed kinase with MAP kinase-like enzymatic activity. As the potential cellular targets for PknB are involved in apoptosis, immune responses, transport, and metabolism, PknB secretion may help the bacterium to evade intracellular killing and facilitate its growth. In apparent agreement with this notion, phosphorylation of the host-cell response coordinating transcription factor ATF-2 by PknB was confirmed by mass spectrometry. Taken together, our results identify PknB as the first prokaryotic representative of the proline-directed kinase/MAP kinase family of enzymes.

Citation: Miller M, Donat S, Rakette S, Stehle T, Kouwen TRHM, et al. (2010) Staphylococcal PknB as the First Prokaryotic Representative of the Proline-Directed Kinases. PLoS ONE 5(2): e9057. doi:10.1371/journal.pone.0009057

Editor: Frank R. DeLeo, National Institute of Allergy and Infectious Diseases, National Institutes of Health, United States of America

Received November 12, 2009; **Accepted** January 18, 2010; **Published** February 4, 2010

Funding: Funding for this work was received from the EU (CEU projects LSHM-CT-2006-019064 and LSHG-CT-2006-037469), the transnational SysMO initiative through project BACELL SysMO, the European Science Foundation under the EUROCORES Programme EuroSCOPE, grant 04-EScope 01-011 from the Research Council for Earth and Life Sciences of the Netherlands Organization for Scientific Research, the Top Institute Pharma project T4-213, and the Deutsche Forschungsgemeinschaft (TR34). The funders had no role in study design, data collection and analysis, decision to publish, or preparation of the manuscript.

Competing Interests: The authors have declared that no competing interests exist.

* E-mail: j.m.van.dijl@med.umcg.nl

Introduction

Despite their clinical relevance, the mechanisms employed by pathogenic bacteria to subvert the host immune system remain only partially characterised. It has become clear, however, that pathogens create a beneficial environment for their survival by secreting proteins that mimic the functions of several host proteins. One of the best known bacterial examples is *Yersinia pestis*, the plague bacterium, which injects its effector proteins into the host cells by the type III secretion system [1,2]. These *Yersinia* effector (Yop) proteins include the eukaryotic-like serine/threonine kinase YpkA, also known as YopO [3]. This kinase shows a high degree of sequence similarity to mammalian serine/threonine protein kinase domains. YpkA is translocated into a host cell where it disrupts the actin-based cytoskeletal system and promotes both survival and replication of bacteria by an unknown mechanism [3,4,5]. Nevertheless, the full spectrum of human proteins that are phosphorylated by YpkA has remained elusive so far [6].

Eukaryotic-like serine/threonine protein kinases (STPKs) are present not only in the *Yersinia* genus, but they have also been identified in the soil microorganism *Myxococcus xanthus* [7,8] and in human pathogens, such as *Mycobacterium tuberculosis*, which even encodes 11 STPKs. Only two of these (PknG and PknK) are soluble proteins, while the other nine STPKs contain a transmembrane domain [9]. Moreover STPKs have also been identified in *Pseudomonas aeruginosa* [10,11], *Streptococcus pneumoniae* [12,13,14] and in *Staphylococcus aureus* [15,16,17]. However, the precise biological functions and substrate specificities of these kinases have not yet been defined.

Recently, attention has been focussed on the PknB kinase of *S. aureus*. This Gram-positive bacterium is part of the human microbiota, but it can turn into a dangerous pathogen, causing a wide range of infections [18,19,20]. Although *S. aureus* is mostly considered as an extracellular pathogen, it can invade a variety of mammalian non-professional cells, such as nasal endothelial cells. Moreover *S. aureus* survives phagocytosis by professional phagocytes [21,22,23], such as neutrophils [24,25], mouse or rat macrophages [26,27,28,29], and human macrophages [30,31]. To overcome the stressful conditions imposed by its host, *S. aureus* has evolved various protective and offensive responses

[32,33,34,35], such as sensing of environmental stimuli and the activation and inactivation of response regulators [36,37]. This is generally achieved through cascades of phosphorylation reactions in the host, which focuses a strong interest on the role of kinases, such as the serine/threonine kinase PknB (also known as StpK) in staphylococcal persistence.

The PknB kinase is composed of three extracellular PASTA domains (penicillin binding domains), a central transmembrane domain and an intracellular kinase domain [16,38]. Interestingly, it was recently reported that PknB is not only involved in regulation of the central metabolism of *S. aureus* [15], but also determines staphylococcal infection of mouse kidneys in an abscess model [17]. The latter observation raises the question whether the kinase activity of PknB is directly or indirectly involved in the pathogenicity of *S. aureus*. A direct role of PknB in infection is conceivable since serine/threonine kinases play key roles in mammalian cell signalling, and at least two bacterial equivalents, YpkA of *Yersinia* and PknG of *Mycobacterium tuberculosis*, have been shown to be directly involved in the subversion of host cells during the respective infectious processes [39,40]. However the exact role played by PknB in pathogenesis or staphylococcal persistence has thus far remained unclear.

Here we show that full-size soluble PknB is present in the medium of growing *S. aureus* cells. We therefore investigated whether PknB of *S. aureus* can recognize and phosphorylate known substrates of human serine/threonine kinases. For this purpose, we used peptide microarrays with known human phosphorylation sites. The phosphorylation profile and mass spectrometry results show that PknB is a proline-directed kinase, which can indeed phosphorylate specific human targets. The observed target specificity of PknB indicates possible roles for this enzyme in a wide range of host cell signalling processes during *S. aureus* infection.

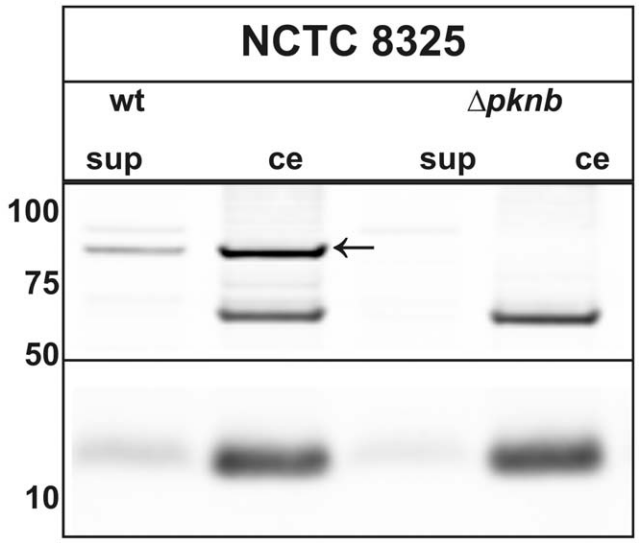

Figure 1. Release of PknB into the growth medium of *S. aureus*. The *S. aureus* strain NCTC 8325 (wt) or a Δ*pknB* derivative were propagated at 37°C in TSB and harvested at OD_{600} 2. Crude extracts (ce) and supernatant (sup) fractions were isolated, corrected for OD and separated by NuPAGE electrophoresis (Invitrogen). Two-fold higher amounts of the supernatant fractions were used for PAGE as compared to the crude extracts. Immunoblotting was conducted using specific antibodies against PknB (upper panel) or TrxA (lower panel). The latter served as an indicator for cell lysis. The position of the specific PknB signal is marked with a black arrow. The band at ~60 kDA corresponds to an unidentified protein, which cross-reacts with the antibodies against PknB. The molecular weight of marker proteins is indicated on the left.
doi:10.1371/journal.pone.0009057.g001

Results and Discussion

Identification of Extracellular PknB

It has previously been reported that different bacteria such as *M. tuberculosis* and *Yersinia* species can secrete their eukaryotic-like serine/threonine kinases directly into the host. This mechanism allows these bacteria to survive intracellularly [9,39], to disrupt the actin cytoskeleton [41], or to cause host cell apoptosis [40]. Since these bacterial ser/thr kinases need to be exported in order to impact on host cells, we investigated whether PknB might be detectable in the extracellular milieu of *S. aureus*. As shown by Western blotting using polyclonal antibodies against PknB, the full-size PknB was detectable both in the cellular and growth medium fractions of cells of *S. aureus* NCTC 8325 harvested at an OD_{600} of 2. As expected, PknB was neither detectable in cellular nor growth medium fractions of the Δ*pknB* mutant. The precise mechanism by which PknB is liberated from the wild-type cells remains to be elucidated. However, there is precedence for the release of membrane proteins, or fragments thereof, into the extracellular milieu of Gram-positive bacteria, such as *S. aureus*, by as yet unknown mechanisms [42]. One possibility is that these proteins are released by cell lysis, remaining stable in the medium due to an intrinsic resistance to extracytoplasmic proteolysis [43]. The idea that PknB is released by lysis would be consistent with the detection of relatively small amounts of the cytoplasmic marker protein thioredoxin A (TrxA) in the growth medium fractions (Fig. 1). TrxA is a cytoplasmic bacterial protein, which acts as an antioxidant by facilitating the reduction of cysteine disulfides in other cytoplasmic proteins. Since TrxA is normally a cytoplasmic protein, it will only be found in the extracellular milieu when bacterial cells have lysed. Notably, compared to the cellular samples, we detected relatively more extracellular PknB than extracellular TrxA, which might suggest that the release of PknB is the consequence of a specific process rather than cell lysis.

Irrespective of the mechanism by which PknB is released into the extracellular milieu of *S. aureus*, its release may impact on human host cell functions. This could be the case upon internalization of *S. aureus*. Although *S. aureus* is primarily an extracellular pathogen, there is strong evidence that it can be internalized by a wide range of human host cells. For example, *S. aureus* invades non-professional phagocytes by a mechanism which requires a specific interaction between the bacterial fibronectin-binding protein and the host cell [44,45,46]. This leads to host signal transduction, activation of tyrosine kinases, cytoskeletal rearrangement and endosome uptake. Bayles and Qazi reported that internalized *S. aureus* is able to escape from the host endosome, and this fact opens up the possibility of direct interactions of released PknB with proteins of the human host [47,48]

Eukaryotic Phosphorylation Sites Recognized by PknB

Peptide arrays (PepChips) have previously been used successfully to profile the activity of kinases in eukaryotic cell lysates [49]. We therefore employed this array-based technology to investigate whether the staphylococcal kinase PknB has the ability to recognize and phosphorylate human phosphorylation sites. When the PepChips were incubated with purified and active PknB [16] and [^{33}P-γ] ATP, radioactivity was efficiently incorporated in a particular subset of the peptides on the chip. In contrast, little radioactivity was incorporated when the arrays were incubated with [^{33}P-γ] ATP in the absence of PknB. We identified 68

potential substrates for PknB, of which the biological functions are summarised in Table 1 (for details, see Table S1). Interestingly, 32 of the potential human substrates of PknB are involved in signal transduction and cell communication. The identified peptides include serine/threonine kinases, cell cycle control proteins, and regulators of protein phosphorylation such as adaptor molecules. Our results suggest that any active PknB released from invasive *S. aureus* cells may target signal transduction mechanisms for host cell subversion. In addition, 13 potential PknB substrates are involved in gene regulation, including transcription factors, transcription regulatory proteins and RNA binding proteins. Three potential substrates play a role in immune responses and recognition, five in transport processes, ten in cell growth and maintenance (cytoskeletal and structural proteins), two in cell metabolism, two in stress responses, and one in apoptosis.

Phosphorylation of the identified potential human PknB targets would result in significant changes in host cell signal transduction. One of the peptides that is best phosphorylated by PknB (^{64}IVADQTPTPTR^{74}) is derived from the Activating Transcription Factor-2 (ATF-2) (see Table S2). ATF-2 belongs to the bZIP (Basic Leucine Zipper Domain) DNA-binding protein family and is expressed by almost all human cells (GeneNote, Ensemlb ID: ENSG00000115966). In unstimulated cells, ATF-2 is maintained in an inactive form by interactions between its own activation domain and its bZIP domain [50]. In response to certain stimuli [51,52,53], the kinases p38 and JNK phosphorylate ATF-2 at amino acids Thr69 and Thr71 [52,53]. The phosphorylated ATF-2 can then form homodimers and heterodimers [54], which bind with high affinity to the consensus sequence 5′-TGACGTCA-3′ [55] in target gene promoters, resulting in their activation. The phosphorylation of ATF-2 thus results in the expression of a broad spectrum of proteins implicated in different processes, such as cell cycle molecules (cyclin D1) [56], cell adhesion molecules [57], growth factors [58], anti-apoptotic factors [59], and invasion-related molecules [60].

To confirm that PknB is able to phosphorylate ATF-2, we incubated ATF-2 with PknB *in vitro* and performed mass spectrometric analyses. As a positive control we incubated ATF-2 with p38. The results show that PknB can indeed phosphorylate ATF-2 (Fig. 2). However, PknB phosphorylated Thr73, whereas p38 phosphorylated Thr69 and Thr71. Interestingly, Thr73 is the known phosphorylation site of the Human Vaccinia-related Kinase 1 (VRK1) [61]. VRK1 is a ser/thr kinase overexpressed in proliferating cells [62,63]. Phosphorylation of ATF-2 on Thr 73 by VRK1 kinase leads to the activation of ATF-2 and, consequently, the induction of cellular protection mechanisms.

Another peptide that was very efficiently phosphorylated by PknB belongs to the Bcl-2 interacting protein Bim (see Table S2). *In vivo* this peptide is recognized by the c-Jun NH_2-terminal kinase (JNK) (Table S1) [64,65]. Bim is a member of the pro-apoptotic Bcl-2 family of proteins, which play a critical role in apoptosis regulation. A short peptide motif, DKSTQT^{56}P, which is present in BimL and BimEL, but absent from BimS, mediates the binding of Bim to the LC8 cytoplasmic dynein light chain. Importantly, the same motif is also recognized and phosphorylated by PknB (Table S1). Exposure of cells to stress causes the activation of JNK kinase, which phosphorylates Bim at Thr56 in the afore-mentioned DKSTQTP motif. The phosphorylation leads to conformational changes in Bim and subsequent dissociation of Bim from dynein motor complexes [66]. The activated Bim may directly activate pro-apoptotic Bax, or indirectly activate Bax by binding anti-apoptotic Bcl-2 family proteins (e.g., Bcl-2 and Bcl-X_L) [67,68]. Judged by the observed phosporylation of the DKSTQT^{56}P peptide, the release of PknB from invasive *S. aureus* cells might have similar effects as its phosphorylation by JNK.

A third intriguing target of PknB identified through phosphorylation profiling is the cytoskeleton-associated protein paxillin. This protein has previously been reported as a target for the phosphatase YopH, which is injected by *Yersinia* into human host cells, thereby affecting cytoskeleton integrity [69]. Taken together, the identified potential targets of PknB are fully consistent with previously reported effects of *S. aureus* and other bacteria on host cell apoptosis [70,71,72,73] and a wide range of cellular processes [4,6,13,39,40,74,75].

Interestingly, a comparison of the identified human phosphorylation sites of PknB with staphylococcal proteins revealed about 300 putative PknB target sequences in proteins of *S. aureus* (data not shown). These include amino acid sequences in proteins that are known to be phosphorylated by PknB, such as triosephosphate isomerase, DnaK, elongation factors, ribosomal proteins and trigger factor [15].

PknB Is a Proline-Directed Serine/Threonine Kinase

To determine which amino acids are preferably phosphorylated by PknB, we generated a sequence logo based on the 15% best-

Table 1. Cellular processes that can be targeted by PknB.

Transport **Total: 5 proteins**	**Cell growth and maintanance** **Total: 10 proteins**
membrane transport proteins, voltage gated channel, water channel proteins	structural proteins, cell cycle regulation proteins, cell adhesion proteins
Metabolism **Total: 2 proteins**	**Immune response and recognition** **Total: 3 proteins**
phosphotransferase, ribosomal subunit	immunoglobulin, cell surface receptors
Signal transduction and Cell communication **Total: 32 proteins**	**Regulation of nucleobase, nucleoside, nucleotide and nucleic acid metabolism** **Total: 13 proteins**
receptors, cell cycle proteins, cell junction proteins, serine/threonine kinases, tyrosine kinases, transport/cargo proteins, adapter molecules	DNA binding site, RNA binding site, ribonucleoproteins, transcription factors, transcription regulatory proteins
Apoptosis **Total: 1 protein**	**Stress** **Total: 2 proteins**
Bcl2- interacting protein BIM	Heat-shock proteins

Functional classes of human proteins that are potentially phosphorylated by PknB, as identified in the present PepChip analysis, are classified by their biological function.

doi:10.1371/journal.pone.0009057.t001

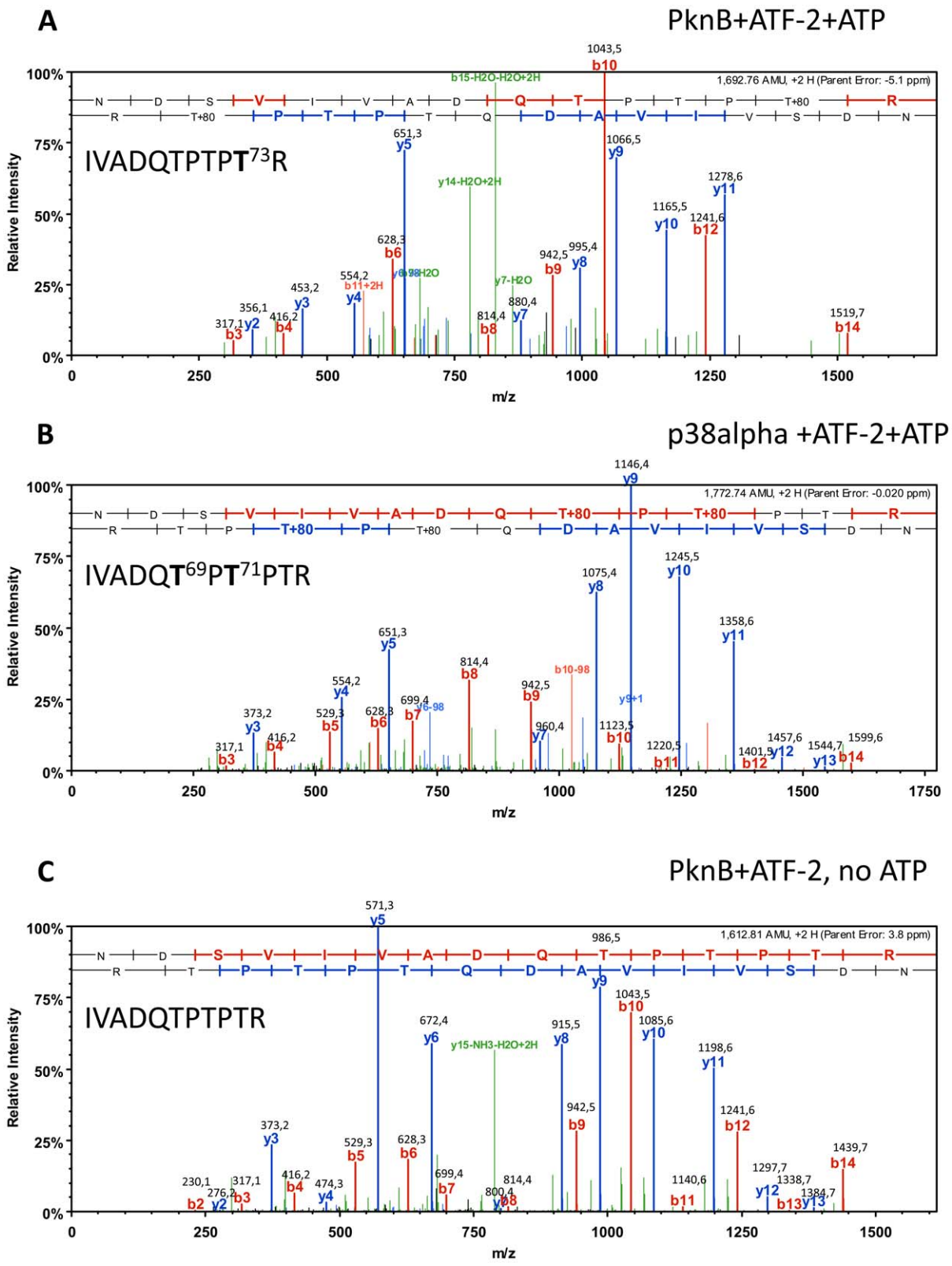

Figure 2. Verification of PknB-dependent phosphorylation of ATF-2. Recombinant ATF-2 was incubated with PknB (A) or p38 (B) in kinase reaction buffer for 30 minutes at 37°C. As a control, ATF-2 was incubated with PknB in the absence of ATP. After tryptic digestion, the resulting peptides were analyzed via online-mass spectrometry. The panels show the spectra for the ATF-2 peptide VIVADQTPTPTR that was either phosphorylated at the Thr73 by PknB, or Thr 69 and Thr 71 by p38. The b- and y-ions are high-lighted and the observed masses are given. Also the peptide sequence is indicated and amino acids that have been identified my mass spectrometric analysis are indicated in bold letters. The upper sequence corresponds to the b- and the lower sequence to the y-ions.
doi:10.1371/journal.pone.0009057.g002

phosphorylated peptides (Fig. 3). The most frequently found amino acids in PknB-phosphorylated peptides are serine and threonine. This observation is in agreement with the serine/threonine kinase signature in the primary sequence of PknB. Apparently, the signature has portability across the eukaryotic/prokaryotic divides. Nevertheless tyrosine phosphorylation can also be unambiguously identified making this study the first demonstration of enzymatic tyrosine kinase activity in a single isolated prokaryotic enzyme. What is also clearly evident in the sequence logo is the presence of a proline residue next to phosphorylated serine, threonine or tyrosine residues. Thus, it seems that proline is part of the PknB recognition and target sequence. This links PknB to the evolutionary well-conserved family of proline-directed kinases, which includes cyclin-dependent protein kinases (CDKs), mitogen-activated protein kinases (MAP kinases) and glycogen synthase kinase-3 (GSK-3; Fig. 3). These kinases play a crucial role in cell cycle, transcription, signal transduction and are involved in many diseases like cancer or Alzheimer's disease [76,77,78]. Like the eukaryotic MAP kinases, PknB has the ability to phosphorylate ATF-2 at least *in vitro*, which implies that PknB has a MAP kinase-like enzymatic activity. This view is supported by the observation that PknB is also involved in the regulation of important cellular functions in *S. aureus*, including central metabolic pathways [15] and cell wall metabolism [79]. Taken together, our results imply that PknB is the first prokaryotic representative of the proline-directed kinases, a cardinal family of regulators of eukaryotic cellular physiology. A major challenge for future studies will be to identify human proteins that are phosphorylated by PknB *in vivo*, for example upon internalization of *S. aureus* by macrophages.

Materials and Methods

Detection of Extracellular PknB by Immunoblotting

S. aureus NCTC 8325 or a *pknB* mutant of this strain [16] were cultivated in 10 ml of TSB (37°C, 250 rpm) and growth was monitored by OD_{600} readings. Samples of 3 ml were harvested at OD_{600} 2 and cells were separated from the growth medium by centrifugation (8000 rpm, 5 min, 4°C). Bacterial cells were washed in PBS, resuspended in sample buffer (NuPage, Invitrogen) and disrupted using a Precellys 24 bead beater (three times 30 s, 6800 rpm; Bertin Technologies). Proteins from the growth medium fraction were collected by TCA-acetone precipitation [80]. Protein samples were mixed with gel-loading buffer with reducing agent and incubated for 5 min at 95°C. To receive a clear signal for the supernatant fractions twice as much as from the crude extract was applied to gel electrophoresis. The proteins were separated on a 10% Bis-Tris gel (Invitrogen) at 200 V for 35 min in NuPAGE® MES SDS Running Buffer (Invitrogen). The separated proteins were transferred to a nitrocellulose membrane (Protran®, Schleicher and Schuell) by semi-dry blotting at 200 mA for 75 min. Membranes were blocked for one hour in Blocking Buffer (Odyssey, Li-Cor biosciences). Rabbit primary antibodies against the kinase domain of PknB were added (1:5000 in blocking buffer) and membranes were incubated for 1 hour. Next, membranes were washed 3 times for 5 minutes in PBS-T (Phosphate Buffered Saline Tween-20) before adding a fluorescent secondary antibody at a 1:20000 dilution in blocking buffer (IRDye 800 CW goat anti-rabbit antibody from LiCor biosciences). Membranes were incubated for 1 hour in the dark, washed three times for 5 min in PBS-T and once in PBS. After

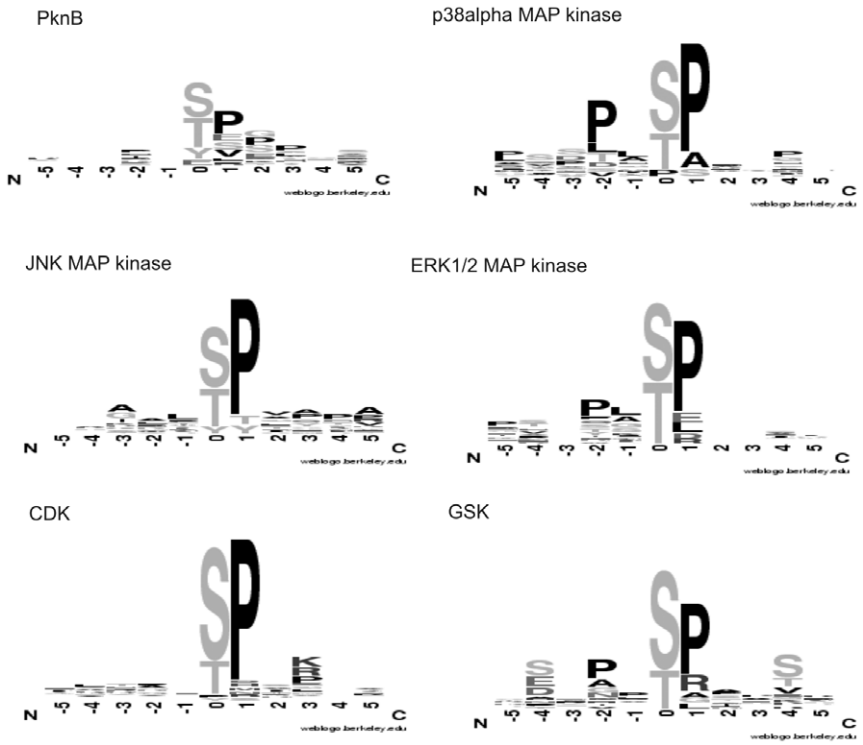

Figure 3. Sequence logo of PknB phosphorylation sites and comparison to known phosphorylation sites of human kinases. The image shows consensus recognition sites for the staphylococcal PknB and other proline-directed ser/thr kinases.
doi:10.1371/journal.pone.0009057.g003

transferring the membranes into fresh PBS, they were scanned using the Odyssey Infrared Imaging System (LiCor Biosciences). As a cell lysis control, antibodies against cytoplasmic protein TrxA were used in the same concentration as PknB antibodies.

Cloning, Expression and Purification of *S. aureus* TrxA

All procedures for DNA purification, restriction, ligation, agarose gel electrophoresis, and transformation of competent *E. coli* DH5α cells were carried out as previously described [81]. Genomic DNA of *S. aureus* RN4220 [82] was isolated using the Genelute Bacterial Genomic DNA kit (Sigma). The *trxA* gene on this genomic DNA was PCR-amplified using the primers GGGGGCATATGGCAATCGTAAAAGTAA and GGGGGC-TCGAGTAAATGTTTATCTAAAACTTC. The PCR product was cloned into *Hinc*II (*Hind*II) restricted pUC18 [83]. After verification of the sequence, the *trxA* gene was excised from this plasmid with *Nde*I and *Xho*I, and ligated into the same restriction sites of pET26b(+) (Novagen, Inc.), downstream of the T7 promoter and upstream of an in-frame His(6)tag sequence. The resulting pET26-SatrxA plasmid was checked by sequencing and used to transform *E. coli* BL21(DE3) (Invitrogen) for high-level *trxA* expression and purification. 10 ml of an overnight culture of this strain was used to inoculate 1 liter fresh LB medium and grown until an OD_{600} of 0.7 was reached. Then, isopropylthiogalactoside (IPTG) was added to a final concentration of 1 mM to induce TrxA production. After 3 hrs of induction, cells were harvested by centrifugation and resuspended in binding buffer (20 mM NaPi, 300 mM NaCl, 10% (v/v) glycerol, 5 mM imidazole, 3 mM DTT, pH 7.4). Next, cells were disrupted by two passages through a French Press (2500 PSI). Cellular debris was removed by centrifugation (30 min at 30000 g, 4°C), and the clarified supernatant fraction was applied to a nickel-charged IMAC column (5 ml HisTrap HP, GE Healthcare). Unbound sample was washed from the column with binding buffer using an ÄKTA explorer (GE Healthcare). Next, the His-tagged TrxA protein was eluted from the column using binding buffer with a gradient of increasing imidazole concentrations (up to 500 mM imidazole). The eluted fractions were checked for the presence of pure TrxA protein using SDS-PAGE and subsequent silver-staining. Further purification was achieved by concentrating the proteins with Vivaspin columns (Vivascience) and loading them on a Superdex 75 gel filtration column (Amersham) pre-equilibrated with 20 mM NaPi, 150 mM NaCl, 10% glycerol and 3.5 mM DTT, pH 7.4. Fractions containing the purified TrxA proteins were pooled and dialyzed 3 times against 20 mM Tris-HCl, pH 7.6, with 150 mM NaCl. Specific polyclonal antibodies against the purified TrxA protein were raised in rabbits (Eurogentec).

Kinome Array Analysis

PepChip™ Kinomics slides containing 976 fully annotated, disease-related kinase phosphorylation sites in triplicate (Pepscan, Lelystad, The Netherlands, http://www.pepscan.com/) were incubated with 50 µl of the ser/thr kinase PknB incubation mix (0.8 µg/ml PknB kinase domain, 60 mM HEPES, pH 7.5, 3 mM $MgCl_2$, 3 mM $MnCl_2$, 1 mM DTT, 50% glycerol, 50 µM ATP supplemented with 1Mbq [γ-^{33}P] ATP, 0.03% Brij-35, 50 µg/ml bovine serum albumin, 3 mM Na_3VO_4, 50 µg/ml PEG 8000) for 90 min in a humidified incubator. As a negative control we used the "empty" incubation mix without PknB. After incubation the peptide arrays were washed twice in 2 M NaCl (1% Tween-20) and PBS-T. Next, the arrays were rinsed twice in demineralised water and air-dried. The dried slides were transferred to a phosphor imager plate (Fuji Storm 860, Stanford, GE, USA) and exposed for 72 hours. The density of the spots was measured and analyzed with array software.

Peptide Array Data Analysis

To analyze the intensity of spots and to correct for background phosphorylation, the ScanAnalyze software and grid tools were used, and the resulting data were exported to an excel sheet. Three replicate data sets were taken for further statistical analysis. To this end, the Spearman correlation coefficient was calculated for each combination of the three sets. The average and standard deviation for each peptide were determined and plotted in an amplitude-based hierarchical fashion. If only background phosphorylation is present, this amplitude-based distribution can be described by a single exponent. Thus, determining the exponent describing amplitude behavior of the 500 least phosphorylated peptides should give an adequate description of array background phosphorylation and, in practice, this was indeed the case. 125 Peptides which exhibited the incorporation of γ-^{33}P in the absence of added kinase were excluded from further analysis. Peptides of which the average phosphorylation minus 1.96 times the standard deviation was higher as the value expected from describing the background distribution were considered to represent true phosphorylation events. Two-sided heteroscedastic t-tests were also performed on each set of values to determine significance ($p<0.05$).

Sequence Logos

Sequence logos were created with the weblogo server at http://weblogo.berkeley.edu/logo.cgi using either the preferred substrates of PknB, or known phosphorylation sequences for human kinases as available at http://www.phosphosite.org/homeAction.do

In Vitro Phosphorylation of ATF-2 by Staphylococcal PknB

In order to confirm the phosphorylation of ATF-2 by PknB, the *in vitro* assay was performed. Purified staphylococcal kinase PknB (26 µg) was incubated with 50 µg of Activating Transcription Factor fusion protein (Cell Signaling) in kinase incubation mix (50 mM HEPES, 1 mM DTT, 0.01 Brij35, 3 mM $MnCl_2$, 3 mM $MgCl_2$, 50 µM ATP) for 30 minutes at 37°C in waterbath. As a positive control, 0.1 µg of p38-alpha MAP kinase (Cell Signaling) was incubated with 50 µg of ATF-2. As negative controls, the following reaction mixtures were used: PknB with ATF-2 but without ATP; PknB with ATP but without ATF-2; and ATF-2 with ATP but without PknB.

Phosphorylation Site Identification and Protein Identification by Mass Spectrometry

Trypsin (Promega) was activated by 15 min incubation at 30°C in activation buffer and then added 1:200 to the samples, digestion was allowed to proceed over night at 37°C. The resulting peptides were separated by liquid chromatography and measured online by ESI-mass spectrometry using a nanoACQUITY UPLC™ system (Waters, Milford, MA) coupled to an LTQ Orbitrap™ mass spectrometer (Thermo Fisher Scientific, Waltham, MA). Peptides were desalted onto a trap column (Symmetry® C18, Waters). Elution was performed onto an analytical column (BEH130 C18, Waters) by a binary gradient of buffer A (0.1% (v/v) acetic acid) and B (100% (v/v) acetonitrile, 0.1% (v/v) acetic acid) over a period of 50 min with a flow rate of 400 nl/min. The LTQ Orbitrap was operated in data-dependent MS/MS mode using MSA for phospho-relevant masses. Proteins were identified by searching all MS/MS spectra in .dta format against all *S. aureus* NCTC 8325 proteins and added ATF-2 protein (extracted from the NCBI database) using Sorcerer™-SEQUEST® (ThermoFin-

nigan, San Jose, CA; version v.27, rev. 11). Sequest was searched with a fragment ion mass tolerance of 1.00 Da and a parent ion tolerance of 10 ppm. Up to two missed tryptic cleavages were allowed. Methionine oxidation (+15.99492 Da), Carbamidomethylation (+57.021465 Da) and phosphorylation of STY (+79.966331 Da) was set as variable modification. Proteins were identified by at least two peptides applying a stringent SEQUEST filter. Sequest identifications required at least deltaCn scores of greater than 0.10 and XCorr scores of greater than 1.9, 2.2, 3.75 and 3.75 for singly, doubly, triply and quadruply charged peptides. Phosphorylated peptides which passed this filter were examined manually and accepted only, when b- or y- ions confirmed the phosphorylation site.

Supporting Information

Table S1 PknB-phosphorylated peptides
Found at: doi:10.1371/journal.pone.0009057.s001 (0.15 MB DOC)

Table S2 Peptides phosphorylated by PknB grouped according to function
Found at: doi:10.1371/journal.pone.0009057.s002 (0.16 MB DOC)

Acknowledgments

The authors wish to thank Michel Débabouillé and Tarek Msadek for useful discussions.

Author Contributions

Conceived and designed the experiments: MM AD DB MPP JMvD KO. Performed the experiments: MM SD SR TRHMK SHD AD ER KG. Analyzed the data: MM SD SHD AD DB MPP KO. Contributed reagents/materials/analysis tools: SR TS MPP KO. Wrote the paper: MM SD SR TS TRHMK SHD AD ER KG DB MPP JMvD KO.

References

1. Rosqvist R, Forsberg A, Wolf-Watz H (1991) Microinjection of the Yersinia YopE cytotoxin in mammalian cells induces actin microfilament disruption. Biochem Soc Trans 19: 1131–1132.
2. Rosqvist R, Magnusson KE, Wolf-Watz H (1994) Target cell contact triggers expression and polarized transfer of Yersinia YopE cytotoxin into mammalian cells. EMBO J 13: 964–972.
3. Galyov EE, Hakansson S, Forsberg A, Wolf-Watz H (1993) A secreted protein kinase of Yersinia pseudotuberculosis is an indispensable virulence determinant. Nature 361: 730–732.
4. Juris SJ, Rudolph AE, Huddler D, Orth K, Dixon JE (2000) A distinctive role for the Yersinia protein kinase: actin binding, kinase activation, and cytoskeleton disruption. Proc Natl Acad Sci U S A 97: 9431–9436.
5. Wiley DJ, Shrestha N, Yang J, Atis N, Dayton K, et al. (2009) The activities of the Yersinia protein kinase A (YpkA) and outer protein J (YopJ) virulence factors converge on an eIF2alpha kinase. J Biol Chem 284: 24744–24753.
6. Navarro L, Koller A, Nordfelth R, Wolf-Watz H, Taylor S, et al. (2007) Identification of a molecular target for the Yersinia protein kinase A. Mol Cell 26: 465–477.
7. Munoz-Dorado J, Inouye S, Inouye M (1993) Eukaryotic-like protein serine/threonine kinases in Myxococcus xanthus, a developmental bacterium exhibiting social behavior. J Cell Biochem 51: 29–33.
8. Perez J, Castaneda-Garcia A, Jenke-Kodama H, Muller R, Munoz-Dorado J (2008) Eukaryotic-like protein kinases in the prokaryotes and the myxobacterial kinome. Proc Natl Acad Sci U S A 105: 15950–15955.
9. Av-Gay Y, Everett M (2000) The eukaryotic-like Ser/Thr protein kinases of Mycobacterium tuberculosis. Trends Microbiol 8: 238–244.
10. Wang J, Li C, Yang H, Mushegian A, Jin S (1998) A novel serine/threonine protein kinase homologue of Pseudomonas aeruginosa is specifically inducible within the host infection site and is required for full virulence in neutropenic mice. J Bacteriol 180: 6764–6768.
11. Motley ST, Lory S (1999) Functional characterization of a serine/threonine protein kinase of Pseudomonas aeruginosa. Infect Immun 67: 5386–5394.
12. Pallova P, Hercik K, Saskova L, Novakova L, Branny P (2007) A eukaryotic-type serine/threonine protein kinase StkP of Streptococcus pneumoniae acts as a dimer in vivo. Biochem Biophys Res Commun 355: 526–530.
13. Echenique J, Kadioglu A, Romao S, Andrew PW, Trombe MC (2004) Protein serine/threonine kinase StkP positively controls virulence and competence in Streptococcus pneumoniae. Infect Immun 72: 2434–2437.
14. Novakova L, Saskova L, Pallova P, Janecek J, Novotna J, et al. (2005) Characterization of a eukaryotic type serine/threonine protein kinase and protein phosphatase of Streptococcus pneumoniae and identification of kinase substrates. FEBS J 272: 1243–1254.
15. Lomas-Lopez R, Paracuellos P, Riberty M, Cozzone AJ, Duclos B (2007) Several enzymes of the central metabolism are phosphorylated in Staphylococcus aureus. FEMS Microbiol Lett 272: 35–42.
16. Donat S, Streker K, Schirmeister T, Rakette S, Stehle T, et al. (2009) Transcriptome and functional analysis of the eukaryotic-type serine/threonine kinase PknB in Staphylococcus aureus. J Bacteriol 191: 4056–4069.
17. Debarbouille M, Dramsi S, Dussurget O, Nahori MA, Vaganay E, et al. (2009) Characterization of a serine/threonine kinase involved in virulence of Staphylococcus aureus. J Bacteriol 191: 4070–4081.
18. Deftereos SP, Michailidou E, Karagiannakis GK, Grigoriadi S, Prassopoulos P (2009) Hematogenous infantile infection presenting as osteomyelitis and septic arthritis: a case report. Cases J 2: 8293.
19. Geipel U (2009) Pathogenic organisms in hip joint infections. Int J Med Sci 6: 234–240.
20. Carrillo-Marquez MA, Hulten KG, Hammerman W, Mason EO, Kaplan SL (2009) USA300 is the predominant genotype causing Staphylococcus aureus septic arthritis in children. Pediatr Infect Dis J 28: 1076–1080.
21. Melly MA, Thomison JB, Rogers DE (1960) Fate of staphylococci within human leukocytes. J Exp Med 112: 1121–1130.
22. Kapral FA (1965) The phagocytosis and intracellular fate of staphylococci. Ann N Y Acad Sci 128: 285–300.
23. Rogers DE, Tompsett R (1952) The survival of staphylococci within human leukocytes. J Exp Med 95: 209–230.
24. Gresham HD, Lowrance JH, Caver TE, Wilson BS, Cheung AL, et al. (2000) Survival of Staphylococcus aureus inside neutrophils contributes to infection. J Immunol 164: 3713–3722.
25. Voyich JM, Braughton KR, Sturdevant DE, Whitney AR, Said-Salim B, et al. (2005) Insights into mechanisms used by Staphylococcus aureus to avoid destruction by human neutrophils. J Immunol 175: 3907–3919.
26. Baughn RE, Bonventre (1975) Nonspecific resistance to Listeria monocytogenes in mice infected and elicited with Staphylococcus aureus. Med Microbiol Immunol 161: 243–252.
27. Hebert A, Sayasith K, Senechal S, Dubreuil P, Lagace J (2000) Demonstration of intracellular Staphylococcus aureus in bovine mastitis alveolar cells and macrophages isolated from naturally infected cow milk. FEMS Microbiol Lett 193: 57–62.
28. Jakab GJ, Green GM (1976) Defect in intracellular killing of Staphylococcus aureus within alveolar macrophages in Sendai virus-infected murine lungs. J Clin Invest 57: 1533–1539.
29. Michailova L, Stoitsova S, Markova N, Kussovski V, Jordanova M, et al. (2000) Interaction of alveolar macrophages with Staphylococcus aureus and induction of microbial L-forms during infection in rats. Int J Med Microbiol 290: 259–267.
30. Elliott GR, Peterson PK, Verbrugh HA, Freiberg MR, Hoidal JR, et al. (1982) Influence of subinhibitory concentrations of penicillin, cephalothin, and clindamycin on Staphylococcus aureus growth in human phagocytic cells. Antimicrob Agents Chemother 22: 781–784.
31. Kubica M, Guzik K, Koziel J, Zarebski M, Richter W, et al. (2008) A potential new pathway for Staphylococcus aureus dissemination: the silent survival of S. aureus phagocytosed by human monocyte-derived macrophages. PLoS ONE 3: e1409.
32. Foster TJ, Hook M (1998) Surface protein adhesins of Staphylococcus aureus. Trends Microbiol 6: 484–488.
33. Lowy FD (1998) Staphylococcus aureus infections. N Engl J Med 339: 520–532.
34. Foster TJ (2005) Immune evasion by staphylococci. Nat Rev Microbiol 3: 948–958.
35. Sibbald MJ, Ziebandt AK, Engelmann S, Hecker M, de Jong A, et al. (2006) Mapping the pathways to staphylococcal pathogenesis by comparative secretomics. Microbiol Mol Biol Rev 70: 755–788.
36. Koziel J, Maciag-Gudowska A, Mikolajczyk T, Bzowska M, Sturdevant DE, et al. (2009) Phagocytosis of Staphylococcus aureus by macrophages exerts cytoprotective effects manifested by the upregulation of antiapoptotic factors. PLoS ONE 4: e5210.
37. Arbibe L, Mira JP, Teusch N, Kline L, Guha M, et al. (2000) Toll-like receptor 2-mediated NF-kappa B activation requires a Rac1-dependent pathway. Nat Immunol 1: 533–540.
38. Treusch AH, Vergin KL, Finlay LA, Donatz MG, Burton RM, et al. (2009) Seasonality and vertical structure of microbial communities in an ocean gyre. ISME J.
39. Walburger A, Koul A, Ferrari G, Nguyen L, Prescianotto-Baschong C, et al. (2004) Protein kinase G from pathogenic mycobacteria promotes survival within macrophages. Science 304: 1800–1804.

40. Park H, Teja K, O'Shea JJ, Siegel RM (2007) The Yersinia effector protein YpkA induces apoptosis independently of actin depolymerization. J Immunol 178: 6426–6434.
41. Wiley DJ, Nordfeldth R, Rosenzweig J, DaFonseca CJ, Gustin R, et al. (2006) The Ser/Thr kinase activity of the Yersinia protein kinase A (YpkA) is necessary for full virulence in the mouse, mollifying phagocytes, and disrupting the eukaryotic cytoskeleton. Microb Pathog 40: 234–243.
42. Tjalsma H, Bolhuis A, Jongbloed JD, Bron S, van Dijl JM (2000) Signal peptide-dependent protein transport in Bacillus subtilis: a genome-based survey of the secretome. Microbiol Mol Biol Rev 64: 515–547.
43. Westers L, Westers H, Zanen G, Antelmann H, Hecker M, et al. (2008) Genetic or chemical protease inhibition causes significant changes in the Bacillus subtilis exoproteome. Proteomics 8: 2704–2713.
44. Dziewanowska K, Patti JM, Deobald CF, Bayles KW, Trumble WR, et al. (1999) Fibronectin binding protein and host cell tyrosine kinase are required for internalization of Staphylococcus aureus by epithelial cells. Infect Immun 67: 4673–4678.
45. Lammers A, Nuijten PJ, Smith HE (1999) The fibronectin binding proteins of Staphylococcus aureus are required for adhesion to and invasion of bovine mammary gland cells. FEMS Microbiol Lett 180: 103–109.
46. Ahmed S, Meghji S, Williams RJ, Henderson B, Brock JH, et al. (2001) Staphylococcus aureus fibronectin binding proteins are essential for internalization by osteoblasts but do not account for differences in intracellular levels of bacteria. Infect Immun 69: 2872–2877.
47. Bayles KW, Wesson CA, Liou LE, Fox LK, Bohach GA, et al. (1998) Intracellular Staphylococcus aureus escapes the endosome and induces apoptosis in epithelial cells. Infect Immun 66: 336–342.
48. Qazi SN, Counil E, Morrissey J, Rees CE, Cockayne A, et al. (2001) agr expression precedes escape of internalized Staphylococcus aureus from the host endosome. Infect Immun 69: 7074–7082.
49. Diks SH, Kok K, O'Toole T, Hommes DW, van Dijken P, et al. (2004) Kinome profiling for studying lipopolysaccharide signal transduction in human peripheral blood mononuclear cells. J Biol Chem 279: 49206–49213.
50. Li XY, Green MR (1996) Intramolecular inhibition of activating transcription factor-2 function by its DNA-binding domain. Genes Dev 10: 517–527.
51. Raingeaud J, Gupta S, Rogers JS, Dickens M, Han J, et al. (1995) Pro-inflammatory cytokines and environmental stress cause p38 mitogen-activated protein kinase activation by dual phosphorylation on tyrosine and threonine. J Biol Chem 270: 7420–7426.
52. Gupta S, Campbell D, Derijard B, Davis RJ (1995) Transcription factor ATF2 regulation by the JNK signal transduction pathway. Science 267: 389–393.
53. Livingstone C, Patel G, Jones N (1995) ATF-2 contains a phosphorylation-dependent transcriptional activation domain. EMBO J 14: 1785–1797.
54. Vlahopoulos SA, Logotheti S, Mikas D, Giarika A, Gorgoulis V, et al. (2008) The role of ATF-2 in oncogenesis. Bioessays 30: 314–327.
55. Lin YS, Green MR (1988) Interaction of a common cellular transcription factor, ATF, with regulatory elements in both E1a- and cyclic AMP-inducible promoters. Proc Natl Acad Sci U S A 85: 3396–3400.
56. Beier F, Taylor AC, LuValle P (2000) Activating transcription factor 2 is necessary for maximal activity and serum induction of the cyclin A promoter in chondrocytes. J Biol Chem 275: 12948–12953.
57. Laferriere J, Houle F, Taher MM, Valerie K, Huot J (2001) Transendothelial migration of colon carcinoma cells requires expression of E-selectin by endothelial cells and activation of stress-activated protein kinase-2 (SAPK2/p38) in the tumor cells. J Biol Chem 276: 33762–33772.
58. Maekawa T, Bernier F, Sato M, Nomura S, Singh M, et al. (1999) Mouse ATF-2 null mutants display features of a severe type of meconium aspiration syndrome. J Biol Chem 274: 17813–17819.
59. Ma Q, Li X, Vale-Cruz D, Brown ML, Beier F, et al. (2007) Activating transcription factor 2 controls Bcl-2 promoter activity in growth plate chondrocytes. J Cell Biochem 101: 477–487.
60. Song H, Ki SH, Kim SG, Moon A (2006) Activating transcription factor 2 mediates matrix metalloproteinase-2 transcriptional activation induced by p38 in breast epithelial cells. Cancer Res 66: 10487–10496.
61. Sevilla A, Santos CR, Vega FM, Lazo PA (2004) Human vaccinia-related kinase 1 (VRK1) activates the ATF2 transcriptional activity by novel phosphorylation on Thr-73 and Ser-62 and cooperates with JNK. J Biol Chem 279: 27458–27465.
62. Nezu J, Oku A, Jones MH, Shimane M (1997) Identification of two novel human putative serine/threonine kinases, VRK1 and VRK2, with structural similarity to vaccinia virus B1R kinase. Genomics 45: 327–331.
63. Vega FM, Gonzalo P, Gaspar ML, Lazo PA (2003) Expression of the VRK (vaccinia-related kinase) gene family of p53 regulators in murine hematopoietic development. FEBS Lett 544: 176–180.
64. Putcha GV, Le S, Frank S, Besirli CG, Clark K, et al. (2003) JNK-mediated BIM phosphorylation potentiates BAX-dependent apoptosis. Neuron 38: 899–914.
65. Lei K, Davis RJ (2003) JNK phosphorylation of Bim-related members of the Bcl2 family induces Bax-dependent apoptosis. Proc Natl Acad Sci U S A 100: 2432–2437.
66. Puthalakath H, Strasser A (2002) Keeping killers on a tight leash: transcriptional and post-translational control of the pro-apoptotic activity of BH3-only proteins. Cell Death Differ 9: 505–512.
67. Cheng EH, Wei MC, Weiler S, Flavell RA, Mak TW, et al. (2001) BCL-2, BCL-X(L) sequester BH3 domain-only molecules preventing BAX- and BAK-mediated mitochondrial apoptosis. Mol Cell 8: 705–711.
68. Zong WX, Lindsten T, Ross AJ, MacGregor GR, Thompson CB (2001) BH3-only proteins that bind pro-survival Bcl-2 family members fail to induce apoptosis in the absence of Bax and Bak. Genes Dev 15: 1481–1486.
69. Black DS, Bliska JB (1997) Identification of p130Cas as a substrate of Yersinia YopH (Yop51), a bacterial protein tyrosine phosphatase that translocates into mammalian cells and targets focal adhesions. EMBO J 16: 2730–2744.
70. Haslinger-Loffler B, Kahl BC, Grundmeier M, Strangfeld K, Wagner B, et al. (2005) Multiple virulence factors are required for Staphylococcus aureus-induced apoptosis in endothelial cells. Cell Microbiol 7: 1087–1097.
71. Weglarczyk K, Baran J, Zembala M, Pryjma J (2004) Caspase-8 activation precedes alterations of mitochondrial membrane potential during monocyte apoptosis induced by phagocytosis and killing of Staphylococcus aureus. Infect Immun 72: 2590–2597.
72. Nilsdotter-Augustinsson A, Wilsson A, Larsson J, Stendahl O, Ohman L, et al. (2004) Staphylococcus aureus, but not Staphylococcus epidermidis, modulates the oxidative response and induces apoptosis in human neutrophils. APMIS 112: 109–118.
73. Schnaith A, Kashkar H, Leggio SA, Addicks K, Kronke M, et al. (2007) Staphylococcus aureus subvert autophagy for induction of caspase-independent host cell death. J Biol Chem 282: 2695–2706.
74. Barz C, Abahji TN, Trulzsch K, Heesemann J (2000) The Yersinia Ser/Thr protein kinase YpkA/YopO directly interacts with the small GTPases RhoA and Rac-1. FEBS Lett 482: 139–143.
75. Mills SD, Boland A, Sory MP, van der Smissen P, Kerbourch C, et al. (1997) Yersinia enterocolitica induces apoptosis in macrophages by a process requiring functional type III secretion and translocation mechanisms and involving YopP, presumably acting as an effector protein. Proc Natl Acad Sci U S A 94: 12638–12643.
76. Nigg EA (2001) Mitotic kinases as regulators of cell division and its checkpoints. Nat Rev Mol Cell Biol 2: 21–32.
77. Pearson G, Robinson F, Beers Gibson T, Xu BE, Karandikar M, et al. (2001) Mitogen-activated protein (MAP) kinase pathways: regulation and physiological functions. Endocr Rev 22: 153–183.
78. Lu KP, Liou YC, Vincent I (2003) Proline-directed phosphorylation and isomerization in mitotic regulation and in Alzheimer's Disease. Bioessays 25: 174–181.
79. Beltramini AM, Mukhopadhyay CD, Pancholi V (2009) Modulation of cell wall structure and antimicrobial susceptibility by a Staphylococcus aureus eukaryote-like serine/threonine kinase and phosphatase. Infect Immun 77: 1406–1416.
80. Jiang L, He L, Fountoulakis M (2004) Comparison of protein precipitation methods for sample preparation prior to proteomic analysis. J Chromatogr A 1023: 317–320.
81. Sambrook J, Fritsch EF, T M (1989) Molecular cloning: a laboratory manual. New York: Cold Spring Harbor Laboratory Press.
82. Kreiswirth BN, Lofdahl S, Betley MJ, O'Reilly M, Schlievert PM, et al. (1983) The toxic shock syndrome exotoxin structural gene is not detectably transmitted by a prophage. Nature 305: 709–712.
83. Norrander J, Kempe T, Messing J (1983) Construction of improved M13 vectors using oligodeoxynucleotide-directed mutagenesis. Gene 26: 101–106.

9.5 Acknowledgements

Thanks to everybody helping me to make this work possible, especially to:

Thilo for your supervision and the opportunity to do my PhD in your lab.

The whole Stehle lab for a great working atmosphere and coffee and other breaks.

Ulla and Georg for their helpful answers and good suggestions.

Stefanie Krieger and Knut Ohlsen for the cooperation on PknB.

Christoph M. Ernst, Dirk Kraus und Andreas Peschel for the cooperation on MprF.

Andreas Maurer and Hubert Kalbacher for their mass spectrometry measurements.

The robot team; please be careful with my favorite robot.

Dirk, Michi, Eva, Felix and Karo for great times in our office.

Markus, Michael and Karo for their student assistance in purification.

All the early-morning coffee drinkers, especially Irmi, for a good start in the day.

Johannes für alles.

Allen Freunden außerhalb der Uni. Besonders Chris und Isa für die lustigen Skatrunden.

Meinen Eltern für all ihre Unterstützung.